Interactions between Vegetation and Water Cycle In the Context of Rising Atmospheric Carbon Dioxide Concentration: Processes and Impacts on Extreme Temperature

Léo LEMORDANT

Submitted in partial fulfillment of the requirements for the degree of Doctor of Philosophy in the Graduate School of Arts and Sciences

COLUMBIA UNIVERSITY

2019

ABSTRACT

Interactions between Vegetation and Water Cycle In the Context of Rising Atmospheric Carbon Dioxide Concentration: Processes and Impacts on Extreme Temperature

Léo Lemordant

Predicting how increasing atmospheric carbon dioxide concentration will affect the hydrologic cycle is of utmost importance for water resource management, ecological systems and for human life and activities. A typical perspective is that the water cycle will mostly be altered by atmospheric effects of climate change, precipitation and radiation, and that the land surface will adjust accordingly. Terrestrial processes can however feedback significantly on the hydrologic changes themselves. Vegetation is indeed at the center of the carbon, water and energy nexus.

This work investigates the processes, the timing and the geography of these feedbacks. Using Earth System Models simulations from the Coupled Model Intercomparison Project, Phase 5 (CMIP5), with decoupled surface (vegetation physiology) and atmospheric (radiative) responses to increased atmospheric carbon dioxide concentration, we first evaluate the individual contribution of precipitation, radiation and physiological forcings for several key hydrological variables. Over the largest fraction of the globe the physiological response indeed not only impacts, but also dominates the change in the continental hydrologic cycle compared to either radiative or precipitation changes due to increased atmospheric carbon dioxide concentration. It is however complicated to draw any conclusion for the soil moisture as it exhibits a particularly nonlinear response.

The physiological feedbacks are especially important for extreme temperature events.

The 2003 European heat wave is an interesting and crucial case study, as extreme heat waves are anticipated to become more frequent and more severe with increasing atmospheric carbon dioxide concentration. The soil moisture and land-atmosphere feedbacks were responsible for the severity of this episode unique for this region. Instead of focusing on statistical change, we use the framework of Regional Climate Modeling to simulate this specific event under higher levels of surface atmospheric carbon dioxide concentration and to assess how this heat wave could be altered by land-atmosphere interactions in the future. Increased atmospheric carbon dioxide concentration modifies the seasonality of the water cycle through stomatal regulation and increased leaf area. As a result, the water saved during the growing season through higher water use efficiency mitigates summer dryness and the heat wave impact. Land-atmosphere interactions and carbon dioxide fertilization together synergistically contribute to increased summer transpiration if rainfall does not change. This, in turn, alters the surface energy budget and decreases sensible heat flux, mitigating air temperature rise during extreme heat periods.

This soil moisture feedback, which is mediated and enabled by the vegetation on a seasonal scale is a European example of the impacts the vegetation could have in an atmosphere enriched in carbon dioxide. We again use Earth System Models to systematically and statistically investigate the influence of the vegetation feedbacks on the global and regional changes of extreme temperatures. Physiological effects typically contribute to the increase of the annual daily maximum temperature with increasing atmospheric carbon dioxide concentration, accounting for around 15% of the full trend by the end of the XXIth Century. Except in Northern latitudes, the annual daily maximum temperature increases at a faster pace than the mean temperature, which is reinforced by vegetation feedbacks in Europe but reduced in North America.

This work highlights the key role of vegetation in influencing future terrestrial hydrologic responses. Accurate representation of the response to higher atmospheric carbon

dioxide concentration levels, and of the coupling between the carbon and water cycles are therefore critical to forecasting seasonal climate, water cycle dynamics and to enhance the accuracy of extreme event prediction under future climates in various regions of the globe.

TABLE OF CONTENTS

List of Figures

List of Tables

ACKNOWLEDGEMENTS

The CMIP5 data is made accessible by the Working Group on Coupled Modelling on the ESGF portal: https://esgf-node.llnl.gov/search/cmip5/

We acknowledge the World Climate Research Programme's Working Group on Coupled Modelling, which is responsible for CMIP, and we thank the climate modeling groups for producing and making available their model output. For CMIP the U.S. Department of Energy's Program for Climate Model Diagnosis and Intercomparison provides coordinating support and led development of software infrastructure in partnership with the Global Organization for Earth System Science Portals.

Yeti and Habanero Columbia HPC have been instrumental in the achievement of this research.

I acknowledge funding from the Alliance Program Doctoral Mobility Grant, which partially supported this research. Marc Stéfanon, co-author of Part II published paper, acknowledges funding from the LABEX BASC (ANR-11-LABX-0034). This work is a contribution to the HyMeX program (HYdrological cycle in The Mediterranean Experiment (Drobinski et al. 2014)). It was also supported by the IPSL group for regional climate and environmental studies, and the IPSL HPC and data center CLIMSERV.

DEDICATION

Dear reader, you should expect that section to be the only non-original section of the dissertation, the classical, consensual, politically correct, and full of banalities section of dedication. But at the same time, these clichés are so true that I write them heartfully.

Let me start with the very unavoidable “cream pie” -as we say in French: it has been a real adventure, paved with good –and less good, but let’s focus on the good ones, right?- things. Before all, I would like to naturally thank my advisor Pierre Gentine who ignited the whole thing by enrolling me in his nascent group. His confidence in my capabilities was very much reassuring for a beginning PhD student, and later on for the pursuing PhD student, and then for the ending PhD student. He got to be more than my PhD advisor, a friend I would enjoy to work with again someday in the future.

Other faculty and scientists have been key in putting the final point to this thesis. First of all, Pr. Kevin Griffin, as a teacher of the plant physiology class, opened to my eyes a whole new world of interesting topics. His class has been a real turning point of my PhD journey. Pr. Upmanu Lall has been an understanding mentor. Co-authors helped me understand how to shape a raw work into a nice publishable story: thank you Philippe Drobinski, Ben Cook, Marc Stéfanon, Alexis Berg, Abby Swann, Jack Scheff, Simone Fatichi. And the anonymous peer-reviewers who helped me a lot enhance my papers.

Travelling for conferences, as invited scientist or for summer schools is vital for research as it enlarges our horizons. It turns out, it enables very nice encounters as well. People who are working on tangential topics, bring up new ideas, and can become eventually true friends. Wink to mates of Ecole Polytechnique’s Summer School ‘13: Anaïs, Karina, Marine, Loïc. Wink to the Valsavarenche Alpine Summer School ’15 friends: Donatella, Francesca, Julio, Angela,

Theo, Maria, Adrien, Greg, Aude, Ned, Annemiek, Maik. Very talented people, with a great future (and already great present).

Thanks also to faculty of summer schools or who hosted me, and interacted with me on the long run: Fabio D'Andrea, Jordi Villa, Stefan Dekker, Kirsten Findell, Alexis Berg, among many others.

Dear co-workers, of the graduate-and –interns room in Mudd 817, you enjoy a very quiet place, no much fun around, but that's the game to get some work done. Marceau, Prad, David, James, Julia, Daniel, Ipsita, Luc, Laureline, Jessica, Nicolas… thanks for the exchanges and the support.

Liebe Alexandra, wie versprochen, bekommst du deine Erwähnung. Ihre Unterstützung zu einem kritischen Zeitpunkt war mir sehr wichtig. Unser Treffen war etwas Gutes, Entscheidendes, das ist mir auf dieser Reise passiert. Mein Leben ist jetzt transformiert, als du meine Wahrnehmung des Lebens geändert hast. Ich habe die Sehnsucht unserer Geistverbindung und unseren Gesprächen. Ich hoffe so stark, dass es möglich in Zukunft wird, wir uns zu sammeln.

Being a student at Columbia is very precious to meet talented and bright people. It enlightens the PhD tunnel. Thanks fellow students from IFP Hart, Stephen, Manuel, Hasan, Rob, Dalila, Victoria, Hanno, Kevin, Georges. Thanks Jess.

And thanks to all my New Yorker friends for the support, Alexis, Jorge and Steph, Marie G and many more.

INTRODUCTION

The atmospheric concentration of [CO_2] has risen globally from the pre-industrial level of 285 ppm to more than 400 ppm in 2015(Etheridge et al. 1996). This unprecedented fast increase has caused the climate to progressively change. However, despite international political agreement in Paris in 2015, [CO_2] continues to rise according to the NOAA Mauna Loa observatory, setting the trajectory of future [CO_2] on the path of the highest emissions scenario of the International Panel on Climate Change(Stocker & Qin 2013). The [CO_2] levels could reach a doubling of current levels, and even surpass a concentration of 1000 ppm by the end of the century.

The rise of global mean temperature is one of the most visible and best known feature of climate change. However, in recent times, extreme climatic events have more clearly highlighted the dramatic turn climate change could have in the future. An international effort of the scientific community has gathered observational evidence of the features of climate change already occurring. At the same time, the community has worked on model-based estimations of climate change in the future. Both observations and modeling studies enable the community to better understand the processes and interactions at play. Oceans are a very important component and global regulator of the climate. The oceanographic community has historically been among the pioneers of the climate change science. Models have long excluded any terrestrial feedback on the atmosphere. The common view was that climate change was driven exclusively by atmospheric and oceanic processes and the land area would then adjust to the new state. Sellers et al. (Sellers et al. 1996) introduced the idea of coupling a land model to an usual atmospheric model within a Global Climate Model, to capture the feedbacks between the terrestrial landmass and the climate. This work convincingly demonstrated that the impacts of this land/atmosphere coupling can be significant.

Terrestrial feedbacks are sometimes referred to as land-atmosphere interactions. Koster et al. (Koster et al. 2004) were among the first to focus specifically on land-atmosphere

interactions. They found that specific geographical and ecological regions were particularly sensitive to these interactions. In these hotspots, precipitation was found to be heavily influenced by soil moisture anomalies, both positively and negatively depending on the specific region. Seneviratne et al.(Seneviratne et al. 2006) found that soil moisture anomalies could create the conditions for exceptional heat-waves. Land-atmosphere interactions play a fundamental role in determining the severity of those heat waves (Fischer et al. 2007; Teuling et al. 2010).

Land-atmosphere interactions are in fact mediated by vegetation. Vegetation is indeed at the heart of the carbon, water and energy cycles. Plants take CO_2 from the atmosphere via their stomata, small pores at the surface of the leaves, to convert it into carbohydrates and biomass. In the process, they release water vapor through the stomata as they transpire. Transpiration accounts for 40% of the precipitation and 60% (Schlesinger & Jasechko 2014) to 90% (Jasechko et al. 2013) of the evapo-transpiration on land. The transpired water is taken from the ground through the roots. The soil moisture is dependent on the vegetation consumption of soil water. Plants are therefore the major player of the water cycle in terrestrial areas. While releasing water the plants are modulating the partition of energy. Transpiration releases energy in the form of latent heat while conduction and convection release energy as sensible heat. Latent heat is the most efficient pathway for energy dissipation (Bateni & Entekhabi 2012) and releasing more energy as latent heat decreases the surface temperature. For this reason, the vegetation is a key part of the energy cycle.

How plants will react to an atmosphere enriched in CO_2, and what are the impacts on the water cycle, are two questions that have been investigated in field experiments. At the leaf level, the size of the stomatal aperture is a direct function of the gradient of $[CO_2]$ between the air and the intercellular $[CO_2]$, and controls how much water is transpired. The stomatal aperture is reduced under higher $[CO_2]$, reducing stomatal conductance without reducing

photosynthesis and therefore increases the water use efficiency (the rate of carbon gain per unit water transpired). As a consequence, less energy is dissipated as latent heat and leaf temperatures increase. Reduced transpiration has been observed *in situ* using tree rings measurements (Frank et al. 2015; Saurer et al. 2004; Peñuelas et al. 2011), and reproduced in experiments specifically designed to study the effect of large [CO_2] increases, the Free-Air CO_2 Enrichment (FACE) experiments (Ainsworth & Long 2005; Norby & Zak 2011).

Another potential but debated physiological effect of increased [CO_2] is known as the fertilization effect. For certain species and under certain circumstances (Peñuelas et al. 2011), especially depending on sufficient nutrient availability, higher CO_2 levels can stimulate growth. The phenomenon has been reported in most experiments (Ainsworth & Long 2005; Norby & Zak 2011; Mccarthy et al. 2007), but the long-term behavior of the vegetation remains uncertain. If a CO_2 fertilization effect persists, this additional biomass could mean more transpiration at the canopy level and could at least partially offset the stomatal conductance reduction effect on transpiration.

Tree ring measurements can only attempt to explore the effects of past increase in atmospheric [CO_2] while FACE experiments can simulate the effects of future atmospheric [CO_2]. However, the spatial footprint of FACE experiments is currently limited to at most a few hundred meters in diameter and thus as consequence, they cannot investigate larger scale feedbacks. Of particular importance is the feedback on the boundary layer and the atmosphere, with spatial scale around 10 km. Modelling experiments are a way to get around this difficulty and gain insights on both the future climate under higher [CO_2] and the processes involved. In this way, the effect of global increase in [CO_2] can be investigated across multiple CO_2 levels and at many spatial and temporal scales.

This dissertation builds on both the recent works and body of literature presented above. I use both observations and model simulation to address the following three research questions:

1- What role will the vegetation play in future hydrologic cycles?
2- How and how much will vegetation impact extreme temperature events under higher [CO_2]?
3- How will the effects of vegetation of future hydrologic cycles and extreme temperature events vary regionally and globally?

I use coupled climate models to disentangle the physiological from the atmospheric feedbacks replicas of the same run. The first run of the model is in its original parameterization with. The [CO_2] increasing in the two inter-dependent but district components of the model, namely the *atmospheric model* that manages all atmospheric and climate variables, and the *land model*, that manages the vegetation and other terrestrial processes. This represents the control run, where both atmospheric and physiological effects occur simultaneously. Next, I alter the increase of atmospheric [CO_2] within the model while holding all other parameters constant. To estimate the atmospheric impacts, the [CO_2] is increasing in the atmospheric model, but remains constant in the land model, I note this run ATMO or RAD. Reciprocally, to estimate the physiological effects, the [CO_2] is increasing in the land model but not in the atmospheric model, I note this run PHYS or FER. Comparing these runs with the control run enables the estimation of the relative contribution of the atmospheric effects, the physiological effects, and the additional indirect feedbacks to the overall effect of rising [CO_2]. I verify the key underlying assumption of this experiment design that the radiative processes are independent from the physiological processes, so that the decomposition of the control run into the ATMO and the PHYS run is relevant.

In part I, I estimate the individual contributions of precipitation, radiation and

physiological CO_2 forcing to several key hydrological variables in an atmosphere enriched in CO_2. The variables considered include: leaf area index, evapo-transpiration, the dryness index Precipitation minus evapo-transpiration, the evaporative fraction, and the soil moisture. This set of variables has been chosen to address the focus of various scientific communties, such as agronomy, ecology, hydrology, climate science, land-atmosphere interactions. The analysis reveals that the change in the continental hydrologic cycle is dominated by the physiological response to CO_2 compared to the response to either radiative or precipitation changes. Soil moisture exhibits however a more nonlinear response compared to the other variables investigated. This study sheds light on the regionaly dominant processes and feedbacks, and demonstrates the key role of the vegetation in influencing future terrestrial hydrologic responses. The study also highlights that the precipitation does not play as big of a role as previously thought.

The Part II develops a novel methods for the study of mega-heatwaves in the future. Instead of looking at statistical data, past extreme events are simulated for future [CO_2]. Specifically I use a regional climate modelling framework to study the European mega-heatwave of 2003, and again use various model parameterizations to isolate the effects of physiological processes from soil-moisture feedbacks. A seasonal analysis shows that the water saved during the spring due to the improved water use efficiency, translates into higher soil moistue during the summer, which is then consumed by the vegetation to cope with the extreme temperatures. The stimulated latent heat flux acts as a proxy for reduced temperature in these simulations and shows that the vegetation can reduce hydrologic stress. As such, the physiological effects could have a dampening effect on the expected increased severity of future heat-waves.

The Part III builds on the results of the Part II, by using a more common statistical

analysis of the model runs used in Part I to investigate the change in extreme temperature events globally. The set up enales me to disentangle and evaluate the global contribution of atmospheric vs. physiological effects on the annual daily maximum temperature Txx change with rising [CO_2]. I show that the vegetation effects typically increase Txx, accounting for around 15% of the full Txx trend. Except in Northern latitudes, Txx increases at a faster pace than the mean temperature, which is reinforced by vegetation feedbacks in regions like Europe, but can also be reduced in other regions like North America.

PART I: Vegetation physiology controls continental water cycle responses to increasing carbon dioxide concentration

Predicting how increasing atmospheric CO_2 will affect the hydrologic cycle is of utmost importance for ecological systems and for human life and activities. A typical perspective is that hydrologic change will mostly be caused by atmospheric effects of climate change, precipitation and radiation, and that the land surface will adjust. Recent work suggests that terrestrial processes may play a greater role than originally predicted. I investigate several key hydrological variables over the largest fraction of the globe using Earth System Models with decoupled surface (vegetation physiology) and atmospheric (radiative) CO_2 responses. Estimating the individual contribution of precipitation, radiation and physiological CO_2 forcing, I show here that the CO_2 physiological response dominates the change in the continental hydrologic cycle compared to either radiative or precipitation changes due to increased atmospheric CO_2, except for soil moisture which exhibits a more nonlinear response. This highlights the key role of vegetation in influencing future terrestrial hydrologic response.

Lemordant, L., Swann, A., Cook, B., Scheff, J., Gentine, P., 2018. Vegetation physiology controls continental water cycle responses to increasing CO_2. *Proceedings of National Academy of Sciences*. DOI: 10.1073/pnas.1720712115

Chapter 1: Introduction to Part I

Most of our understanding of changes in water availability is based on the analysis of changes in the imbalance between precipitation (P) and total evaporation (E) (Held & Soden 2006; Seager et al. 2014). Over open water bodies, evaporation is at its potential rate, i.e. potential evaporation E_p (Penman 1948; Durack et al. 2012). However, over land, soil and vegetation limit the supply of moisture to the atmosphere so that the actual evapotranspiration (ET) is lower than the atmospheric demand E_p. Hence on vegetated surfaces, the analysis of P - E_p fails to explain the projected changes in actual water fluxes (Greve & Seneviratne 2015; Swann et al. 2016; Milly & Dunne 2016), or even the direction of the change in many regions of the globe, and in particular in the subtropics (Byrne & O'Gorman 2015; He & Soden 2016; Greve & Seneviratne 2015). The supply of ET is controlled by the transport of water from the soil and plant roots to the atmosphere and thus depends on moisture available in the soil, biomass (particularly leaf area), plant hydraulic stress, and the opening of stomata (small pores at the leaf surface) among other things. The atmospheric demand of ET is driven by the temperature and dryness of the air, wind speed, and available radiation (as given by the Penman-Monteith equation). As a result, ET, and P-ET, over land can substantially differ from their potential rates E_p, and P - E_p respectively (Milly & Dunne 2016; Swann et al. 2016; Scheff & Frierson 2014).

Plant transpiration accounts for the largest fraction of terrestrial ET (Good et al. 2015), and rising atmospheric [CO_2] affects transpiration through the regulation of stomata (Norby & Zak 2011). With increasing [CO_2] at the leaf surface, the density of stomata at the leaf surface is decreased and their individual opening is reduced and therefore less water is transpired per unit leaf area (de Boer et al. 2011; Lammertsma et al. 2011). In other words, leaf-level water use efficiency increases (Ainsworth & Long 2005; Norby & Zak 2011; Warren et al. 2011),

potentially increasing surface soil moisture (Lemordant et al. 2016; Leuzinger & Körner 2007) and runoff (Betts et al. 2007). On the other hand, leaf biomass tends to also increase with increasing [CO_2], as reported in several field experiments (Ainsworth & Long 2005; Norby & Zak 2011; Mccarthy et al. 2007; Warren et al. 2011), generating a larger evaporative surface that can partly offset the reduction in stomatal conductance and negate the soil water savings (Lemordant et al. 2016). Our objective is therefore to quantify how such plant [CO_2] effects influence future hydrological variable responses compared to radiative effects (Sellers et al. 1996) – the atmospheric impact of the "greenhouse effect". Radiative effects impact precipitation, i.e. water supply, and evaporative demand, through increase in radiation, temperature, and atmospheric dryness as estimated by the vapor pressure deficit (VPD), i.e. saturation minus actual vapor pressure (Figure 1.1).

Several dryness indices based on E_p have been previously defined and used to assess changes in water stress, but give contradictory responses (Berg, Findell, et al. 2016; Scheff & Frierson 2015; Greve et al. 2014). We therefore decided to not use such indices (Swann et al. 2016) as they are not pertinent in the future because of plant physiological effects (Milly & Dunne 2016; Swann et al. 2016). We instead focus on actual physical variables that can be used as land aridity indicators pertinent to various applications. P-ET is a good proxy for long-term runoff, as soil and groundwater storage variations over several years are negligible, and a useful variable for agricultural and ecological impacts. In addition to P-ET, we focus on three variables (Figure 1.2) of specific interest for scientific communities: soil moisture (agronomy and ecology), evapotranspiration (ET) (hydrology, climate), and evaporative fraction (EF) (land-atmosphere interactions), i.e. the ratio of ET to surface available energy.

Chapter 2: Data and Methods

We used outputs from six Earth System Models (ESM) from the idealized single-forcing CMIP5 (Taylor et al. 2011) experiments with [CO_2] increasing at a rate of one percent per year in the atmospheric model, in the vegetation model or in both models. The combined vegetation and atmospheric model [CO_2] increase is called CTRL (1pctCO2 in CMIP5 terminology). We call PHYS the vegetation model [CO_2] increase with no atmospheric model increase (esmFixClim1 in the CMIP5 terminology). We call ATMO the converse simulations, with atmospheric and no vegetation [CO2] increase (esmFdbk1 in CMIP5 terminology). The three runs are otherwise replicas of the same experiment, in which the [CO_2] is increased for 140 years by 1% each year starting from preindustrial [CO_2] levels in 1850 (except for HadGEM2-ES which starts in 1860). The [CO_2] of the 140th year of experiment is about 1145 ppm, significantly higher than the 2100 [CO_2] level in the RCP 8.5 scenario (935 ppm) often taken as the reference scenario for future CO_2 concentration.

The data is available for 6 models: BCC-CSM1-1, CanESM2, CESM1-BGC, GFDL-ESM2M, HadGEM2-ES, NorESM1-ME. For those experiments only one run is available for most of the models -one ensemble member- (r1i1p1 in the CMIP5 terminology), so that we consider only the r1i1p1 ensemble member for all models and ignore ensemble with other members if available.

The 6 models are fully coupled global climate–carbon model including interactive vegetation and global carbon cycle. Land models have several common features. There all based on Plant Functionnal Types (PFT). The various vegetation species are grouped into 5 to 16 different types of vegetation. The models use either the Ball−Berry-type or the Leuning stomatal conductance formulation. Ball-Berry (Ball et al. 1987) is based on relative humidity, whereas Leuning (1995) is based on vapor pressure deficit. Photosynthesis formulation is based

on Farquhar et al. (1980) and Collatz et al. (1991; 1992), except BCC-CSM1-1 which uses a different formulation. It should be noted that half of the models use an atmospheric model derived from the NCAR's CAM4 atmospheric model. BCC-CSM-1 integrates the GFDL's ocean model MOM4.

Model name	BCC-CSM1-1	CanESM2	CESM1-BGC	GFDL-ESM2M,	HadGEM2-ES	NorESM1-ME
Main references	(Ji 1995; Wu et al. 2013)	(Arora et al. 2011; Christian et al. 2010)	(Lawrence et al. 2011; Lindsay et al. 2014)	(Dunne et al. 2012; Dunne et al. 2013)	(Cox et al. 1998; Jones et al. 2011)	(Bentsen et al. 2013; Iversen et al. 2013; Tjiputra et al. 2013)
Atmospheric model name	BCC_AGCM2.0	CanCM4	WACCM	AM2	HadGEM2-AO	CAM4-Oslo
Atmospheric model lineage	NCAR's CAM3 + inhouse parametrizations	Canadian Centre for Climate Modelling and Analysis	NCAR's CAM4 + enhancements	GFDL's CM2.1 + enhancements	MET Office Hadley Centre	NCAR's CAM4
Ocean Model name	MOM4_L40 (Modified GFDL's MOM4)	CMOC	-	MOM4p1	HadGEM2-AO	Modified MICOM

Model name	**BCC-CSM1-1**	**CanESM2**	**CESM1-BGC**	**GFDL-ESM2M,**	**HadGEM2-ES**	**NorESM1-ME**
Land Model name	AVIM	CTEM	CLM4	LM3.0	TRIFFID	CLM4
Stomatal conductance model	Ball-Berry	Leuning	Ball-Berry	Leuning	« Simplified » Leuning	Ball-Berry
Photosynthesis	Custom	Farquhar and Collatz	Farquhar and Collatz	Farquhar and Collatz	Farquhar and Collatz	Farquhar and Collatz
Number of PFTs	15	9	16	5	5	16

The sum of ATMO and PHYS is very close to CTRL (SI Appendix, Figure 1.5, 1.6) indicating that the processes occurring in ATMO and PHYS are sufficiently independent from one another, and justifies the linear decomposition of CTRL into ATMO and PHYS. In particular, for example, rare and extreme events caused by increased warming do not significantly impact PHYS effects on the future mean state in these simulations. Soil moisture, which shows more non-linearities, is an exception. We also emphasize that because of slight differences in each ensemble member initial conditions one should not expect to obtain a perfect match between the combined ATMO+PHYS and CTRL. In particular, regional variations should be expected and due to the internal climate variability.

These idealized runs differ from the more typical CMIP5 Representative Concentration Pathways 8.5, an emission scenario from 2005 to 2100 that includes prescribed changes in Land Use and Land Cover (LULC) scenarios, as well as aerosol and ozone forcing. Also, the [CO_2] increase is different between RCP 8.5 (ending at 936 ppm in 2100) and the 1% per year runs (ending at 1145 ppm after 140 years of simulation). For comparison with the idealized 1% runs, we combined RCP 8.5 with the data from historical runs simulating the period 1850-2005 (historical in CMIP5 terminology). The resulting data 1850-2100 is shown in Figures 1.1, 1.5, and 1.6, and is comparable in terms of geographical features to the 1% simulations.

Our analysis is based on monthly-averaged outputs. We consider one value of a given water stress indicator for each year, and suggest the use of the most relevant period of the year for each variable and localization. It makes more sense to use annual average for precipitation and ET, and P-ET in order to obtain the total water fluxes – as ET is very small in cold winter regions. We also use the annual average for the net radiation and LAI. However, summer is the dominant growing season whether in tropics, mid-latitudes or high latitudes, but not around the

equator, and so plant soil moisture stress is more present and relevant in summer than at other times of year. Hence, we use the summer-time mean (i.e. JJA for latitudes between [10; 90] and DJF for latitudes between [-90; -15]) for EF, VPD, and soil moisture, three variables that indicate a stress, except around the equator (latitudes between [-15; 10]) where, in the Congo for instance, there are two dry/wet seasons. Around the equator selecting only one season would thus lead to a subjective assessment of dryness, as there is minimal dryness in the wet seasons, and ultimately the annual signal is dominated by the dry seasons. The [-15; 10] latitude range was chosen so that the transition with the local summer averaging zones looks smooth, and so that the equatorial range stays as small as possible.

We re-grid each model to a common $1° \times 1°$ grid in order to later compute the intermodel average. The change of a variable X is normalized before the intermodel averaging by the interannual variability and is calculated according to the following formula: $\Delta X = \frac{\bar{X}_{fut} - \bar{X}_{hist}}{\sigma(X_{hist})_{CTRL}}$ where $\bar{X}_{fut}$ is the mean of X over years 89-118 of the runs CTRL, PHYS and ATMO (resp. 2070-2099 for RCP 8.5), $\bar{X}_{hist}$ is the mean of X over years 1-20 (resp. 1939-1968), and $\sigma(X_{hist})_{CTRL}$ is the standard deviation of X over the same period of the run CTRL. We have chosen the averaging periods so that the mean CO_2 concentrations in all four sets of runs are similar (see Table S1). We then compute the standardized change ΔX intermodel average. For comparison, Figure 1.11 and 1.12 show for all the variables presented in Figure 1.1 and 1.2 the change in ATMO and PHYS relative to CTRL: $\frac{RUN}{CTRL} = \frac{\left[\bar{X}_{fut} - \bar{X}_{hist}\right]_{RUN}}{\left[\bar{X}_{fut} - \bar{X}_{hist}\right]_{CTRL}}$

Net radiation is computed using the net downward minus upward longwave and shortwave radiation fluxes. EF is defined as the monthly ratio of the latent heat flux to the sum of the latent and the sensible heat fluxes. VPD is computed from the relative humidity and the saturation vapor pressure, calculated from the monthly averaged temperature. Soil moisture at

2 m and at 30 cm are interpolated using the model soil moisture profiles. As the number of layers varies across models, we first linearly interpolate the profiles of each model and each annual data point (e.g. after the seasonal averaging), extract the value at 2m depth and 30cm depth, and then apply the same routine as for the other variables.

Figure 1.13 shows the number of models that agree with the sign of the ΔX intermodel average. Only the soil moisture intermodel average change shows wide areas of mismatch with individual model change sign.

We decompose changes in each water stress variable X (P-ET, LAI, etc…) into three terms (Figure 1.3, SI Appendix, Figure 1.7): the change due to the effect of R_n, the change due to the effect of P, and the change due to the effect of the physiology. Changes due to R_n are not differentiated from correlated changes in air temperature and VPD, as they are too collinear to yield unique linear decomposition.

This translates into the following equation (1) decomposing changes in water cycle variables, due to R_n and precipitation changes in ATMO and physiological changes in PHYS (and related changes in atmospheric VPD and R_n through land-atmosphere interactions, as seen in Figure 1.1 and 1.2):

$$\Delta X = \left\{\left[\frac{\partial X}{\partial Rn}.\Delta Rn\right]_{ATMO} + \left[\frac{\partial X}{\partial P}.\Delta P\right]_{ATMO} + [Decomposition\ error]_{ATMO}\right\} + [\Delta X]_{PHYS} + [Decomposition\ error\ into\ ATMO\ \&PHYS] \quad (1)$$

First we re-grid X to 1x1° and temporally (annually except for the soil moisture at 2m) average it as for Figure 1.2. Then we apply a multiple linear regression of the variable X of ATMO with respect to the drivers P or R_n, over the 140 years of the 6 models data of X. Hence we regress against 140 x 6 values for each grid point and each variable X, P, R_n. Those decomposed PHYS and ATMO runs help us uniquely define the sensitivity. This contrasts with

CTRL where all variables are evolving jointly in response to both surface physiological and radiative changes so that a uniquely defined decomposition is nearly impossible. The decomposition error terms are reported in Figure 1.5 and 1.6, the fraction of variance explained by the multiple linear regression (R^2) is in coherence with the fact that LAI and EF are dominated by physiological effects (SI Appendix, Figure 1.9d and 1.3d), and but large for P-ET (SI Appendix, Figure 1.14).

A linear regression on net radiation and precipitation cannot account for all the variance explained as we did not include other modified variables such as temperature, relative humidity or wind. However, given the very strong correlation (nearly 1) of temperature with net radiation, a unique linear decomposition cannot be found. The other terms (relative humidity, wind and nonlinearities), as well as non-linearities and ensemble variations, explain the non-unity R^2 (SI Appendix, Figure 1.14). However, in most regions R^2 is very high, emphasizing that precipitation and net radiation (and related temperature changes) are the primary drivers of the change. In the CO_2 physiological runs, precipitation changes as well as mean temperature changes are small (Figure 1.1), so that it is fair to ignore precipitation influence on the changes due to physiological effects.

It should also be noted that PHYS and ATMO are strictly independent and cannot have cross-correlation. The decomposition of CTRL into ATMO and PHYS is not perfect but works well, as shown in Figure 1.5 and 1.6. The effect of the linearization in (1) in the independent PHYS and ATMO runs are further compared to the full nonlinear response of the CTRL runs in Figure S2 and S3. ATMO and PHYS contributes quite independently and linearly to CTRL (SI Appendix, Fig 1.5 and 1.6). However, if we use the decomposition of ATMO changes along the precipitation and the net radiation (as in Figure 1.3 and SI Appendix, Figure 1.7) to reconstruct an equivalent to CTRL, the result is satisfactory except for EF at northern latitudes and in Eastern Africa (SI Appendix, Figure 1.5 and 1.6) and especially for the soil moisture (SI

Appendix, Figure 1.5 and 1.6), indicating non-linearities, consistent with an overall low R^2 (SI Appendix, Figure 1.14). This further emphasizes the difficulty to predict the change in soil moisture.

We end up with a triplet (R, G, B) with R, G and B in [0;1] for each pixel defined as the absolute normalized sensitivity to net radiation, physiology and precipitation changes respectively:

$$R = \frac{\left|\left[\frac{\partial X}{\partial Rn}.\Delta Rn\right]_{ATMO}\right|}{\left|\left[\frac{\partial X}{\partial Rn}.\Delta Rn\right]_{ATMO}\right|+\left|\left[\frac{\partial X}{\partial P}.\Delta P\right]_{ATMO}\right|+\left|[\Delta X]_{PHYS}\right|} \quad (2)$$

$$G = \frac{\left|[\Delta X]_{PHYS}\right|}{\left|\left[\frac{\partial X}{\partial Rn}.\Delta Rn\right]_{ATMO}\right|+\left|\left[\frac{\partial X}{\partial P}.\Delta P\right]_{ATMO}\right|+\left|[\Delta X]_{PHYS}\right|} \quad (3)$$

$$B = \frac{\left|\left[\frac{\partial X}{\partial P}.\Delta P\right]_{ATMO}\right|}{\left|\left[\frac{\partial X}{\partial Rn}.\Delta Rn\right]_{ATMO}\right|+\left|\left[\frac{\partial X}{\partial P}.\Delta P\right]_{ATMO}\right|+\left|[\Delta X]_{PHYS}\right|} \quad (4).$$

The triplet (R,G,B) is used to color the pixel with the combination of (red, green, blue) in Figure 3, as an indicator of absolute net radiation, physiology and precipitation changes. On all plots we discard pixels where LAI is below 0.2. Figure 1.3 reports also pie charts of global averages of R, G and B values, weighted by the total effect including error terms, reported in these pie charts as a dashed grey area.

Chapter 3: Disentangling atmospheric and physiological responses to increasing CO_2

We quantify changes in these water cycle parameters using a multi-model ensemble from Phase 5 of the Coupled Model Intercomparison Project CMIP5(Taylor et al. 2011), and assess the impact of atmospheric (ATMO) vs. physiological (PHYS) CO_2 effects(Sellers et al. 1996) using an idealized experiment where [CO_2] is increased from preindustrial levels by one percent each year only in the atmospheric model (ATMO) or in the vegetation model (PHYS), or in both (CTRL) (Methods). These conceptual experiments give geographically consistent results with the more commonly used RCP8.5 experiments (Figure 1.4, 1.5 and 1.6), and enable us to disentangle the greenhouse gas warming (ATMO), from the physiological effects of increased [CO_2] (PHYS) on hydrologic responses. We further decompose the global warming effects in ATMO into the contribution of precipitation and net radiation (and related increases in temperature and VPD) (Methods). We are then able to estimate the relative contribution of each of the three main hydrologic drivers: precipitation, net radiation, and physiological effects (Figure 1.3, Figure 1.7), as well as nonlinearities that could result from the interactions between surface physiology and atmospheric changes (Chap. 2, Methods).

The drivers of water supply and evaporative demand - precipitation, radiation and VPD - are primarily controlled by atmospheric greenhouse effects (ATMO) (Figure 1.1). On the supply side of the water balance, annual precipitation increases throughout the globe in CTRL, because of the increased energy input into the surface due to increased greenhouse gas effects and because of the increased atmospheric water vapor, especially at northern latitudes (Figure 1.1a) where the present pattern is exacerbated by warming-induced changes in water vapor (Held & Soden 2006; Sarah B. Kapnick & Delworth 2013; Krasting et al. 2013). Precipitation decreases in several places such as in Southwest North America, southern Africa, the Amazon,

and the Mediterranean region(Seager et al. 2014), primarily because of global warming (Figure 1.1b) and changes in atmospheric dynamics and not because of physiological effects, which mainly have an impact on tropical precipitation (Figure 1.1c).

On the demand side of the water balance, net radiation (R_n), one of the main drivers of E_p(Penman 1948), increases relatively uniformly over the Earth (Figure 1.1d) in CTRL, primarily driven by greenhouse gas radiative effects (Figure 1.1e). Nonetheless, physiological effects also increase R_n throughout the globe except in equatorial Africa and in Indonesia (Figure 1.1f). The reduction in low cloud cover imposed by the decreased EF(Gentine et al. 2013) (Figure 1.2i) drives a downwelling shortwave radiation increase, while the limited differential changes in surface skin and air temperature keep longwave radiation changes small.

Enhanced VPD not only increases evaporative demand (Penman's equation(Penman 1948)) but also decreases stomatal conductance, and therefore ET. VPD increases strongly across the Earth with increasing [CO_2] (Figure 1.1g) due to its exponential dependence on temperature (Figure 1.1h, SI Appendix, Figure 1.8). In addition to warming effects (Figure 1.1h), the closure of stomata under higher [CO_2] implies reduced water flux into the air. The resulting shift in EF (Figure 1.2i) contributes to higher temperatures, which, combined with lower humidity, increases VPD throughout the globe, especially in the wet tropics (Figure 1.1i). Climate change also drives differential land and ocean warming, reducing relative humidity over land(Byrne & O'Gorman 2016), as highlighted in ATMO.

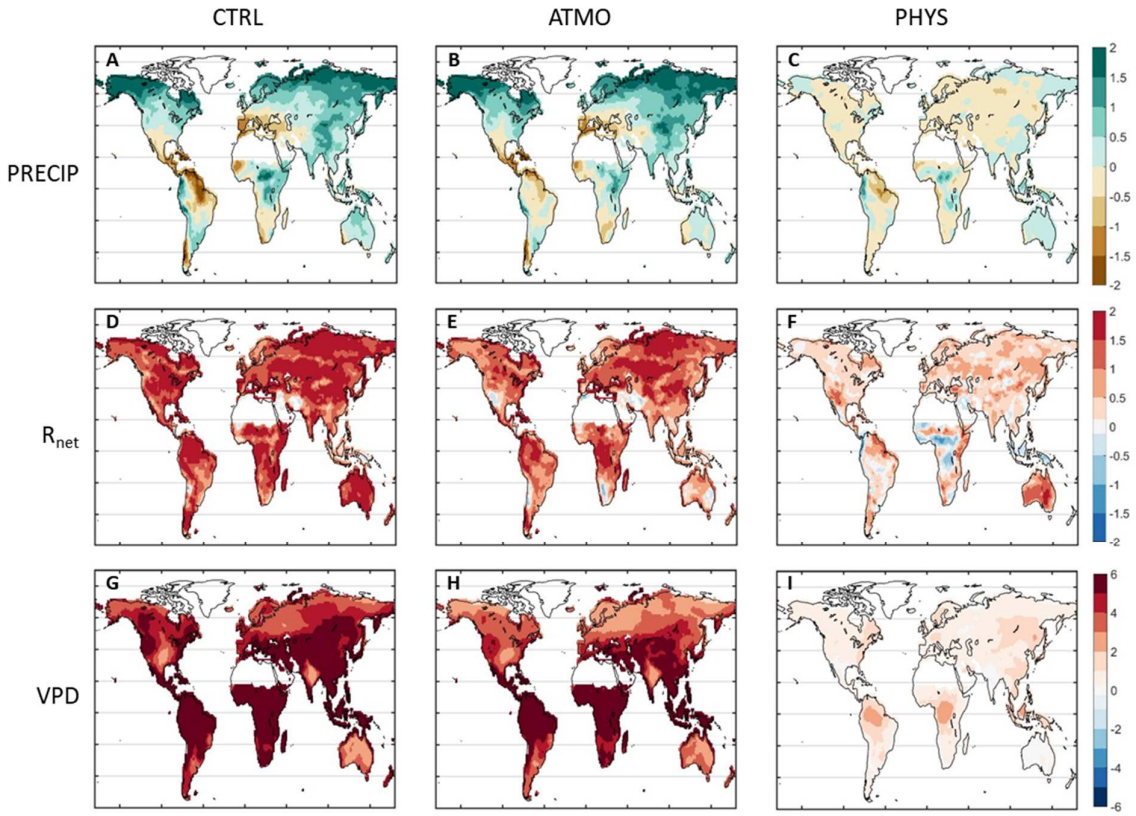

Figure 1.1 Supply and demand for water.
Precipitation (A, B, C; annual) is the supply; demand for water is driven by two factors: Net radiation (D, E, F; annual) and VPD (G, H, I; growing season), for respectively CTRL (left column), ATMO (center column) and PHYS (right column) runs. Change is quantified by the difference of the years 89-118 of the simulation and the years 1-20, normalized by the standard deviation of CTRL over the years 1-20 (Methods). The changes observed for VPD are much larger in amplitude than for R_n and P, so that the scale was adjusted accordingly for VPD in G.

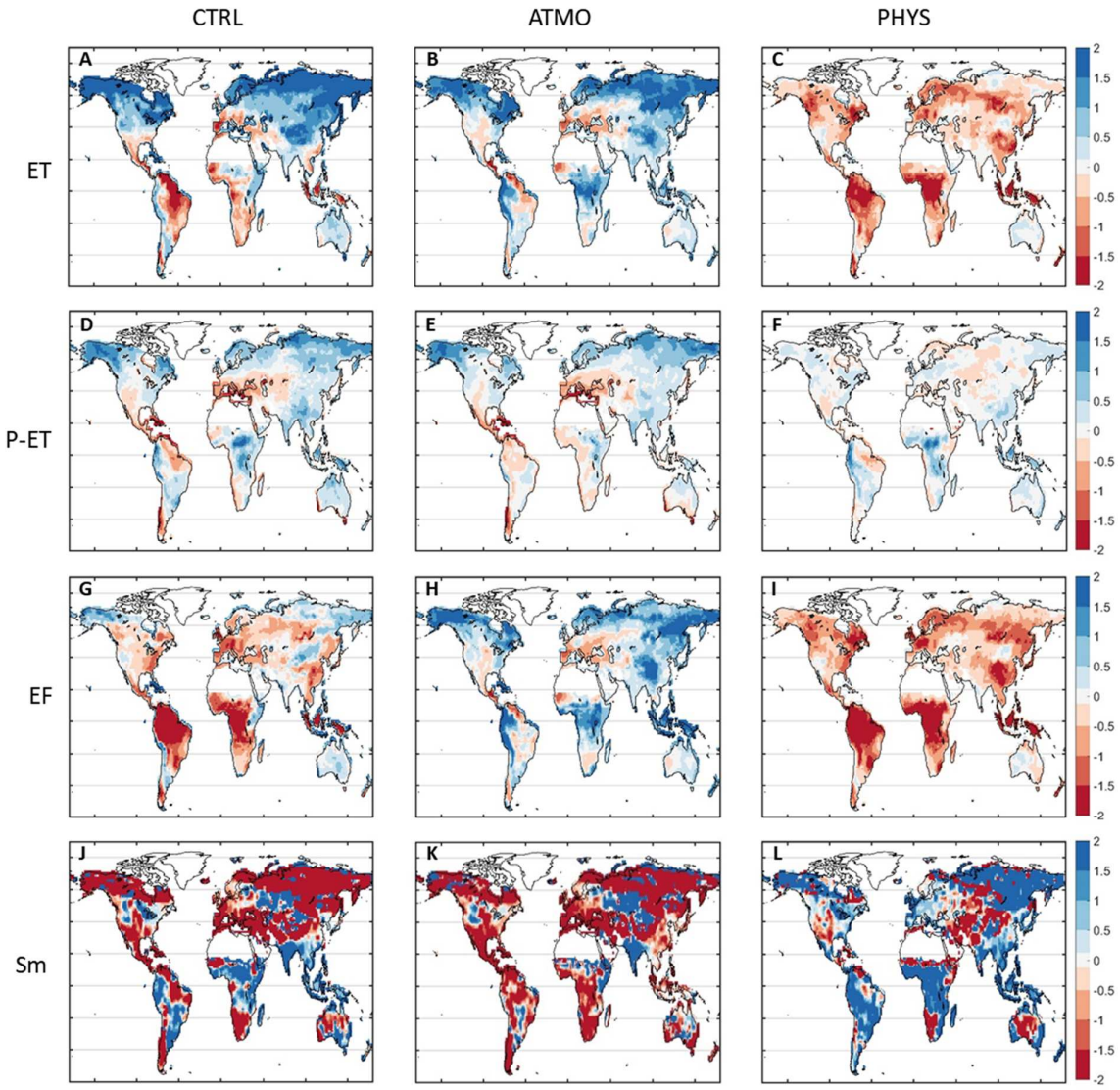

Figure 1.2 Hydrologic cycle response to increased [CO_2].
ET (A, B, C; annual), P-ET (D, E, F; annual), EF (G, H, I; growing season), soil moisture at 2m (J, K, L; growing season), changes in CTRL (left column), ATMO (center column), and PHYS (right column) runs, are quantified by the difference of the years 89-118 of the simulation and the years 1-20, normalized by the standard deviation of CTRL over the years 1-20 (Chap 2 Methods).

Chapter 4: Physiological effects have a critical impact on the variables of the water cycle

Field experiments (Ainsworth & Long 2005; Mccarthy et al. 2007; Norby & Zak 2011) and observations (Campbell et al. 2017) have shown that higher [CO_2] can stimulate plant growth within an observed range of nearly zero up to ~12% at a doubling of [CO_2] depending on species, climates, nutrient availability and other stresses. Land-surface models capture a similar range (Zhu et al. 2016). We find that LAI indeed increases almost everywhere except in Amazonia and central Africa (Figure 1.9a), where LAI is already high and further growth is thus limited (Norby & Zak 2011). The physiological effect (SI Appendix, Figure 1.9c) is, as expected, the primary driver of LAI changes over 89% of land accounting for two thirds of the change globally (SI Appendix, Figure 1.9d, Figure 1.10a). Exceptions are the northern latitudes where radiative effects (SI Appendix, Figure 1.9d) induce warmer temperatures and a longer growing season (Zhu et al. 2016) (SI Appendix, Figure 1.9b), and the Amazon basin, where the combined negative contributions of the precipitation decline (SI Appendix, Figure 1.9d, Figure 1.1b) and the radiatively induced R_n increase (SI Appendix, Figure 1.9d, Figure 1.1e) cancel out the physiological effects (SI Appendix, Figure 1.9d, 1.9c).

Changes in ET under elevated [CO_2] vary widely across the globe (Figure 1.2a) and are mostly controlled by physiological effects, which account for 58% of the changes globally (Figure 1.3a, SI Appendix, Figure 1.7c). In the energy-limited northern latitudes, higher ET is however mostly due to radiative effects and accompanying increased precipitation (Figure 1.2b, Figure 1.3a, and SI Appendix, Figure 1.7a). Tropical rainforests, which are also energy-limited, display an increase in ET from radiative effects (Figure 1.2b) but this effect is overcompensated by the physiological response of stomata to [CO_2] (Figure 1.2c). The Mediterranean, Central America and West Africa all exhibit reduced ET (Figure 1.2a) in

response to radiatively driven precipitation declines (Figure 1.2b), but are also largely physiologically controlled (Figure 1.3a, , SI Appendix, Figure 1.7a, b, c, 1.10b).

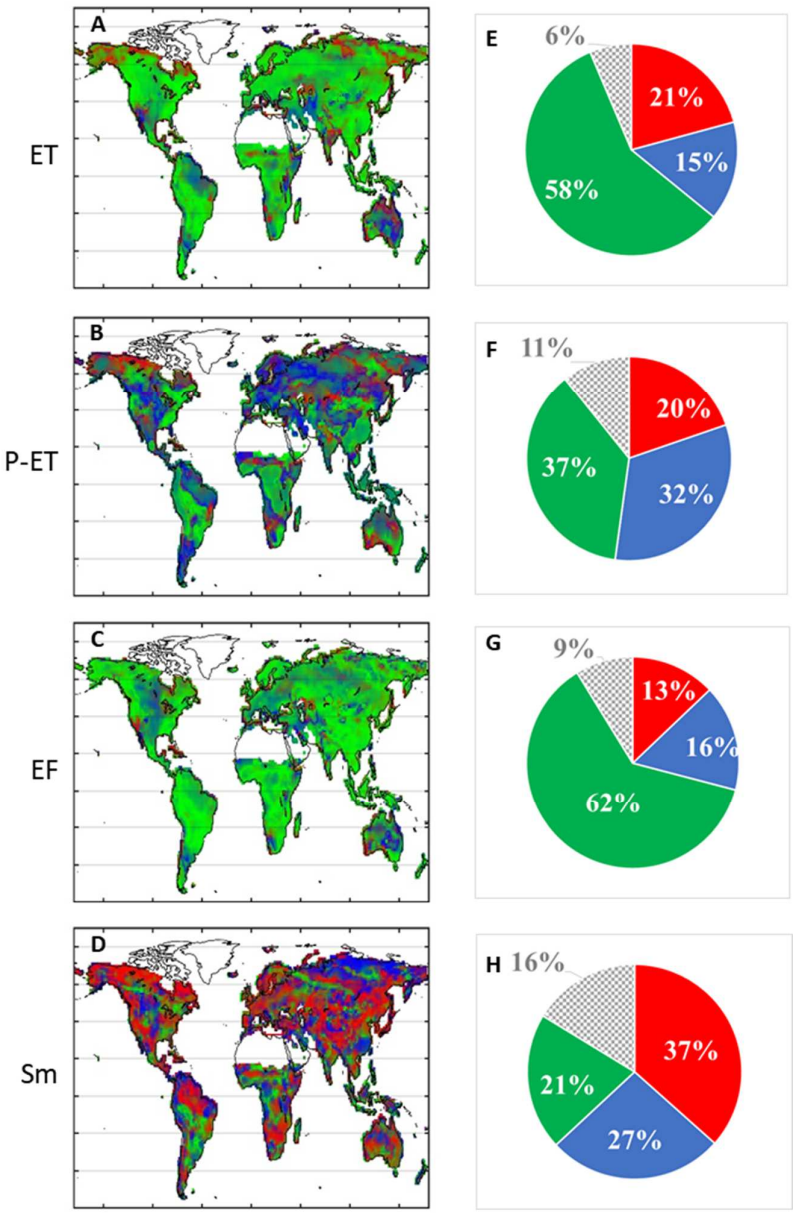

Figure 1.3 Decomposition along the three main drivers of ET (A), P-ET (B), EF (C), Sm (D) in CTRL

Green quantifies the effect of the vegetation physiology based on the run PHYS; red and blue quantify the contribution of, respectively, net radiation and precipitation, based on a multiple linear regression of ATMO. Pie charts show for ET (E), P-ET (F), EF (G), Sm (H) the global average of each contribution, weighted by the total effect including error terms, reported as a grey shaded area.

The response of P-ET, i.e. long term runoff (Figure 1.2d), reflects the changes in both P and ET, and is expected to be more strongly related to radiative changes than just ET changes as radiative changes mostly alter precipitation. Nonetheless, physiology still slightly dominates changes of P-ET over precipitation, 37% vs. 32% of the total changes respectively (Figure 1.3b). In CTRL, the response is a smoothed version of the precipitation response (Figure 1.1a) and does not reflect the increase in E_p (Figure 1.3b) (Swann et al. 2016), further confirming that E_p is not a pertinent variable of changes in ET in the future (Swann et al. 2016). The geographical structure of P-ET thus largely reflects global warming changes (Figure 1.2e). Physiological effects and their impact on ET (Figure 1.2c) drive the P-ET response in the regions where ET changes are the largest (Eastern US, central South America, South-East Asia and central Africa) (Figure 1.12i); they contribute most to P-ET in about one third of the globe (Figure 1.3b, Figure 1.7f). Precipitation accounts for about a third of the P-ET changes (Figure 1.3b, Figure 1.7e) and dominates the P-ET response in one quarter of the globe (Figure 1.10c), which is a much larger fraction than for other stress indices such as LAI, ET, EF or soil moisture. Over Western Europe, the northern part of Amazon and southern South America, the decreasing trend in precipitation (Figure 1.1a) has a large impact on P-ET. Radiation and related temperature increase drives P-ET change in the northern latitudes and in some semi-arid regions (Figure 1.3b, Figure 1.7d). However, a third of the globe surface is not dominated by one single factor, and only their combined effects can explain the overall response (Figure 1.10c). This multi-model analysis of P-ET shows that both total greenhouse gas effects (as assessed in ATMO) and PHYS play a very significant role in long-term runoff similarly to a previous single earth system model analysis (Betts et al. 2007).

The evaporative fraction (latent heat flux divided by the total energy input), and its associated quantity the Bowen Ratio (sensible heat flux divided by latent heat flux), measure the surface energy partitioning towards ET and its impact on the overlying atmosphere (Gentine

et al. 2007; Gentine et al. 2011), and reflects ecosystem stress. While changes in EF are constrained by ET, they are impacted by the energy cycle changes as well. Both the radiative flux and EF changes impact the global changes in evaporation and precipitation (Held & Soden 2006). Since ET equals EF times the radiative flux, the responses of ET and EF are related but distinct, especially in regions where radiative changes are large, such as in cold regions. The linear combination of radiative and physiological effects very well explains the spatial patterns of EF in CTRL (Figure 1.2g). Radiative (Figure 1.2h, Figure 1.10d) and physiological effects (Figure 1.2i, Figure 1.10d) show strong and opposite control on EF. Radiative effects increase EF (Hartmann 2016), except in the Mediterranean, Central America, West Africa and around the Amazon delta (Figure 1.2h, Figure 1.10d, Figure 1.3c, Figure 1.7g). On the contrary, physiological effects have a large negative impact on EF (Figure 1.2i, Figure 1.10d) in most regions (79% of the globe, Figure S7d) and especially in tropical regions (Figure 1.3c, Figure 1.7i), as decreases in transpiration due to stomatal closure under rising [CO_2] are not compensated by saved soil moisture resources (Gray et al. 2016; Lemordant et al. 2016) or increased LAI, which is already very high in tropical regions. In Alaska, Siberia, Australia and the horn of Africa, the physiological-induced decrease of EF indicates increased partitioning towards sensible heating compared to ET and thus increased temperature through land-atmosphere feedback (Seneviratne et al. 2010). It is therefore critical to correctly represent physiological effects in models to estimate future land-atmosphere interactions and extremes (Lemordant et al. 2016). Precipitation (Figure 1.3c, Figure 1.7h) is a major driver of EF changes in Europe, Australia, in the Great Plains, and some of central and South America. In the Northern West coast of South America, EF decreases significantly, while ET tends to increase because of increased radiative effect (Figure 1.2a, b, g). In Northern latitudes regions like Québec or Central Northern Russia, EF increases slightly but ET increases much more because

of the additional radiative heating (Figure 1.2a, b, g). Overall though, physiology accounts for the majority (almost two thirds) of the EF changes (Figure 1.3c, Figure 1.7i).

Growing season soil moisture at 2m depth (SM_{2m}) (Methods) changes almost everywhere but the sign and magnitude of the response varies widely across the globe (Figure 1.2j). SM_{2m} is influenced by changes in seasonality imposed by changes in phenology and LAI (Figure 1.9c) (Lemordant et al. 2016; Boisier et al. 2015). Most of the soil moisture decrease (Figure 1.2j) is due to radiative effects (Figure 1.2k, Figure 1.3d, Figure 1.7j), whereas physiological effects tend to increase SM_{2m} (Figure 1.2l), especially in equatorial Africa, South America, South Asia and Indonesia (Figure 1.2j). Soil moisture does not homogeneously change over the whole soil column, consistent with recent findings(Berg, Sheffield, et al. 2016). Soil moisture changes are often thought to be driven by changes in P, but this is confirmed only over a very small fraction of the globe (Figure 1.3d, Figure 1.7k, 1.10e), and, overall, soil moisture changes have no unique global driver. Large fractions of the globe are impacted by radiative changes, including the Amazon and most of Western Europe (Figure 1.3d, Figure 1.7j), where precipitation also declines (Figure 1.1a). Vegetation and land-atmosphere interactions are the main drivers of soil moisture changes in regions including South America, Eastern US, South East Asia and some places in Central Africa (Figure 1.12o). In addition, soil moisture variations are strongly non-linear so that a linear decomposition does not explain all the features observed (Figure 1.4, 1.5, 1.6, 1.9e), emphasizing that predicting soil moisture is more complicated than other stress indices.

Chapter 5: Discussion

The control of precipitation on the future terrestrial water cycle is weak in general and represents the dominant control for only a small fraction of the Earth, consistent with recent remote sensing observations showing stronger vegetation response to atmospheric aridity compared to precipitation (Konings et al. 2017). In particular, precipitation trends are only a minor factor for biomass growth (as measured by LAI, Fig. 1.9a-c) and energy partitioning (as indicated by EF, Fig. 1.2g-i). We note that the response over the Amazon basin is heavily influenced by net radiation changes rather than by physiological or precipitation effects (Fig. 1.3). In energy-limited ecosystems such as the Amazon, changes in radiation will become one of the primary drivers of transpiration and ecosystem functioning (Pieruschka et al. 2010). Our conclusions are not strongly affected by additional land-use and land cover changes or the addition of aerosols, as present in the RCP 8.5 simulations, which overall behave similarly to the simplified one-percent yearly increase CO2 experiments (Fig. 1.4). Soil moisture appears to be the most complex and non-linear variable and is also affected by uncertain land-use and land-cover change and vegetation response (Alkama & Cescatti 2016). Our study illustrates how deeply the physiological effects due to increasing atmospheric [CO_2] impact the continental water cycle. Contrary to previous wisdom, changes in precipitation and radiation do not play the primary role in future drying and moistening in most regions. Rather, biosphere physiological effects and related biosphere-atmosphere interactions (Green et al. 2017) are key for predicting future continental water stress as represented by evapotranspiration, long-term runoff, evaporative fraction or leaf area index. In turn, vegetation water stress largely regulates land carbon uptake (Poulter et al. 2014), further emphasizing how tightly the future carbon and water cycles are coupled so that they cannot be evaluated in isolation.

Chapter 6: Supplementary Materials of Part I

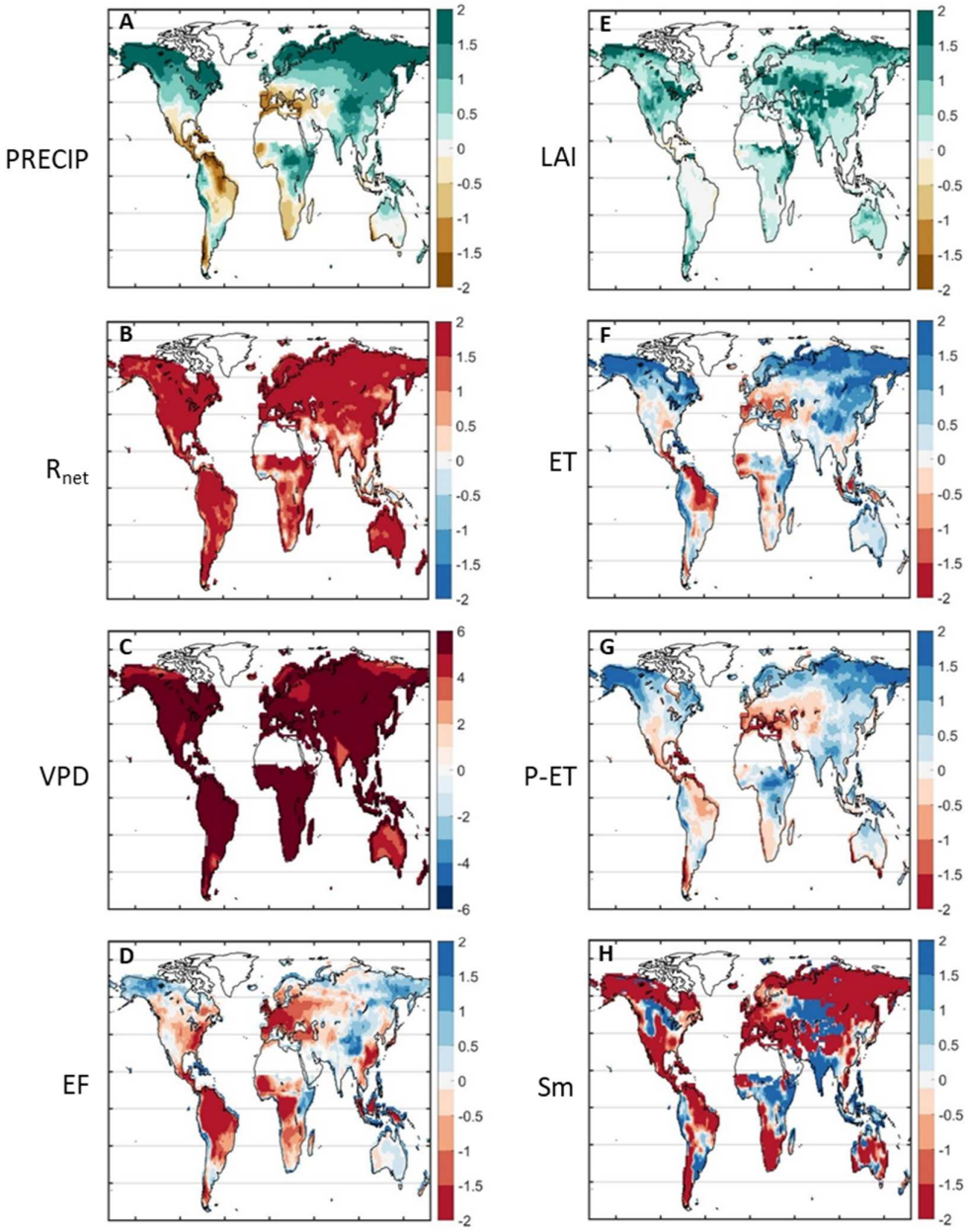

Figure 1.4 Standardized changes in RCP 8.5.
All forcings (land use and land cover change, aerosols, ozone, etc…) are taking into account for precipitation (A), net radiation (B), VPD (C), EF (D), LAI (E), ET (F), P-ET (G) and soil moisture at 2m (H).
Change is quantified by the difference of the years 89-118 of the simulation and the years 1-20, normalized by the standard deviation of CTRL over the years 1-20 (Methods).

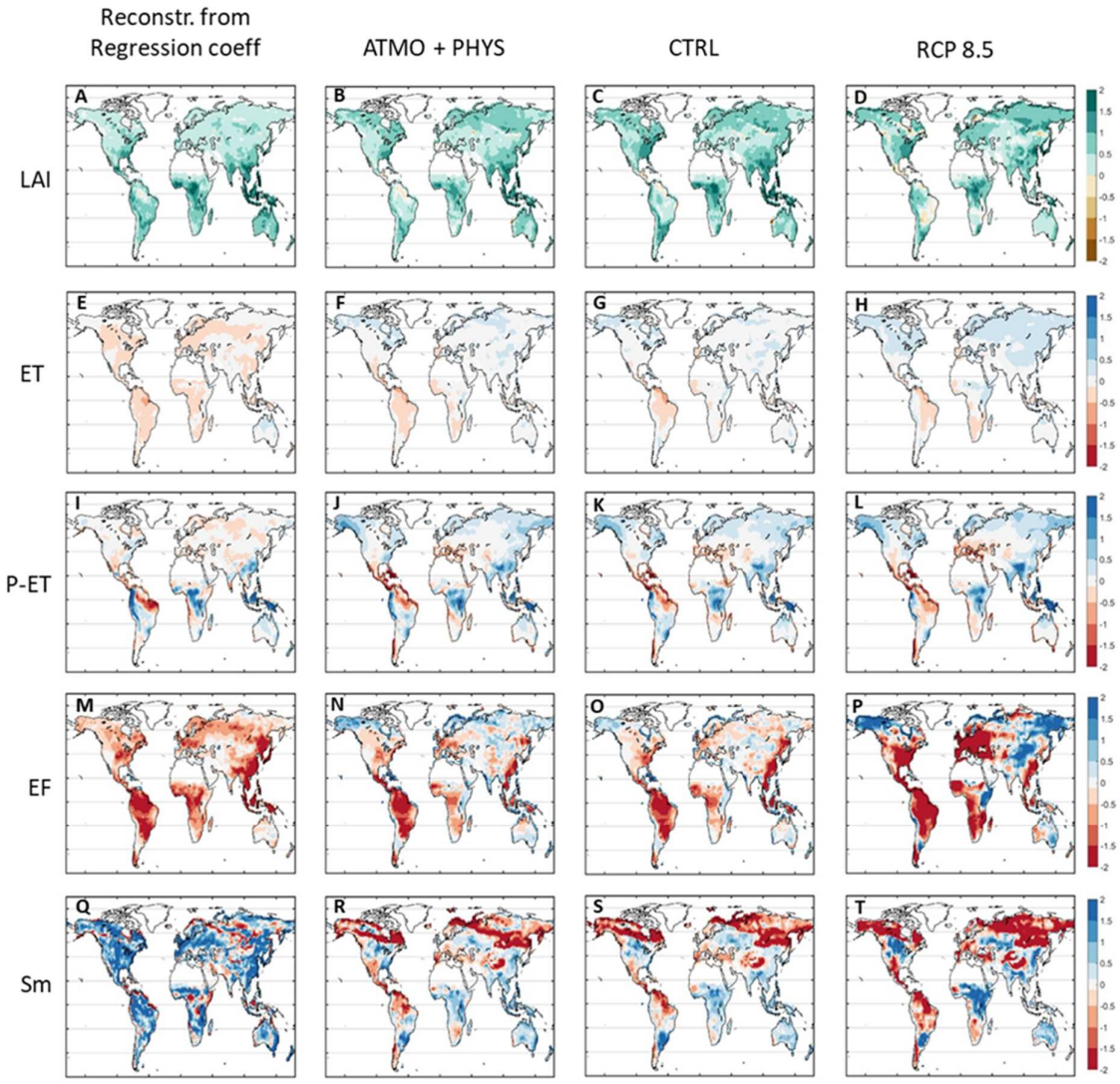

Figure 1.5 Reconstruction of the change.
Difference between years 89-118 and years 1-20 from the multiple linear regression (first column), the sum of changes in ATMO and PHYS (second column), and the comparison with CTRL (third column) and RCP 8.5 (fourth column) is shown for LAI (A, B, C, D), P-ET (E, F, G, H), EF (I, J, K, L), and SM_{2m} (M, N, O, P).

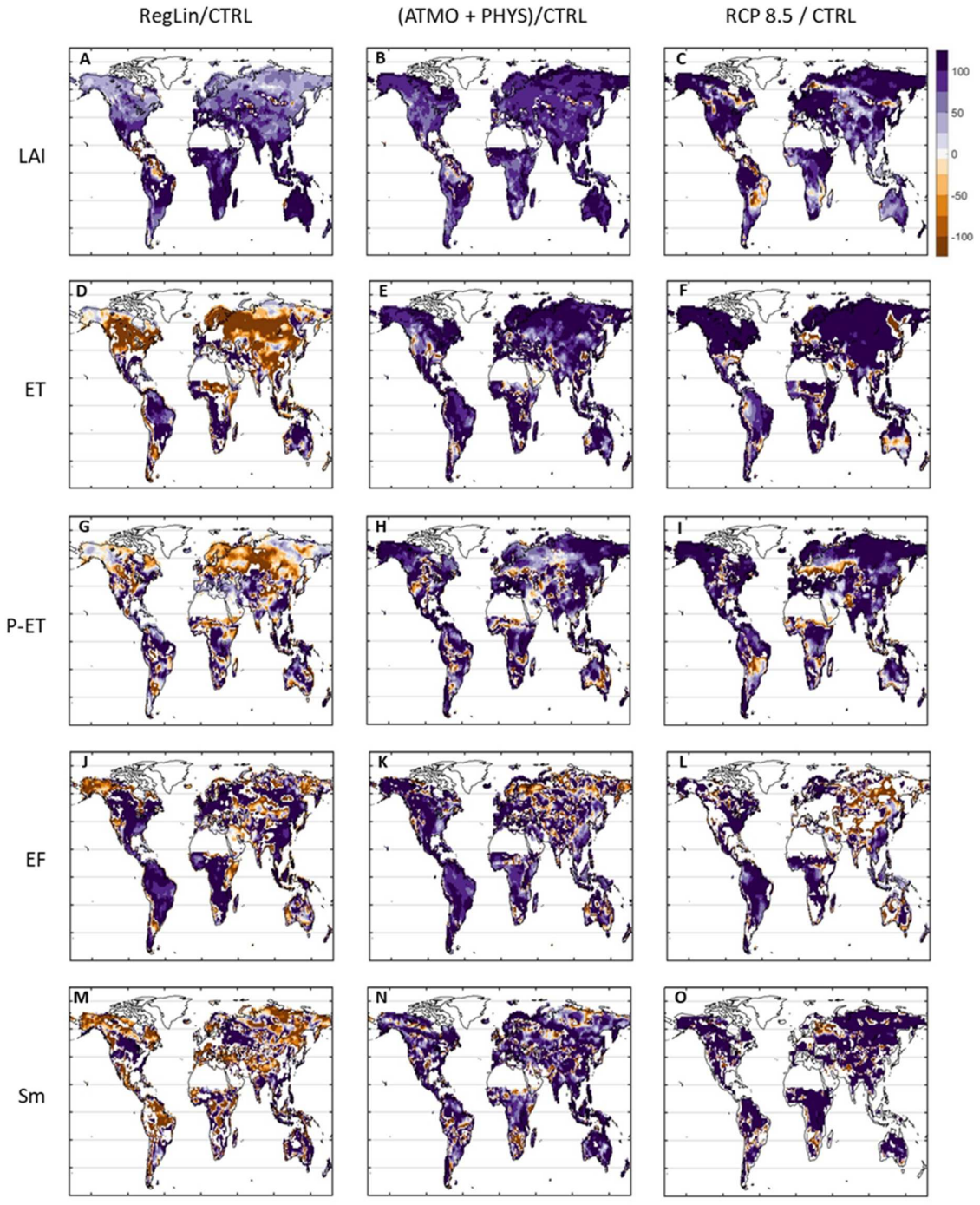

Figure 1.6 Comparison of the ratios to CTRL.
Difference between years 89-118 and years 1-20 from the multiple linear regression (first column), the addition of changes in ATMO and PHYS (second column), and the comparison with CTRL (third column) and RCP 8.5 (fourth column) is shown for LAI (A, B, C), ET (D, E, F), P-ET (G, H, I), EF (J, K, L) and SM_{2m} (M, N, O).

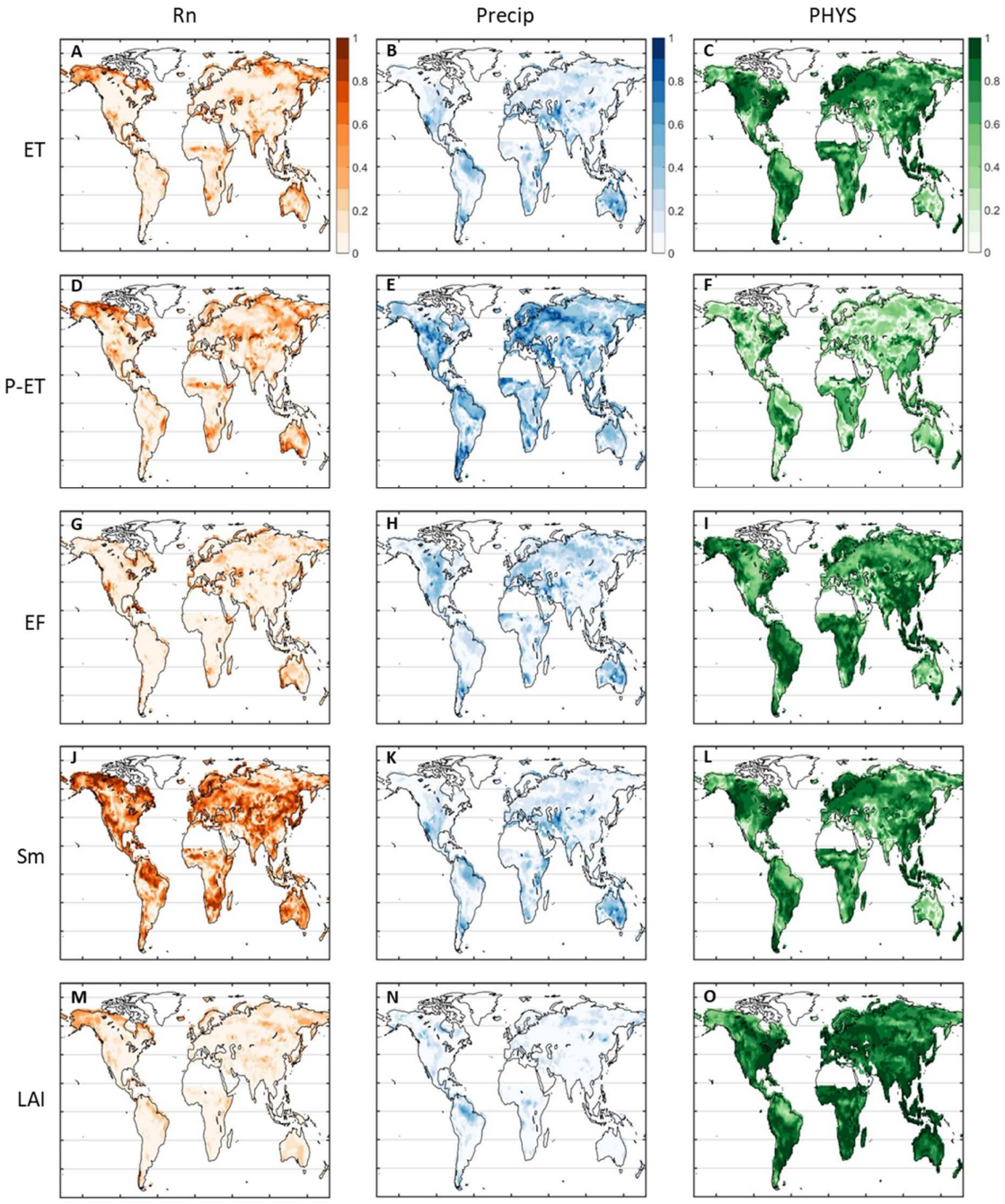

Figure 1.7 Individual contributions of net radiation, precipitation and physiological effects. Contribution of net radiation to ET (A), P-ET (D), EF (G), Sm (J) and LAI (M) in CTRL according to the decomposition.
Individual contribution of precipitation to ET (B), P-ET (E), EF (H), Sm (K) and LAI (N) in CTRL. Individual contribution of physiological effects to ET (C), P-ET (F), EF (I), Sm (L) and LAI (O) in CTRL.

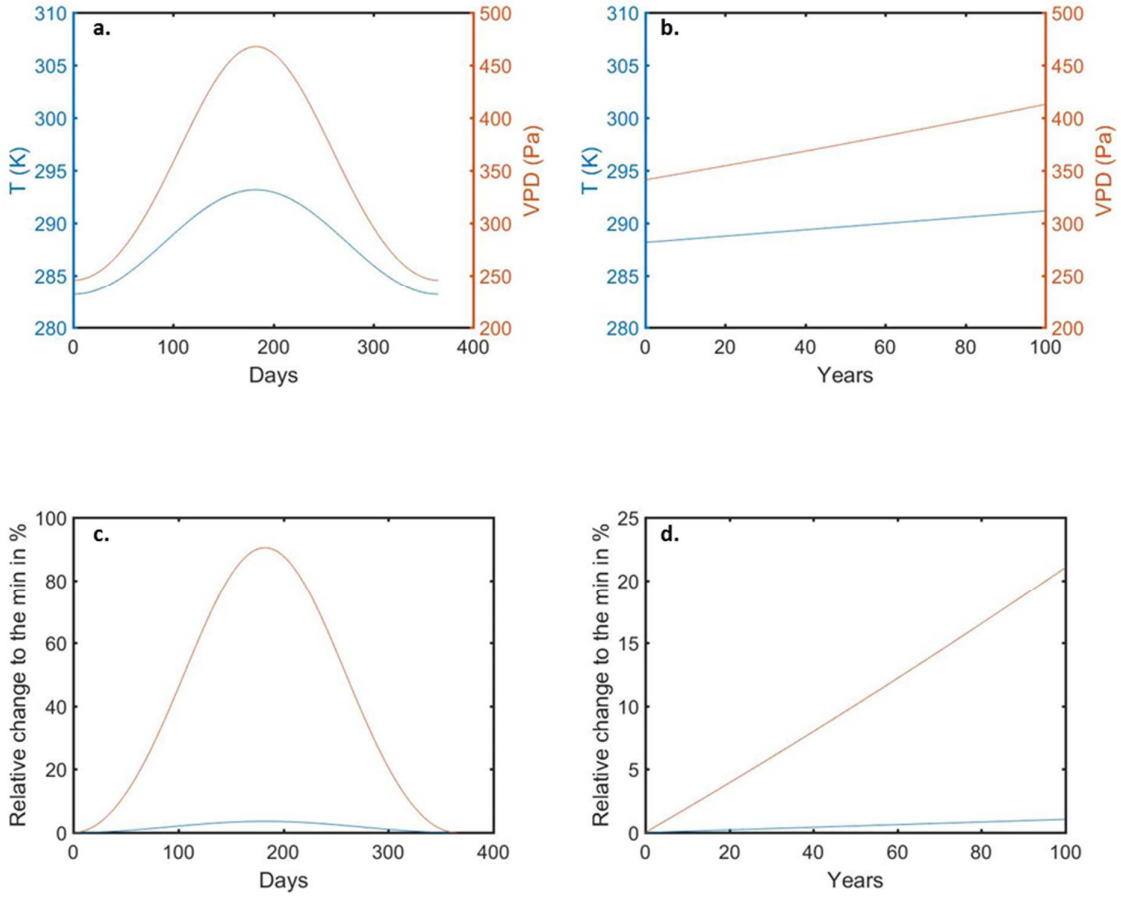

Figure 1.8 The VPD exponential dependence on temperature.
The VPD exponential dependence on temperature alone explains that a 3K temperature variations, or less than 10% change, lead to large seasonal (A) and long run climate change (B) variations of VPD, dozens of percent variations relatively to the minimum (C and D respectively). Relative humidity is kept constant at 80%.

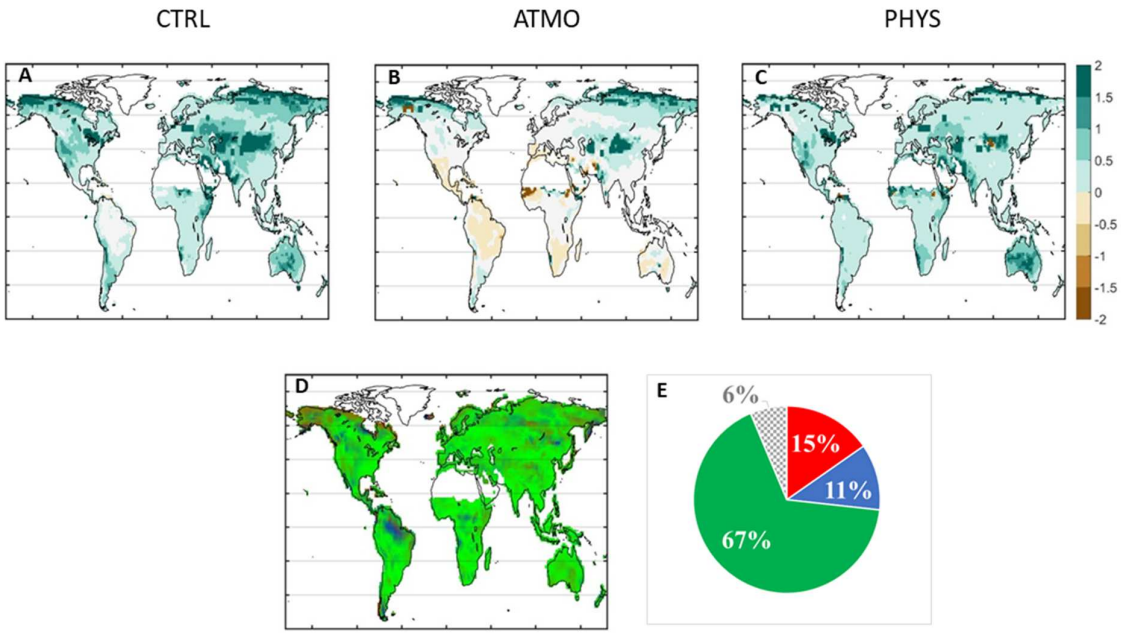

Figure 1.9 LAI (annual) changes in CTRL (A), ATMO (B), and PHYS (C). Changes are calculated as the difference of the years 89-118 of the simulation and the years 1-20, normalized by the standard deviation of CTRL over the years 1-20 (Methods). For the decomposition along the three main drivers of LAI (D), Green quantifies the effect of the vegetation physiology based on the run PHYS; red and blue quantify the contribution of, respectively, net radiation and precipitation, based on a multiple linear regression of ATMO. The pie chart (E) shows for each variable the global average of each contribution, weighted by the total effect including error terms, reported as a grey shaded area.

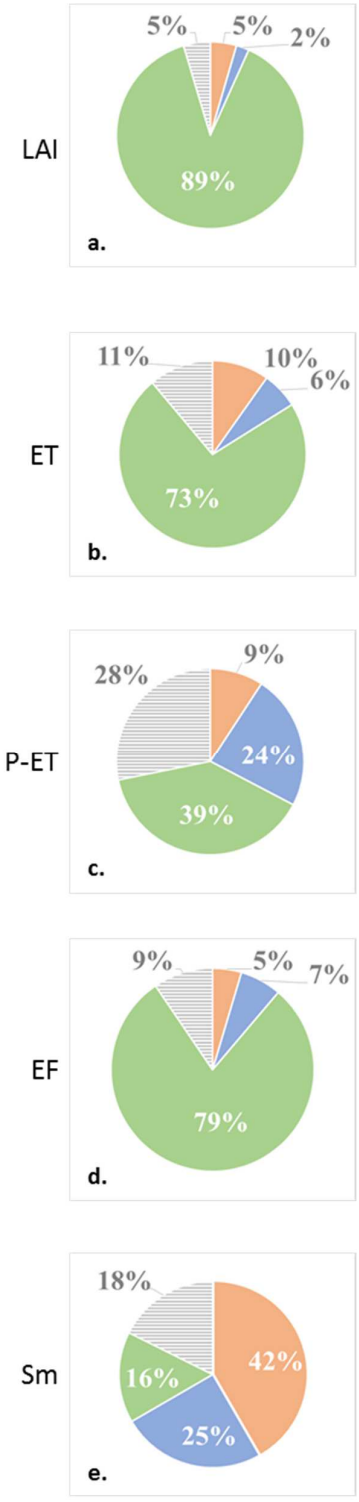

Figure 1.10 Main influence of drivers.
After the decomposition along the three main drivers of LAI (A), ET (B), P-ET (C), EF (D), Soil moisture at 2m (E) in CTRL, the pie charts show for each variable the fraction (labelled in %) of land under the main influence (more than 50% of the changes is attributed to this driver) of one the three main drivers (green for grid points dominated by vegetation

physiology, red for grid points dominated by net radiation, and blue for grid points dominated by the precipitation), and under no single driver influence (dashed area).

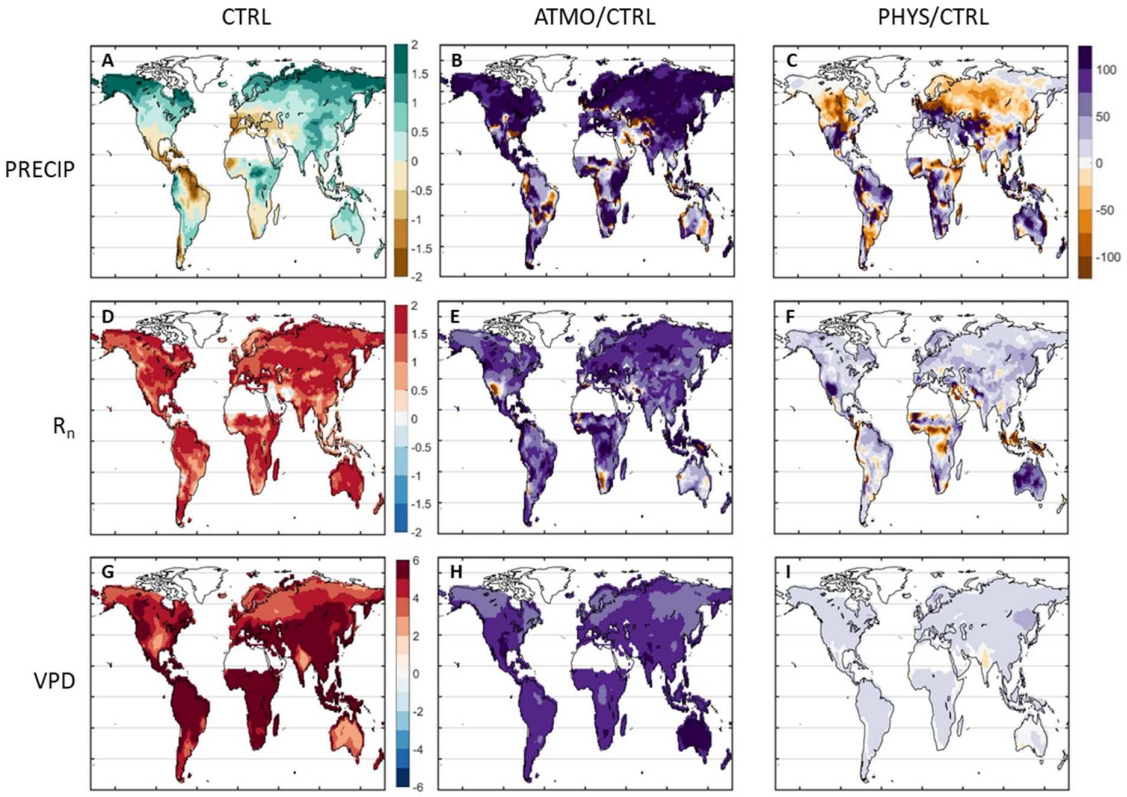

Figure 1.11 Changes in Precipitation (A, B, C; annual), Net radiation (D, E, F; annual) and VPD (G, H, I; growing season) are presented.
The left column shows results for CTRL as changes normalized by the standard deviation of CTRL over the years 1-20 (Methods), whereas the center and right columns show the changes of ATMO and PHYS relative to the changes of CTRL in % (purple to orange colorbar). Change is quantified by the difference of the years 89-118 of the simulation and the years 1-20. The changes observed for VPD are much larger in amplitude than for R_n and P, so that the scale was adjusted accordingly for VPD in G.

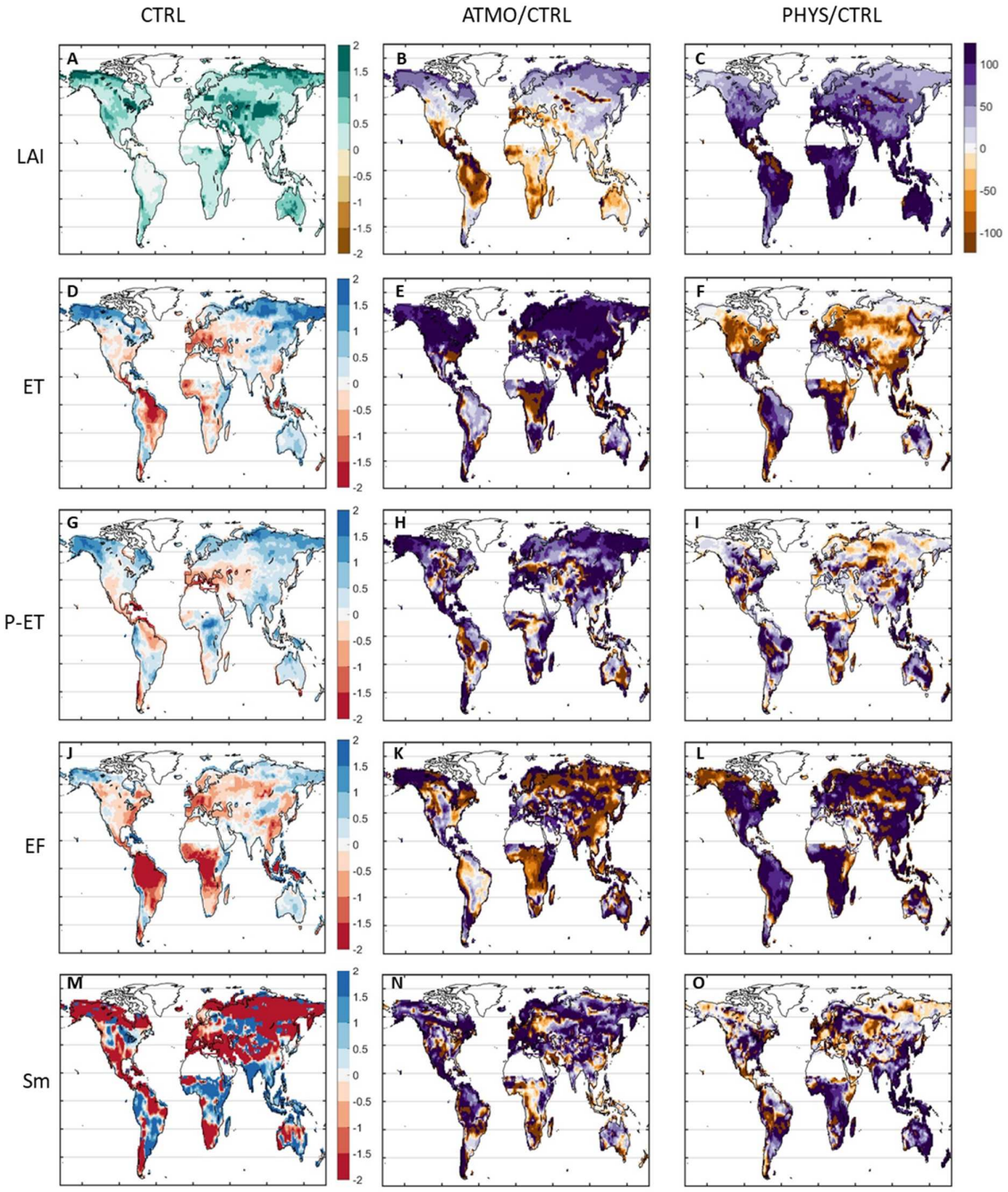

Figure 1.12 Variables, normalized by the standard deviation.
LAI (A, B, C; annual), ET (D, E, F; annual), P-ET (G, H, I; annual), EF (J, K, L; growing season), soil moisture at 2m (M, N, O; growing season) changes are shown on the left column for CTRL, normalized by the standard deviation of CTRL over the years 1-20 (Methods). The center and right columns show the changes of ATMO and PHYS relative to the changes of CTRL in % (purple to orange colorbar).

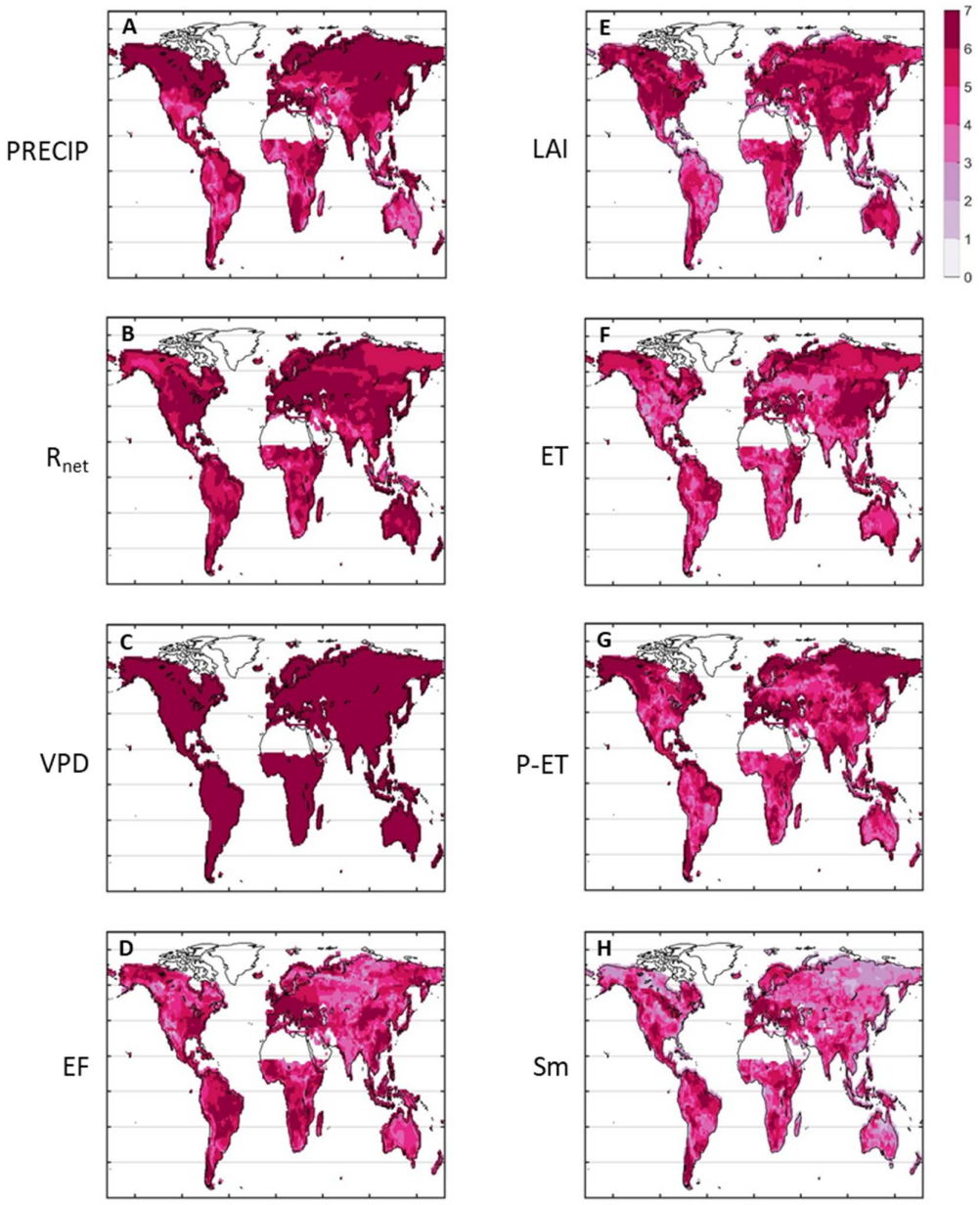

Figure 1.13 Numbers of models that agree with the inter-model average sign from 1 to 6, for Precipitation (A), R_n (B), VPD (C), EF (D), LAI (E), ET (F), P-ET (G), SM_{2m} (H).

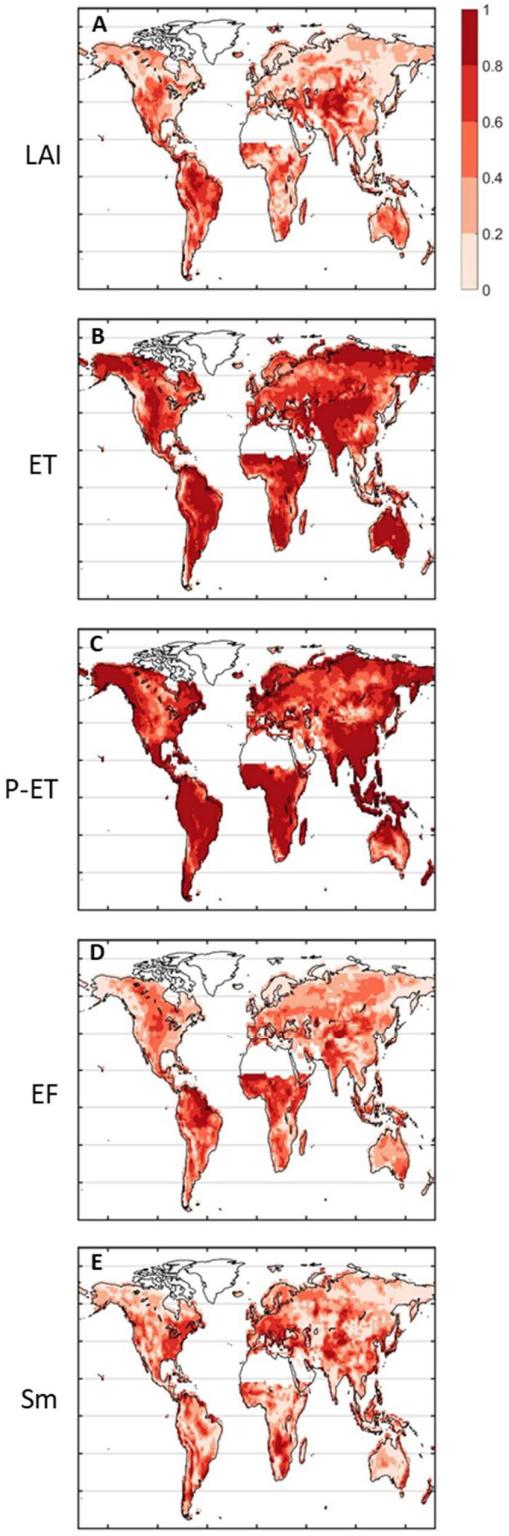

Figure 1.14 Fraction of variance explained by the multiple linear regression (R^2) for LAI (A), ET (B), P-ET (C), EF (D), SM_{2m} (E).

	1pctCO2		RCP 8.5	
historic period	1850	1869	1941	1970
historic years id	*1*	*20*	*91*	*120*
historic [CO_2] min-max (ppm)	284	347	310	325
historic [CO_2] average (ppm)	313		315	
future years	1939	1968	2070	2099
future years id	*89*	*118*	*220*	*249*
future [CO_2] min-max (ppm)	690	920	670	927
future [CO_2] average (ppm)	800		799	

Table 1.1 Years considered for temporal averaging to match similar levels of [CO_2] in 1pctCO2 runs

PART II: Modification of land-atmosphere interactions by carbon dioxide effects: implications for summer dryness and heatwave amplitude

Plant stomata couple the energy, water and carbon cycles. We use the framework of Regional Climate Modeling to simulate the 2003 European heat wave and assess how higher levels of surface CO_2 may affect such an extreme event through land-atmosphere interactions. Increased CO_2 modifies the seasonality of the water cycle through stomatal regulation and increased leaf area. As a result, the water saved during the growing season through higher water use efficiency mitigates summer dryness and the heat wave impact. Land-atmosphere interactions and CO_2 fertilization together synergistically contribute to increased summer transpiration. This, in turn, alters the surface energy budget and decreases sensible heat flux, mitigating air temperature rise. Accurate representation of the response to higher CO_2 levels, and of the coupling between the carbon and water cycles are therefore critical to forecasting seasonal climate, water cycle dynamics and to enhance the accuracy of extreme event prediction under future climate.

Lemordant, L., Gentine, P., Stéfanon, M., Drobinski, P., Fatichi, S., 2016. Modification of land-atmosphere interactions by CO_2 effects: implications for summer dryness and heatwave amplitude. *Geophysical Research Letters*. Available at: http://doi.wiley.com/10.1002/2016GL069896.

Chapter 7: Introduction to Part II

Western Europe experienced an unprecedented heatwave event and severe soil dryness conditions during the summer of 2003 (Schär et al. 2004). The impact on the ecosystems was widespread, as this event roughly negated four years of net carbon storage in Western Europe forests (Ciais et al. 2005). France experienced the highest temperature anomaly within Europe with mean daily temperatures in the 95^{th} percentile from 8 to 16 June and from 2 to 16 August 2003 (Stéfanon et al. 2012). This meteorological episode had a great impact on society, as France, for example, recorded 15,000 excess deaths in August (Canouï-Poitrine et al. 2006). Such extreme heat waves are believed to occur more frequently (Quesada et al. 2012) and more intensely in future climate (Meehl & Tebaldi 2004) in a context of globally warmer and locally drier conditions (Sherwood & Fu 2014) in the mid-latitudes.

Land-atmosphere interactions play a fundamental control on the severity of those heat waves (Fischer et al. 2007; Seneviratne et al. 2006; Teuling et al. 2010. There are several ways rising CO_2 levels affect the canopy conductance, which regulates both the water and energy cycles. First, the stomatal conductance is reduced with increasing surface CO_2 concentrations (Figure 2.1a), increasing the plant water use efficiency (WUE) (Katul et al. 2012; Norby & Zak 2011; Ainsworth & Long 2005; Morgan et al. 2011), defined as the ratio of net photosynthesis to transpiration. Reduced water vapor losses, in turn, conserve soil water and allows more heat to be dissipated as sensible heat flux, resulting in higher surface temperatures (Bateni & Entekhabi 2012). This effect is called the *stomatal response* (Figure 2.1a).

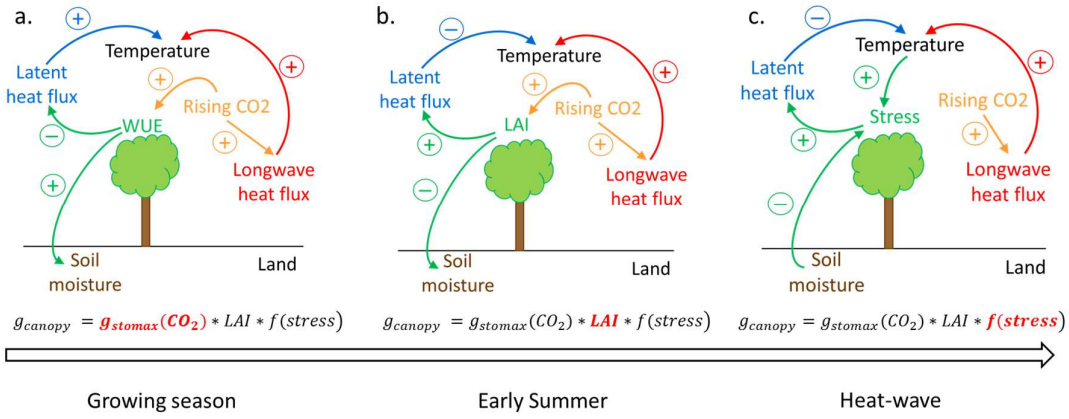

Figure 2.1 Dominant carbon, energy and water feedbacks.
During the growing season, the water use efficiency due to higher CO_2 concentrations reduces latent heat flux, increasing air temperature and soil moisture (a). In early summer, the increase in LAI due to CO_2 fertilization increases the latent heat flux and leads to a temperature reduction (b). During a heat wave, the spring soil moisture savings decrease the stress of the vegetation and increase the transpiration leading to a decrease of the peak temperature (c). Minus (positive) sign reads decrease (increase).

Second, the potential stimulation of biomass production by CO_2 fertilization (Warren et al. 2011; Norby & Zak 2011; Ainsworth & Long 2005; Mccarthy et al. 2007) can counteract some of the stomatal conductance reduction by increasing the leaf area (Wullschleger et al. 2002) hence sustaining higher transpiration and lower sensible heat flux, resulting in reduced temperature. This is referred to as *fertilization effect* (Figure 2.1b).

Numerous field experiments have been conducted to investigate the vegetation response to higher atmospheric CO_2 levels using various methodologies such as the Free-Air CO_2 Enrichment (FACE) experiments or using tree-rings isotopes (Frank et al. 2015; Norby & Zak 2011; Peñuelas et al. 2011; Saurer et al. 2004). These experiments show that transpiration is typically reduced and water use efficiency increased with increasing CO_2, while local, above canopy temperature might increase due to higher sensible heating. Decrease in stomatal conductance accompanied by leaf area index (LAI) increase (Ainsworth & Long 2005; Norby & Zak 2011; Warren et al. 2011) has been reported across several experiments and across a broad range of species. In particular, the stomatal conductance of crops and grass strongly and unequivocally responds negatively, i.e. the stomata close, to elevated CO_2 while maintaining relatively similar rates of photosynthesis (Ainsworth & Long 2005). As a result, the water-use efficiency of crops and grass have been reported to increase with elevated CO_2, the impact being even greater in water-stressed conditions (Wullschleger et al. 2002). The LAI increase can in some cases partly compensate some of the transpiration reduction by stomatal conductance (Wullschleger et al. 2002; Mccarthy et al. 2007). Higher LAI also increases canopy conductance so that more heat is released as turbulent heat fluxes (Figure 2.1b). Nonetheless individual species response to elevated CO_2 varies across FACE experiments. Multi-year droughts, in particular, may affect the availability of the deep soil moisture itself, as well as the biomass production stimulation and the capacity of trees to access the soil water (Warren et al. 2011; Morgan et al. 2004). The Swiss Canopy Crane project - a long-term FACE

experiment in a mature forest (Bader et al. 2013) - is the only available on-site data for 2003 within the domain of our study. The elevated CO_2 plot showed notably reduced stomatal conductance and reduced transpiration in normal weather conditions (Figure 2.1a) (Keel et al. 2007). But during the 2003 centennial drought significantly higher transpiration was recorded for some species, translating into locally reduced temperature during the extreme drought and heat wave (Leuzinger et al. 2005). The stomatal response during the growing season (Figure 2.1a) leads to a larger soil moisture availability later in the year, which could potentially decrease vegetation stress and increase evapotranspiration during a subsequent summer heat-wave and thereby mitigate its severity. This is referred to as *water cycle feedback* (Figure 2.1c).

These field experiments give crucial evidence at a small spatial scale of the different processes at play. Because of their small footprint, FACE experiments cannot be used to investigate the regional land-atmosphere impact of CO_2 fertilization nor the regional coupling and feedbacks with the atmosphere (Leuzinger et al. 2015) that may, for instance, affect the atmospheric water vapor pressure deficit (Wullschleger 2002). Our study is specifically designed to investigate the impact of CO_2–driven physiological effects on extremes through changes in land-atmosphere interactions, here taking the 2003 European heat wave as a case study. Previous studies have not taken into account the impact of the surface CO_2 physiological effect on land-atmosphere interactions when studying regional extreme events (e.g. (Seneviratne et al. 2006)). We use a Regional Climate Model (RCM) to investigate the physical mechanisms of land-atmosphere interactions, similarly to other authors (Seneviratne et al. 2006; Stéfanon et al. 2012). We purposely do not use GCMs as, in addition to their coarse resolution and initialization issues, they only allow characterizing *statistical* changes of frequency and intensity of heat waves and droughts, and cannot directly quantify the relative contribution of each physical or physiological process on a specific weather event. In addition, GCMs have difficulties representing large-scale blocking conditions especially in the Euro-

Atlantic region (D'Andrea et al. 1998; Sillmann & Croci-Maspoli 2009), and are thus not ideal for investigating mid-latitude heat waves. Unlike GCMs, RCMs are aimed at understanding physical processes by repeating near-twin runs using the same large-scale forcing but with a different set of parameters or processes (see Methods and Table 1.1). For each run, we can estimate the contribution of the process and parameter under the same prescribed synoptic conditions (Seneviratne et al. 2006).

Chapter 8: Data and Methods

8.1 Model Setup

In this experiment the WRF (Weather and Research Forecasting - v.3.1.1) limited-area model is coupled with the ORCHIDEE (Organizing Carbon and Hydrology In Dynamic Ecosystems – v.1.9.5) land-surface model (Drobinski et al. 2012). WRF is an atmospheric model with non-hydrostatic core used for regional climate simulations (Skamarock et al. 2008). ERA-Interim reanalysis of the European Centre for Medium-Range Weather Forecasts (ECMWF) (Dee et al. 2011) provides the initial and lateral weather conditions (temperature, wind and humidity). At the boundaries, if the temperature is prescribed, the fluxes are not, and can reflect the changes within the boundaries. ORCHIDEE simulates the surface processes of the terrestrial biosphere – in particular the soil water budget and the photosynthesis – as well as the phenology and the carbon dynamics (Krinner et al. 2005; Stéfanon et al. 2012). This coupled model setup has been shown to produce results consistent with observations of the 2003 heat wave (Stéfanon et al. 2012). A spin-up is first applied by repeating the year 2002 twice so that the leaf area index and soil moisture are in a dynamic equilibrium at the beginning of 2003.

The study focuses on the summer and especially the heat wave of 2003, which exhibited more than 4K temperature anomaly over Western Europe. This anomaly is similar in amplitude to the expected temperature changes in 2100 under the Representative Concentration Pathway 8.5 scenario of the International Panel on Climate Change (IPCC) report – likely in the range of 2.4 to 4.8 K in the global mean, and from 4 to 8 K during the summer in Central Europe. Therefore, our setup gives preliminary insights on how the CO_2 physiological effects might affect surface fluxes and regional temperature patterns in a typical summer at the end of the

century, the particularities of the setup (block, precipitation pattern, boundary conditions, etc…) are nonetheless not quite identical in this study as the simulated RCP 8.5 climate change.

Two sets of simulations are performed on domains of different sizes. In the first set of simulations, the domain extends from 6.4˚W to 10.4˚E and from 41.5˚N to 51.7˚N, with a 0.26˚ grid cell. At this scale, the lateral boundary conditions control is substantial, so that there cannot be large-scale temperature deviations across simulations while still resolving the regional impact of land-atmosphere interaction changes. The second set of simulations is run on an extended domain from 10.5˚W to 26.5˚E and from 35˚N to 59˚N, with a 0.22˚ grid cell. On this larger domain, the influence of the boundary conditions becomes less important and larger-scale patterns can be altered. In other words, this larger domain tests the sensitivity of the results to the prescribed lateral boundary conditions and domain size. However, as is elaborated below, the main results and conclusions are not modified over the larger domain and confirm the findings of the smaller domain.

8.2 ORCHIDEE and the vegetation model

The surface model takes into account 12 different Plant Functional Types (PFTs). Agricultural C3 crop is the most frequent PFT throughout the domain, followed by C3 grass and temperate broad-leaved summer green plant (deciduous forests), covering similar areas. ORCHIDEE has been shown to produce results consistent with local flux tower data (Anav et al. 2010) and LAI satellite observations (Lafont et al. 2012). ORCHIDEE has also been evaluated in the context of elevated CO_2 (Cheaib et al. 2012) and has been successfully validated against multiple FACE datasets in a recent inter-model comparison study, where the LAI is however reported to be somewhat overestimated by ORCHIDEE (De Kauwe et al. 2013; Walker et al. 2014). The version used here does not include the nutrient cycle. Table 2.2 points out to the other differences with the model used in De Kauwe et al. (2013).

8.3 Surface CO_2 and other Greenhouse gasses concentrations

Two types of simulations are performed (Supp. Table 2.1). The first is the control run or CTL, and the surface model is set with the observed mean CO_2 concentration of 2003 (376 ppm) while in the second one, FER, the surface model is set with the CO_2 concentration expected for 2100 in the RCP 8.5 (936 ppm) (Moss et al. 2010). In FER, the CO_2 concentration of the atmospheric model is not changed, enabling us to estimate the sole impact of CO_2 physiological effects on the surface vegetation, land-atmosphere interactions and heat wave. Another experiment was performed, named FER_{dry}, a replicate of the FER run but with soil moisture imposed at all time step identical to the CTL values, which are drier than in FER. By doing so, we separate the effect of seasonal CO_2-induced water saving on land-atmosphere feedbacks (Figure 2.1c) from the other effects - namely the CO_2 fertilization and the instantaneous stomatal response feedback (Figure 2.1a and b). The method to constrain the soil moisture level leads to a soil moisture difference between CTL and FER_{dry} of less than 0.6 kg/m^2 or <0.3% of the total amount, and 7% of the maximum difference between CTL and FER. This is due to the variety of PFT fractions of each pixel. We imposed the same average CTL value of the pixel to all PFTs of the pixel, instead of generating the various soil moisture values for each PFT as in the original version of the code.

8.4 Sensitivity analysis with additional runs

A set of additional experiments has been run to test the sensitivity of the results to several critical model parameters. Each parameter is tested with both the CTL and FER surface CO_2 conditions. To test the sensitivity to phenology and LAI, the leaf onset is delayed by increasing the growing degree-day by 50% in ORCHIDEE (Supp. Figure 2.6 a, e). In a second set of experiments, the planetary boundary layer scheme used in WRF for the first experiment (the non-local, counter-gradient, Yonsei University scheme - YSU) is switched to another

scheme (a local 2.5-order turbulent closure Mellor-Yamada-Nakanishi and Niino scheme - MYNN 2.5) (Supp. Figure 2.6 b, f). To test the sensitivity to the stomatal conductance parameterization, we modified the parameter representing the temperature dependence of photosynthesis (Supp. Figure 2.6 c,g) and the parameter representing the soil moisture stress in Vc_{max}, i.e., the maximum rate of Rubisco carboxylation (Supp. Figure 2.6 d, h). This way, we alter either the temperature stress response of the vegetation or its water use efficiency. In both cases, the original parameter value x (between 0 and 1) was modified for the sensitivity analysis to a higher value $x+(1-x)/2$. Supp. Table 2.1 summarizes the model parameters modified from the base case CTL for each simulation.

Chapter 9: Results and Discussion

9.1 Small domain

The small domain is centered over France, which experienced the peak of the 2003 heatwave. FER exhibits significantly less latent heat flux than CTL throughout the growing season (Figure 2.2b), as a direct consequence of the reduction of the stomatal conductance under higher CO_2 concentration (Figure 2.1a). As a result, FER displays increased soil moisture content compared to CTL (Figure 2.2a) consistently throughout the growing season (Figure 2.3a). The stomatal closure also translates into higher sensible heat flux (Figure 2.2d, 2.3h) and higher surface temperature (Figure 2.2c, 2.3c). However, the latent heat flux difference between FER and CTL is reduced from mid-March onward because of the larger LAI due to the CO_2 fertilization effect in FER (Figure 2.1b, Supp. Figure 2.4a, 2.4b).

During the growing season, similarly to FER, lower latent heat fluxes (Figure 2.2b, 2.5d) and higher temperature than CTL are experienced (Figure 2.2c, Supp. Figure 2.5c) in FER_{dry}. Latent heat flux in FER_{dry} and FER are of the same order of magnitude during the growing season. This is expected since the growing season difference is dominated by the CO_2 stomatal closure (Figure 2.1a), as soil water is not limiting early in the season. The daily maximum temperature, as well as the sensible heat flux, are also of the same order of magnitude in both FER and FER_{dry}. However, starting mid-March, due to lower LAI in FER_{dry} than in FER (Supp. Figure 2.4a, 2.4b), fluxes and temperature begin to progressively diverge, FER_{dry} showing less latent heat flux than FER, more sensible heat flux, and higher temperature.

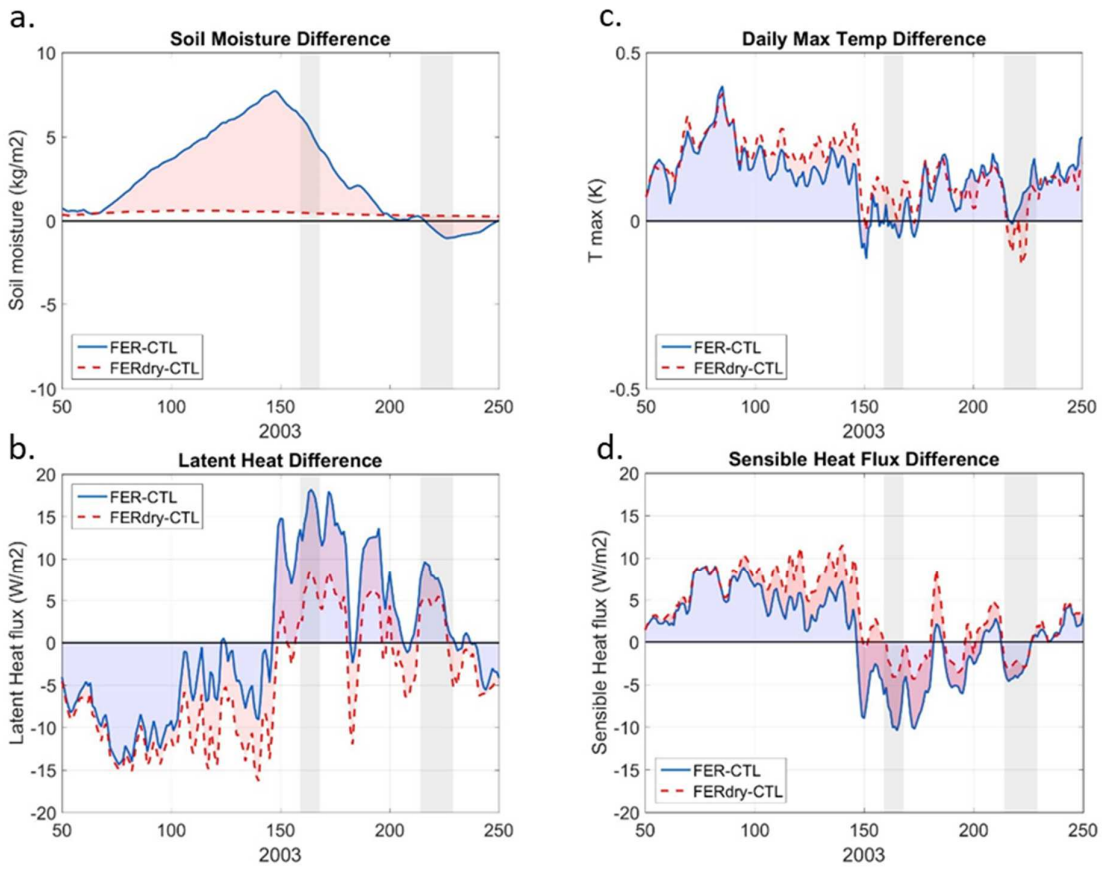

Figure 2.2 Effects of the water cycle feedback on temperature over the small domain. Left column shows averages over the domain of the main components of the water cycle (a) soil moisture (0-200 cm) (kg/m^2) (b) latent heat flux at 15:00 UTC (W/m^2). Right column shows averages over the domain of the (c) daily maximum temperature (K) and (d) sensible heat flux (W/m^2) at 15:00 UTC. Data is shown for the period from 19 February (DOY 50) to 7 September 2003 (DOY 250). All variables are expressed as a difference relative to CTL of the two runs FER (blue) and FER$_{dry}$ (red, dashed). Grey shaded areas correspond to the period where the temperature anomaly was above the 95th percentile in 2003, the periods of an extreme heat wave over the domain. The red and blue shaded areas correspond to respectively the FER$_{dry}$-FER and FER-CTL differences. Except for the soil moisture, the time series are smoothed by a 3-days running average.

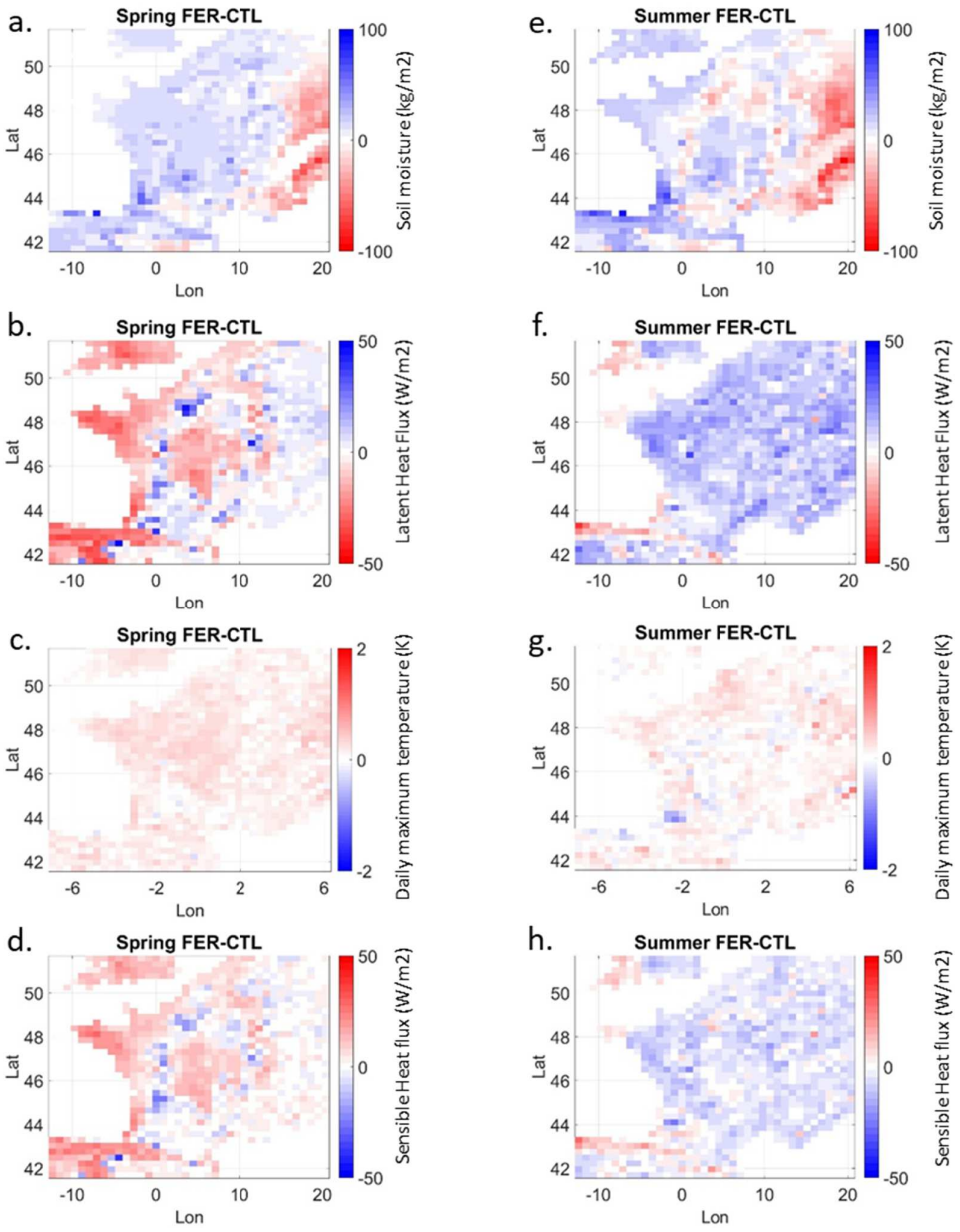

Figure 2.3 Physiological effect (FER) over the small domain during spring and summer. The left column presents an average of the variables for FER expressed as the difference to CTL for spring (15 March to 8 June 2003), while the right column displays the same results for the summer period (8 June to 16 August 2003). The presented variables are the average soil moisture content (kg/m^2) (a, e), the average latent heat flux (W/m^2) at 15:00 UTC (b, f), the daily max temperature (K) (c, g) and the average sensible heat flux (W/m^2) at 15:00 UTC (d, h).

In contrast to the growing season, during the June heat wave, stomatal closure is not the main driver of latent heat flux difference between FER and CTL anymore. The latent heat flux is indeed now higher in FER than in CTL (Figures 2.2b, 2.3f), which holds true for the rest of the summer. The higher LAI in FER could be one of the reasons explaining the increased latent heat flux. LAI is indeed 37% larger in FER than in CTL during the summer (Supp. Figure 2.4). As a consequence of higher latent heat flux, the soil moisture in FER decreases compared to CTL (Figures 2.2a, 2.3e), and the spring soil moisture surplus is depleted to sustain higher transpiration (Figure 2.1c).

We can evaluate the differential impact of the soil moisture surplus on one side and the larger LAI on the other side comparing FER to FER_{dry}. The response to summertime temperatures in FER is unequivocal with more latent heat and less sensible heat fluxes than in CTL (Figure 2.3f and 2.3h). In contrast, the response is spatially different in FER_{dry} with latent and sensible heat fluxes close to the levels in CTL (Supp. Figure 2.5d and 2.5f).

The latent heat difference FER_{dry} -CTL averaged from 8 June to 16 August 2003 over the entire domain is about a quarter that of FER-CTL (Figure 2.2c). LAI in FER_{dry} is 22% higher than in CTL, but latent heat increases by only 4% (Supp. Figure 2.5d). LAI in FER is 37% higher than in CTL, and latent heat increases by 14% (Figure 2.3f). There may be a contribution of the CO2 fertilization effect (Figure 2.1b) to the latent heat flux difference between FER_{dry} and FER during the summer, but the soil moisture saving induced by stomatal closure (Figure 2.1c) as assessed by (FER- FER_{dry}) accounts for the larger share. Figure 2.2 suggests, however, a less categorical conclusion for the most extreme periods of the summer, during which the heat fluxes in FER_{dry} are very different than in CTL, implying an important contribution of the LAI during this period.

The corresponding reduction in sensible heat flux (Figure 2.2d) translates into lower temperature, which is of great importance during the hottest part of the season. Nonetheless, the model set-up with the constraint of prescribed temperature boundary conditions does not allow representing significant temperature differences between FER, FER_{dry} and CTL. Surface fluxes are allowed to evolve freely and are of comparable magnitude to typical global warming impact (e.g. Representative Concentration Pathway RCP 8.5 – with 8.5 W m^{-2}). The prescribed temperature boundary condition is an obvious caveat of the adopted framework.

FACE experiments on crops and grass tend to show less pronounced fertilization than simulated by ORCHIDEE (Ainsworth & Long 2005; De Kauwe et al. 2013). If LAI were lower than simulated by the model (as in FACE), the water savings would be even larger during the growing season, and this water could further sustain transpiration in the summer, thus reducing water stress. This would reinforce our results and further amplify the mitigation of heat stress through increased soil moisture.

9.2 Sensitivity to model parameters

Given the uncertainties in the model parameterization and representation of the coupling between the carbon and water cycle, we performed a series of sensitivity studies to the different model parameters. The additional runs using different bud break date, planetary boundary layer scheme, and dependence of stomatal conductance to temperature and soil moisture (Methods) confirm the results highlighted above. The main result – that the CO_2-induced water savings mitigate the heat wave and summer dryness holds true for all these sensitivity experiments (Supp. Figure 2.6a to 2.6h), but with a different amplitude. The bud break day and the temperature dependence of the stomatal conductance do not have much influence on the results, but the dependence of stomatal conductance on soil moisture (i.e. the modeled intrinsic water use efficiency) does, which further emphasizes that characterization of

the carbon and water cycles coupling is key for accurate seasonal prediction of land-atmosphere interactions and of heat waves in particular. The boundary layer scheme is also important in modulating the impact of land-atmosphere interactions, especially during the heat wave period. Indeed during heatwaves, the unstable boundary layer experiences intense updrafts spanning the entire boundary layer depth and the nighttime boundary layer does not become stable (Miralles et al. 2014). It is therefore expected that a scheme (YSU) that better accounts for non-local turbulent transport and explicitly represents thermals would better model the heat-wave boundary layer. Entrainment and vertical mixing are the most significant differences among boundary layer schemes in WRF, which have considerable consequences on the intensity of the vertical mixing and fluxes (Hu et al. 2010). Nonetheless, only the FER_{dry} run radically affects the pattern of decreased latent heat flux during spring and increased latent heat flux – concurrently with temperature - during summer compared to CTL (Supp. Figure 2.6i and 2.6j).

9.3 Large domain

To test the dependence of the results on the domain size and to the prescribed lateral temperature boundary conditions we performed a second set of simulations (CTL, FER) over a larger domain covering continental Europe (Methods). As many regions of the extended domain did not experience temperatures as extreme as France (Seneviratne et al. 2006) those simulations are also used to investigate the robustness of the findings to less extreme temperature anomalies and more typical summer conditions.

The water-saving feedback observed over the smaller domain similarly occurs over the extended domain (Supp. Figure 2.7). Over France, we observe the same range of magnitude for spring soil water savings and latent heat seasonal change. Evapotranspiration is stronger in FER than in CTL during the summer (Supp. Figure 2.7b and 2.7f), as reduced stomatal opening during the growing season has conserved water. Except in a few sea-dominated locations along the coasts (Iberian Peninsula, extreme south of Italy and south of Greece), the FER simulation

exhibits lower surface average temperatures difference with CTL in the Summer compared to Spring over a significant part of the domain (Supp. Figure 2.7c and 2.7g). This lower temperature difference is due to the higher latent heat flux (Supp. Figure 2.7f) accompanied by a reduction of sensible heat flux (Supp. Figure 2.7h). In other words, the seasonal water cycle feedback and the larger LAI compensates for the stomatal response over this extended domain. These effects are particularly strong over central and Eastern Europe. This more continental part of Europe exhibits indeed strong land-atmosphere temperature coupling (Seneviratne et al. 2006), stronger than over France, and is less influenced by maritime air advection. In continental Europe, the spring stomatal water savings seem however not enough to overcome the transpiration stimulation by the larger LAI, and soil moisture content tends to decrease in FER compared to CTL in these regions even during spring.

Chapter 10: Summary and conclusion of Part II

The present study illustrates the role of plant physiology in altering land-atmosphere interactions under higher CO_2 concentration. CO_2 indirect effects can mitigate heat-wave impacts and the severity of summer dryness in the Western Europe mid-latitude climate. Spring water savings enabled by increased ecosystem water use efficiency modifies the surface energy partitioning, allowing increased latent heat flux later in the summer that more than compensates the reduced stomatal opening induced by increased CO_2. Mitigation of extreme temperature anomalies is more pronounced in regions experiencing summer water stress and in regions of strong land-atmosphere coupling. We demonstrated that the characterization of the surface CO_2 physiological effects is essential to accurately predict seasonal climate and extremes. This has important implications for climate model prediction of continental heat waves and dryness. Future droughts and heat wave intensity might indeed be partially attenuated by the carbon-water feedback, and especially by the water use-efficiency. Such attenuation depends on the competing contributions of the fertilization and stomatal closure effects, which are biome and climate dependent. This calls for additional studies on the statistical changes in heat-wave characteristics induced by vegetation physiology using GCMs.

Other biogeochemical processes and nutrient feedbacks could also play an important role in the context of rising atmospheric CO_2, but these remain poorly represented in current generation models (Zaehle et al. 2014). Water stress regulation of photosynthesis neither is accurately represented in land-surface models nor accounts for the diversity of strategies observed from active (isohydric behavior) to minimal stomatal regulation (anisohydric behavior) under water stress (Mcdowell 2011; Gentine et al. 2016; Konings & Gentine 2016).

In addition to highlighting the importance of the land-atmosphere interactions induced by CO_2 for future model improvements [*Fatichi et al.*, 2016], these findings have important

implications for better estimating summertime heat waves in the context of projected future warming or drying across much of Europe (Seneviratne et al. 2006; Dai 2013; Giorgi & Lionello 2008), emphasizing the role of the plant water use efficiency and its model representation for extreme event prediction.

Chapter 11: Supplementary Materials of Part II

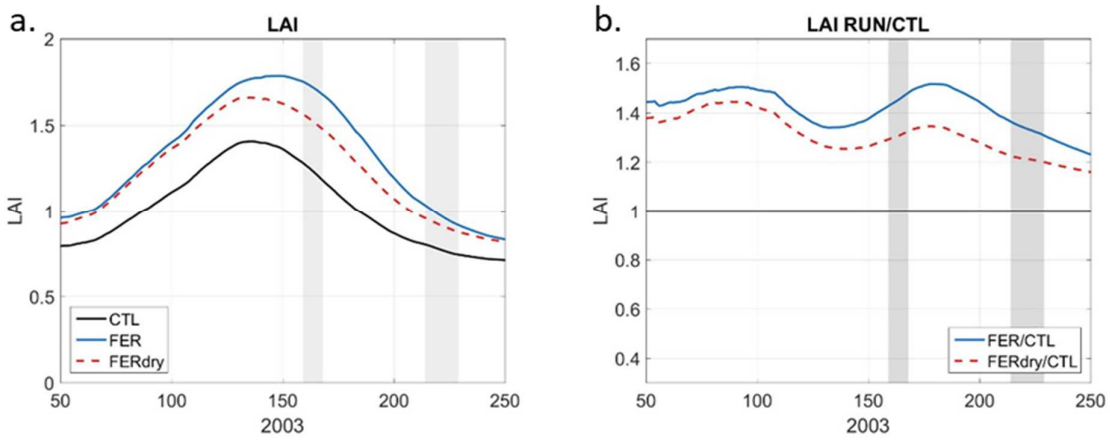

Figure 2. 4 Leaf Area Index averaged over the small domain.
***(a)** displays averaged over domain the Leaf Area Index (LAI) of the runs CTL, RAD, FER and FERdry. **(b)** displays averaged over domain the LAI of the runs RAD, FER and FERdry standardized by the LAI of CTL.*

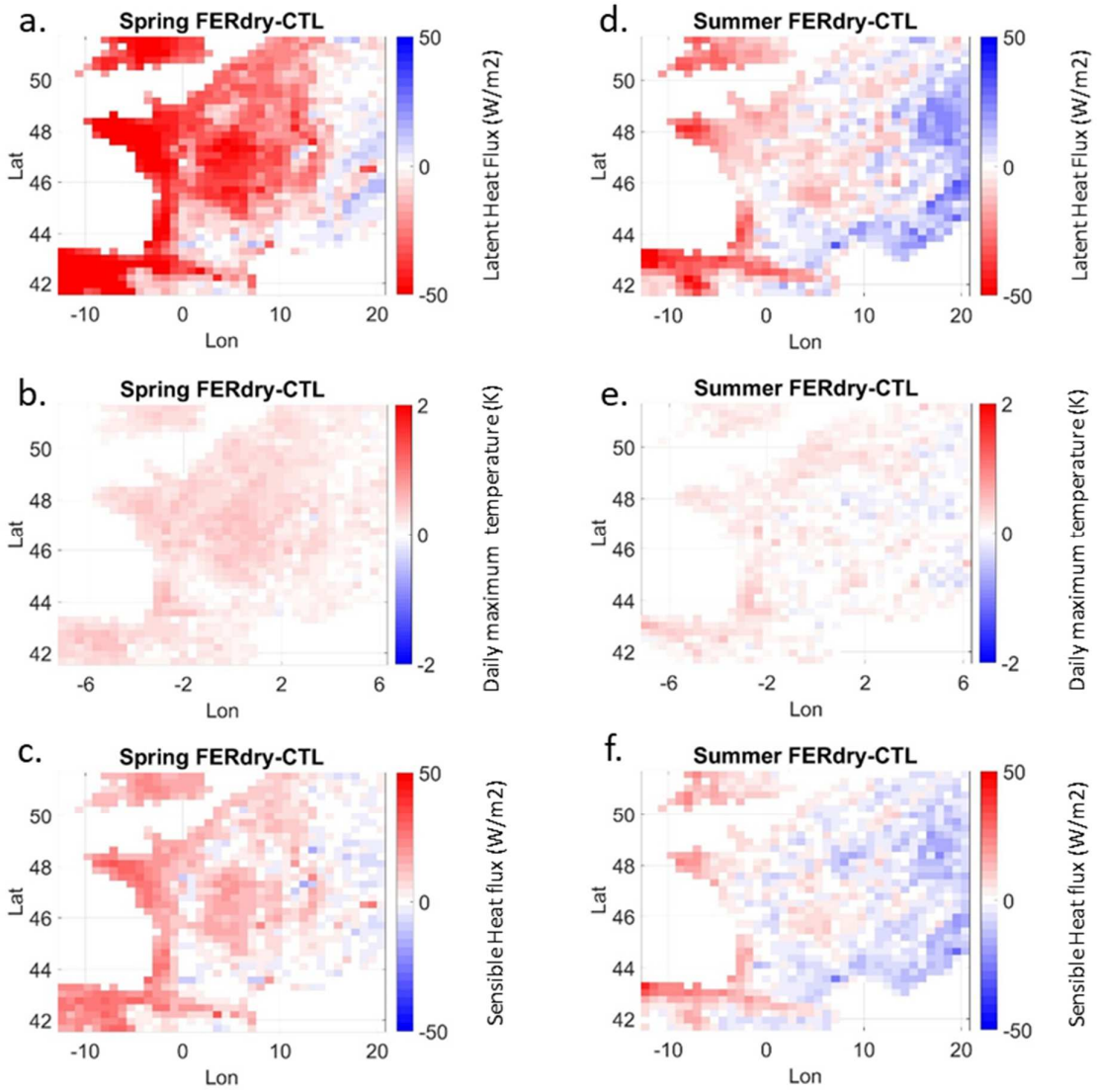

Figure 2.5 Water cycle feedback on temperature over the large domain during the summer. The two columns (from left to right) display averaged over the 2003 spring (March 15th to June 8th) and summer (June 8th to August 16th) the mean daily maximum temperature (K) (a, d), the daily average temperature (b, e) and the latent heat flux (W/m^2) at 15:00 UTC (c, d). The data shown is the difference of FER relative to CTL.

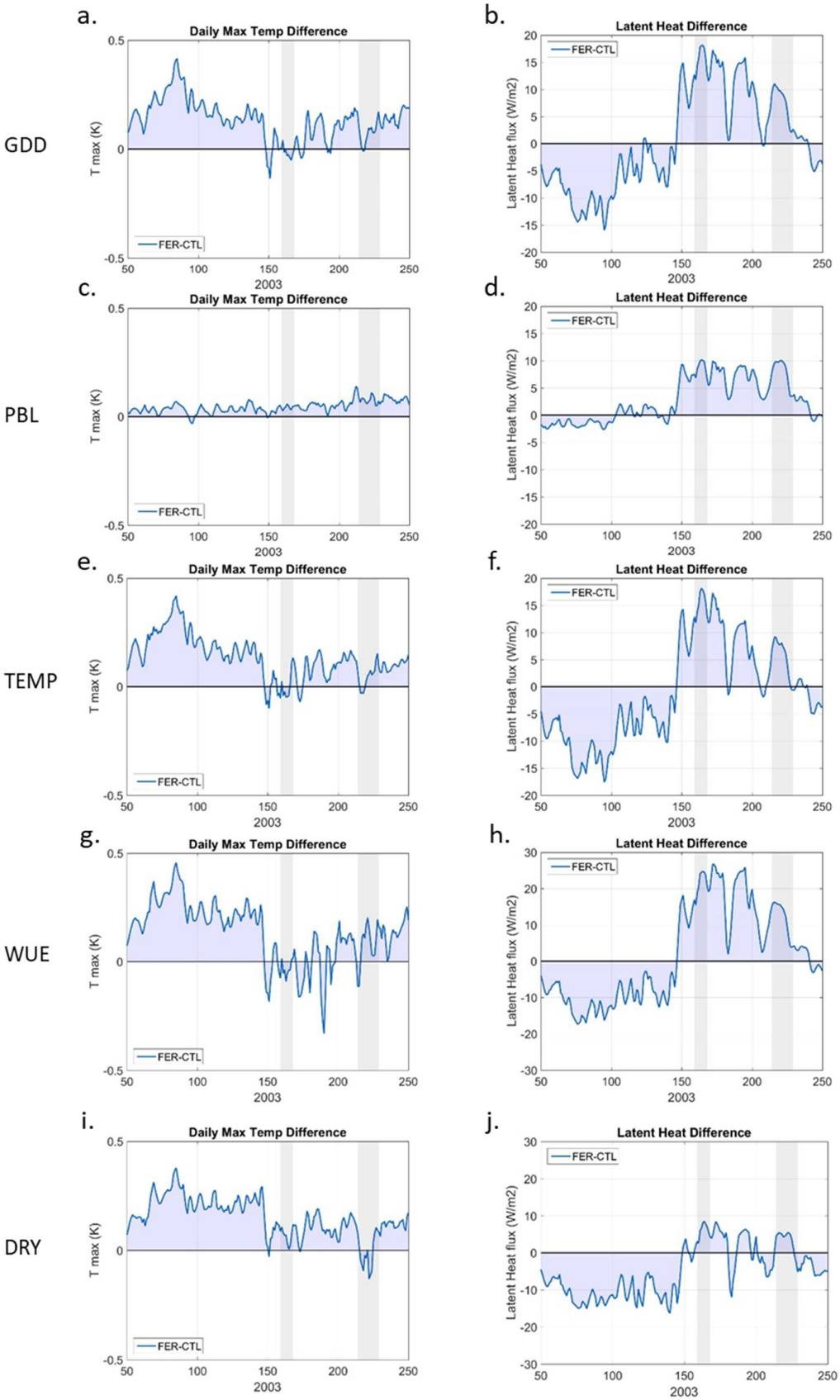
a.
Daily Max Temp Difference
T max (K)
FER-CTL
2003
b.
Latent Heat Difference
Latent Heat flux (W/m2)
FER-CTL
2003
GDD
c.
Daily Max Temp Difference
T max (K)
FER-CTL
2003
d.
Latent Heat Difference
Latent Heat flux (W/m2)
FER-CTL
2003
PBL
e.
Daily Max Temp Difference
T max (K)
FER-CTL
2003
f.
Latent Heat Difference
Latent Heat flux (W/m2)
FER-CTL
2003
TEMP
g.
Daily Max Temp Difference
T max (K)
FER-CTL
2003
h.
Latent Heat Difference
Latent Heat flux (W/m2)
FER-CTL
2003
WUE
i.
Daily Max Temp Difference
T max (K)
FER-CTL
2003
j.
Latent Heat Difference
Latent Heat flux (W/m2)
FER-CTL
2003
DRY

Figure 2.6 The sensitivity analysis to various features of the model.
The two columns display (from left to right) the daily maximum temperature (K) and the Latent Heat flux (W/m^2) at 15:00 UTC for the FER run, averaged over the small domain for four experiments where one parameter of the original settings is altered, and expressed as a difference relative to the run CTL of the original settings. The parameter altered in (a) and (e) is the growing degree day, in (b) and (f) the planetary boundary layer scheme, in (c) and (g) the parameter representing the temperature dependence of photosynthesis in Vc_{max},in (d) and (h) the parameter representing the soil moisture stress in Vc_{max} (Methods).

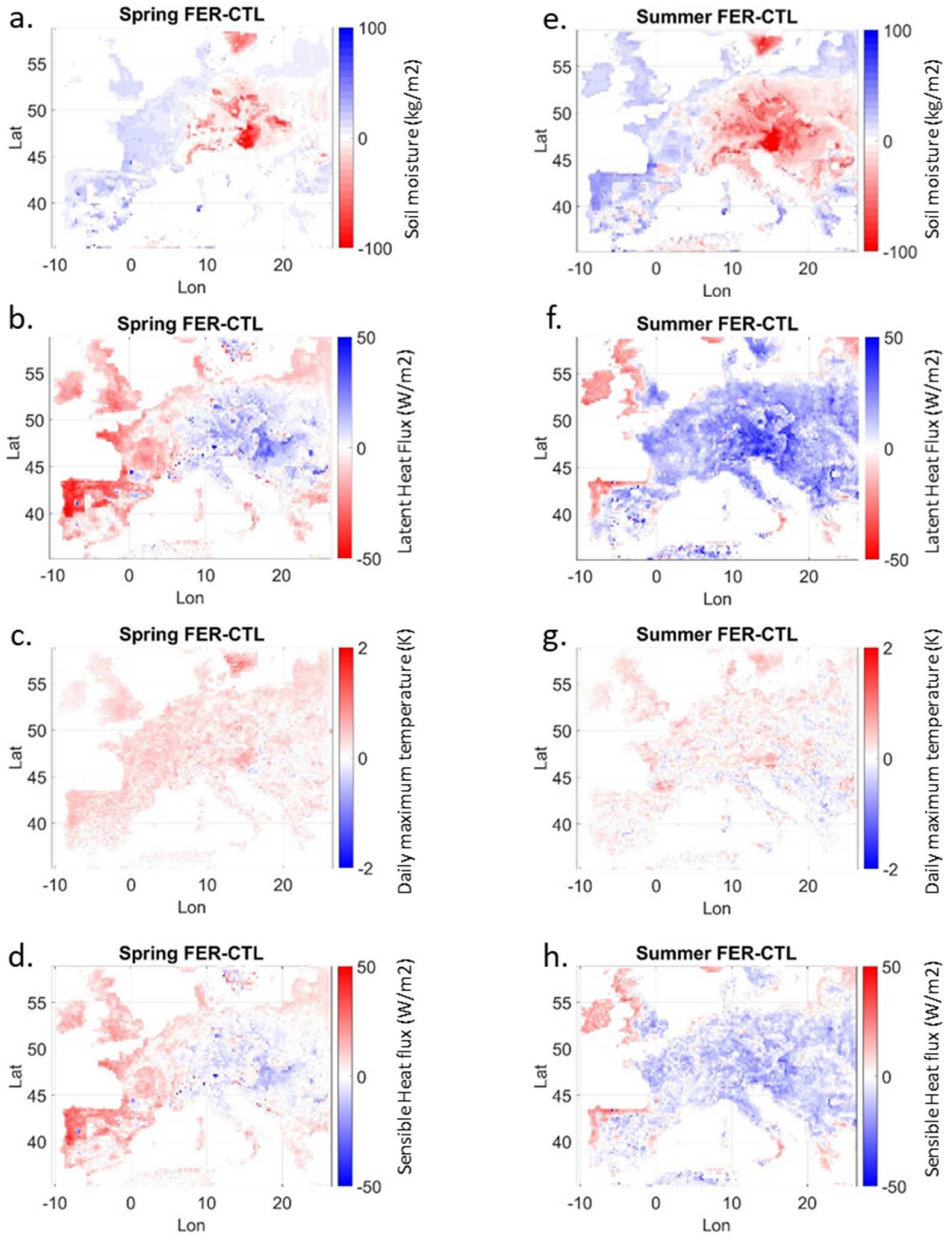

Figure 2.7 Water cycle feedback on temperature over the large domain during the summer. The two columns (from left to right) display averaged over the 2003 spring (March 15th to June 8th) and summer (June 8th to August 16th) the mean daily maximum temperature (K) (a, d), the daily average temperature (b, e) and the latent heat flux (W/m2) at 15:00 UTC (c, d). The data shown is the difference of FER relative to CTL.

	$[CO2]_{atm}$ in the surface model	**Other parameter tweaked in the surface model**
CTL	376 ppm (Base case)	N/A
FER	936 ppm	N/A
FER_{dry}	936 ppm	Soil moisture = soil moisture in CTL
GDD	376 ppm	growing degree-day increased by 50%
PBL	376 ppm	YSU scheme changed for MYNN 2.5
TEMP	376 ppm	Temperature dependence of photosynthesis parameter in Vc_{max} increased from x to x+(1-x)/2
WUE	376 ppm	Soil moisture stress parameter in Vc_{max} increased from x to x+(1-x)/2

Table 2.1 Parameters changed from the base case CTL in each simulation.

	Part II	De Kauwe et al. (2013)
Nitrogen cycle	No	Yes
Reference	Krinner et al. (Krinner et al. 2005)	Zaehle et al. (Zaehle & Friend 2010)
Time step	3 min	30 min
Assimilation	Farquhar et al. (Farquhar et al. 1980) / Collatz et al. (Collatz et al. 1992)	Kull & Kruijt (Kull & Kruijt 1998)

Table 3.2 Differences in the model features of this study compared to those of De Kauwe et al. (De Kauwe et al. 2013)

PART III: Global impacts on extreme temperatures of the vegetation response to rising carbon dioxide concentration

Extreme temperatures are responsible for damages to society and ecosystems. There is evidence that severe episodes of extreme heat have been occurring more frequently and more severely in recent periods. Driven primarily by oceanic and atmospheric effects as well as land-climate feedbacks, those extreme events are expected to increase with climate change. Vegetation, which regulates the energy, water and carbon cycles, is a key player of land-atmosphere interactions that has been proven to be determinant in recent extreme events. Using an ensemble of Earth System Models simulations, we show that physiological effects globally increase the annual daily maximum temperature (Txx) with rising [CO_2], accounting globally for around 13% of the full Txx trend. Due to physiological effects, Txx can reinforce (e.g. Central Europe) or reduce (e.g. Central North America) the mean temperature increase.

Lemordant, L., Gentine, P., 2017. Vegetation response to rising CO_2 impacts extreme temperatures. *Geophysical Research Letters*, in review.

Chapter 12: Introduction to Part III

Observations and climate projections show that increasing atmospheric [CO_2] drives a global temperature rise (Stocker & Qin 2013). Observations also present a consistent increasing trend of occurrence and intensification of temperature extremes during the XX^{th} century (Alexander et al. 2006; Donat et al. 2016; Perkins et al. 2012). Record breaking heat waves and extreme temperatures have been observed in recent years (Alexander et al. 2006; Coumou and Rahmstorf 2012), deeply impacting ecosystem functioning (Ciais et al. 2005; Granier et al. 2007) and societies (Canouï-Poitrine et al. 2006; Watts et al. 2017). Their onset is primarily driven by oceanic and atmospheric effects (Byrne & O'Gorman 2013; Sherwood & Fu 2014).These extreme events are expected to become more frequent (Ding et al. 2010), and more intense (Fischer and Schär 2010; Meehl and Tebaldi 2004; Perkins et al. 2012; Schär et al. 2004) in large parts of the world (Perkins-Kirkpatrick & Gibson 2017).

Land-atmosphere interactions (Teuling et al. 2010), and the interplay of soil moisture in particular, take a significant role in the regulation of temperature extremes at the regional level, shifting the distribution of maximum temperatures compared to the mean (Berg et al. 2014; Seneviratne et al. 2006; Seneviratne et al. 2016; Vogel et al. 2017). In Europe for example, soil moisture feedbacks are responsible for a large fraction of the amplification of extreme temperatures compared to the mean temperature (Miralles et al. 2014; Vogel et al. 2017). The lack of precipitation during spring, and subsequent soil moisture deficit, reduces the latent cooling of the surface during a major heatwave event and consequently induces an increase in duration and intensity of daily maximum temperatures (Fischer et al. 2007; Hauser et al. 2016).

Nonetheless, soil moisture does not control evapotranspiration directly but only indirectly through changes in surface conductance, in places where soil moisture storage is not

the limiting factor of vegetation growth. Vegetation is the primary regulator of evapotranspiration, as transpiration is a major evapotranspiration flux (Jasechko et al. 2013; Schlesinger & Jasechko 2014), modulating the latent heat flux and influencing surface temperature (Frank et al. 2015).

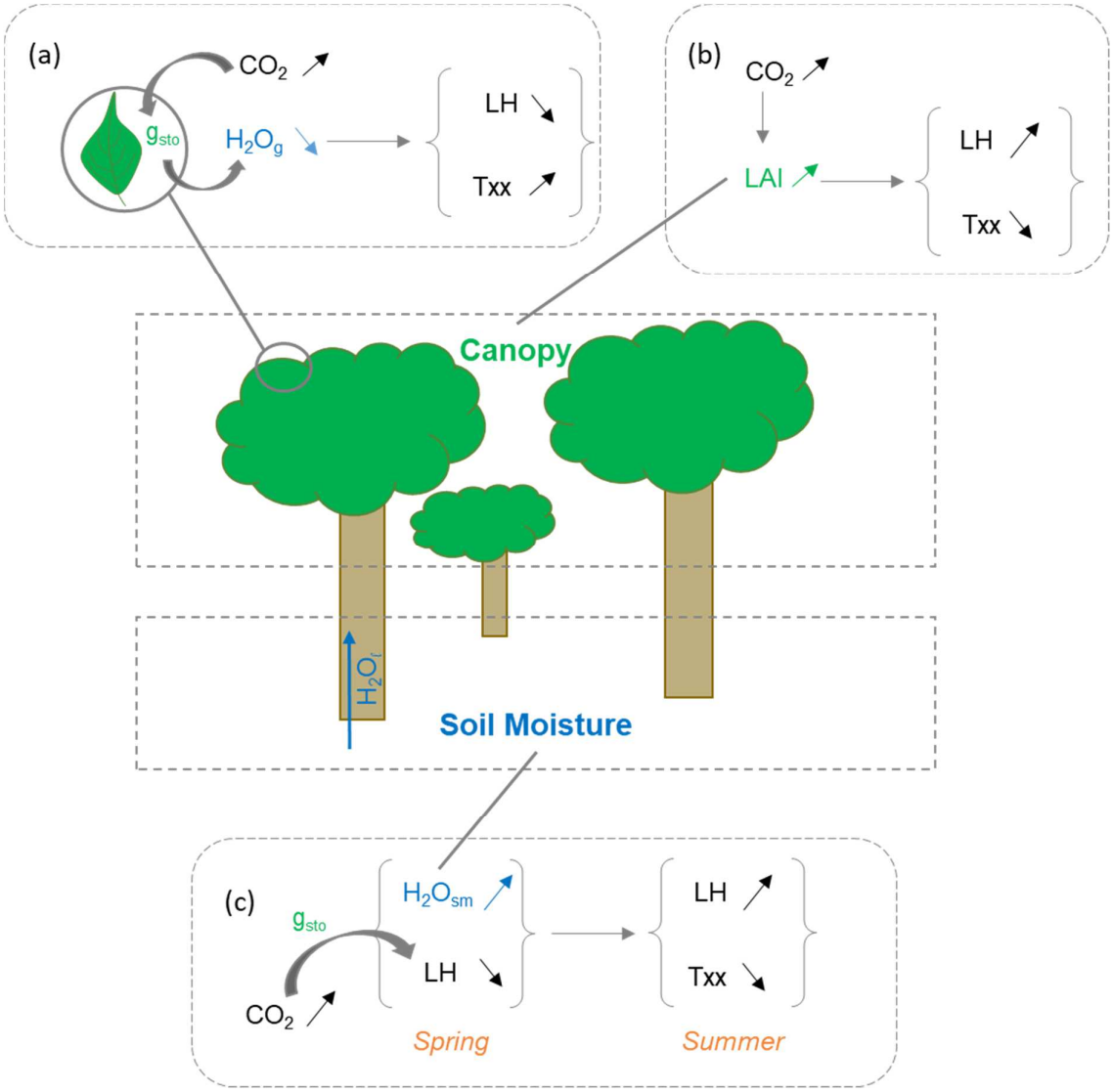

*Figure 3.1 Schematic representation of the physiologically based feedbacks. Leaf-level effect of CO_2 increase decreases the latent heat flux (LH) due to stomatal regulation g_{sto} (**a**), and so decreases the Txx. Potential increased LAI due to higher $[CO2]_{atm}$ would have the opposite effect on LH and Txx (**b**). The increased water use efficiency during the growth phase of the plants means higher soil moisture available during the hottest days of the year in summer, and a reduced Txx (**c**).*

Field observations such as the Free-Air CO_2 Enrichment (FACE) experiments or tree-ring isotope analysis are used to investigate vegetation response to increased [CO_2] (Frank et al. 2015; Norby and Zak 2011; Peñuelas et al. 2011; Saurer et al. 2004). Even though responses vary widely across species and climate, transpiration has been shown to be reduced (Frank et al. 2015) and water use efficiency increased (Ainsworth and Rogers 2007; Morison 1985), while locally, above canopy temperature increases (Figure 3.1a). Leaf area index (LAI) and leaf-level photosynthesis (Kimball et al. 1993; Norby & Zak 2011) have been reported to typically increase. The increase in LAI induces an increased canopy conductance, which implies that more heat is released as turbulent latent heat fluxes, which can then offset the stomatal reduction by transpiration (Mccarthy et al. 2007; Wullschleger et al. 2002), and potentially reduce the canopy temperature (Figure 3.1b). The increase in LAI is sometimes called "fertilization effect" of CO_2 (Strain 1987). Site conditions, especially nutrient availability (Mccarthy et al. 2007) seem critical for this effect and various observations give contradictory results (Morgan et al. 2004). Besides LAI and fertilization effects, evapotranspiration can also increase as a result of enhanced evaporative demand and the lengthening of the growing season (Frank et al. 2015). All these direct physiological effects can contribute to the modulation of extreme temperatures, while also generating additional ecosystem stress and damage to ecosystems (Granier et al. 2007).

Vegetation response to CO_2 can in turn alter soil moisture (Lemordant et al. 2018; Morgan et al. 2004), and evaporative fraction (Lemordant et al. 2018), impacting extreme temperatures(Alexander et al. 2006; Perkins et al. 2012)(Alexander et al. 2006; Perkins et al. 2012)(Alexander et al. 2006; Perkins et al. 2012)(Alexander et al. 2006; Perkins et al. 2012)(Alexander et al. 2006; Perkins et al. 2012)(Alexander et al. 2006; Perkins et al. 2012)(Alexander et al. 2006; Perkins et al. 2012)(Alexander et al. 2006; Perkins et al. 2012)(Alexander et al. 2006; Perkins et al.

2012)(Alexander et al. 2006; Perkins et al. 2012)(Alexander et al. 2006; Perkins et al. 2012)(Alexander et al. 2006; Perkins et al. 2012)(Alexander et al. 2006; Perkins et al. 2012) (Alexander et al. 2006; Perkins, Alexander, and Nairn 2012). During the 2003 centennial European drought, Leuzinger et al. (Leuzinger & Körner 2007) recorded higher transpiration rates for some species and locally reduced temperature in the experimental higher [CO_2] area. A model study (Lemordant et al. 2016) showed that stomatal response to higher [CO_2] can generate soil water savings during the growing season and enhanced water availability during the summer, feeding larger transpiration during a summer heat wave and thereby mitigating its severity (Figure 3.1c).

This study systematically investigates the response of extreme temperatures to rising [CO_2] in Earth System Models (ESMs) at the global scale by separating the radiative greenhouse gas impact from the vegetation physiological response.

Chapter 13: Data and Methods

13.1 CMIP5 ensemble

Daily temperature is available for four Earth System Models (ESM) for the idealized single-forcing Coupled Model Intercomparison Project, Phase 5 (CMIP5) (Taylor et al. 2012) experiments with [CO_2] increasing at a rate of one percent per year, either 1) in the atmospheric model only, i.e. acting as a greenhouse gas but not seen by the leaves, 2) in the vegetation model only, i.e. prescribing transparent CO_2 in the atmosphere or 3) in both. The simulations 1) are called CTRL (1pctCO2 in the CMIP5 terminology). The simulations 2) are called PHYS (esmFixClim1 in the CMIP5 terminology), and simulations 3) are referred to as ATMO (esmFdbk1 in CMIP5 terminology). In all three simulations, CO_2 is increased by 1% each year starting for 140 years from pre-industrial levels in 1850 for CanESM2, IPSL5A-LR, and MPI-ESM-LR, and in 1860 for HadGEM2-ES.

These idealized runs differ from the more common CMIP5 Representative Concentration Pathway 8.5 (RCP 8.5), an emission scenario from 2005 to 2100 that includes prescribed changes in land use and land cover scenarios, as well as aerosol and ozone forcing. All ESMs used here have a dynamic vegetation model, so that LAI can vary.

Daily data is available for four models: CanESM2, IPSL5A-LR, HadGEM2-ES, and MPI-ESM-LR (Taylor et al. 2012). For most of the models only one ensemble member is available -r1i1p1 in the CMIP5 terminology-, so that we consider only one ensemble member per model.

13.2 Data processing and analysis

Our analysis of extremes is based on the annual maximum of the daily maximum temperature, Txx (Zhang et al. 2011). We re-gridded each model to a common 1° x 1° grid in

order to compute the intermodel average. The temporal change of a variable X is calculated as: $\Delta X = \bar{X}_{fut} - \bar{X}_{hist}$. $\bar{X}_{fut}$ is the mean of X over years 89-118, so that the mean CO_2 concentration matches the period 2070-2099 in RCP 8.5, while $\bar{X}_{hist}$ is the mean of X over years 1-20 to correspond with the period 1939-1968 in RCP 8.5. We chose to define $\bar{X}_{fut}$ in this way in order to facilitate the comparison with other studies (Stocker & Qin 2013).

In addition to daily temperature data, our analysis is based on monthly-averaged outputs for sensible heat flux and evaporative fraction (EF), defined as the ratio of the latent heat flux to the sum of the latent and the sensible heat fluxes. For sensible heat flux, we consider the annual average, as physiological impact is small in the winter. For EF, we use the annual average for tropical latitudes between [-15; 10], and the average of local summer months elsewhere (i.e. JJA for [10; 90] and DJF for [-90; -15]). We focus on summer months since this is the dominant growing season and therefore the most relevant for plant water stress and heat-wave events. In the tropics we use the latitudinal range [-15; 10], as it satisfies the two following constraints: the transition with the local summer averaging zones is consistent, and the equatorial range stays as small as possible.

The runs are independent and the Txx response is quasi linear for the different experiments presented here (Figure 3.4). The difference between CTRL and ATMO is indeed very close to PHYS (Figure 3.5) indicating that the ATMO and PHYS effects compare nearly linearly with CTRL, which justifies the decomposition. Soil moisture, which shows more non-linearities, is however an exception (Figure 3.7). Because the initial conditions of each ensemble member are not perfectly identical, one should not expect to obtain a perfect match between the combined CTRL-ATMO and PHYS. In particular, the internal climate variability is causing regional variations.

3 out 4 models agree on the sign change of Txx between the Years 89-118 and 1-20 on 49% of the land pixel of the grid (Figure 3.8), and the 4 models agree on the sign of the change on 27% of the pixels. This leaves out 23% of the grid with insignificant results.

We focus on five regions initially defined in a previous studies of extremes (Seneviratne et al. 2012). We selected these regions as they highlight the behavior of various ecosystem-climate and strong land-atmosphere coupling (Vogel et al. 2017): Amazonia (AMZ), Central Europe (CEU), Central North America (CNA), Northern Australia (NAU), and Southern Africa (SAF).

Chapter 14: Results

The Txx response to increasing [CO2] is nearly linear, in time, for CTRL and ATMO (Figure 3.4, 3.1b). Txx increases in CTRL by 7 K during the 140 years experiment, corresponding to a [CO2] increase from 284 to 1134 ppm. A large fraction of CTRL Txx increase can be seen in ATMO, as in ATMO Txx increases globally by about 5.5 K (Figure 3.4). However, Txx also increases in PHYS, by about 1 K in 140 years, i.e. 15% of the CTRL total increase. The sum of the mean contributions of ATMO and PHYS is slightly lower than CTRL (Figure 3.4, Figure 3.6), by about 0.3 K.

Once plotted against [CO2], the Txx response does not show a linear behavior anymore but rather a curvature (Figure 3.2a). The effect of increasing [CO2] on Txx is more important at lower [CO2] levels. The marginal effect of increasing [CO2] on temperature becomes smaller with increasing [CO2] as a result of both ATMO and PHYS effects, as they both become less efficient at higher concentrations. However, the PHYS effect on Txx becomes more important, in proportion, at [CO2] above 600 ppm, stabilizing at 15% of the CTRL response (Figure 3.5b). We note that the mean temperature response in CTRL is within the range of the whole CMIP 5 ensemble for RCP 8.5 (Seneviratne et al. 2016; Stocker and Qin 2013).

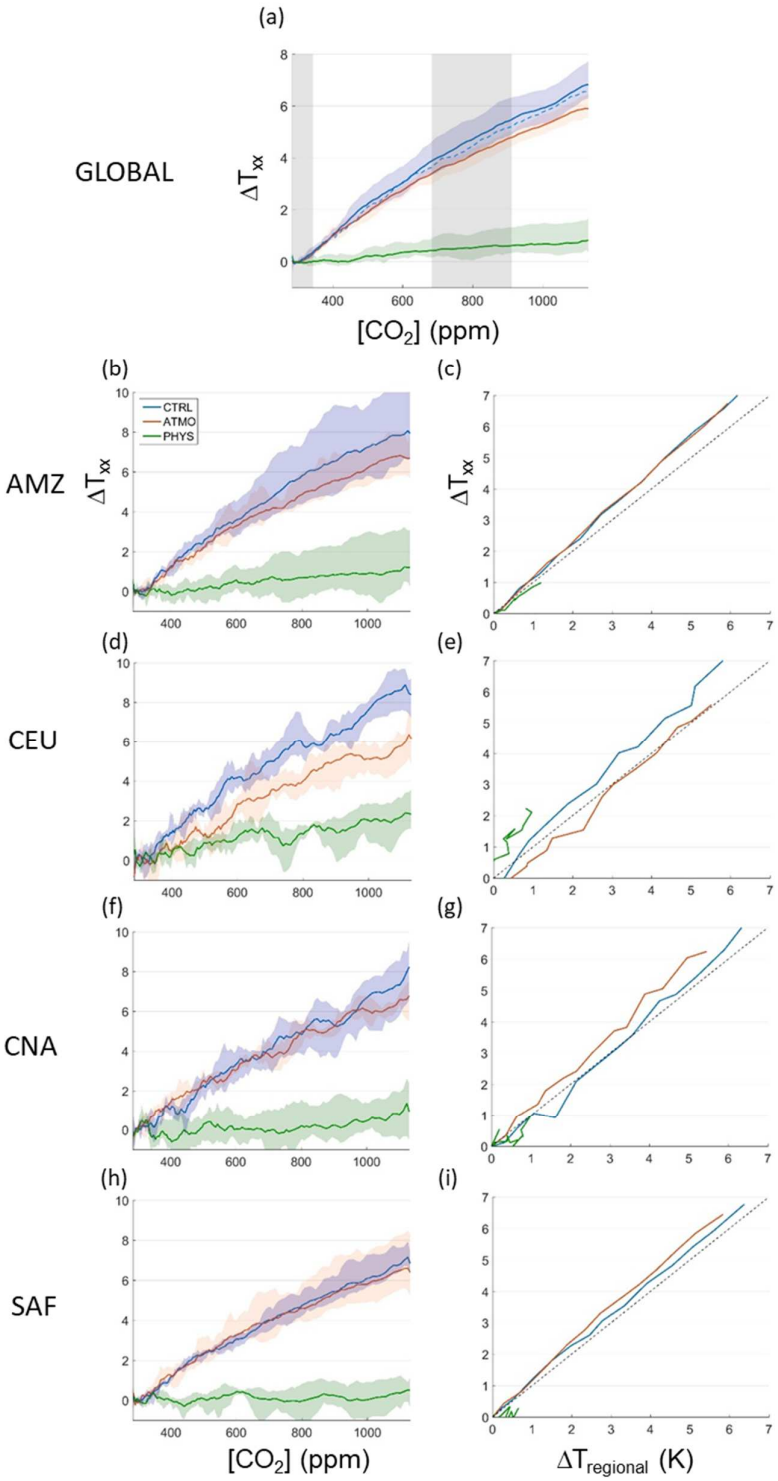

Figure 3.2 Global and Regional terrestrial Txx anomalies and quantification of the physiological effect.

*Global and Regional terrestrial Txx anomalies and quantification of the physiological effect. The global terrestrial Txx anomalies (K) are plotted against [CO_2] in ppm (**a**) for CTRL (blue), ATMO (red) and PHYS (green).*

*(Left column) The regional terrestrial Txx anomalies (K) are plotted against [CO_2] in ppm for CTRL (blue), ATMO (red) and PHYS (green), for AMZ (**b**), CEU (**d**), CNA (**f**) and SAF (**h**).*
*(Right Column) Regional Txx anomalies in K are presented against regional mean temperature anomalies in K for CTRL (blue), ATMO (red) and PHYS (green) for AMZ (**c**), CEU (**e**), CNA (**g**) and SAF (**i**).*
The colored shaded areas present the minimum and maximum values of the individual models. Txx intermodel average is smoothed using a 10-years moving mean algorithm. Anomalies are calculated against the mean of years 1 to 10. Anomalies can be small, translating into shorter lines. Data of only 4 models was available, explaining some of the noise in the results. Grey shaded area indicate the historical and future periods used for the maps of Figure 3.3.

The global Txx averages depicted in Figure 3.2 nonetheless hide strong geographical disparities. Txx is increasing by a few degrees in CTRL everywhere globally over land areas (Figure 3.9a). Mean temperature increases in similar ways to Txx, although the magnitude of the increase is noticeably smaller in Europe and South America, and larger in Northern latitudes (Figure 3.3a). ATMO is showing similar results to CTRL in respect to the regional patterns (Figure 3.9b). Quantitatively ATMO is showing less changes with respect to CTRL (Figure 3.2c) in key areas, resulting in global averages smaller with respect to CTRL (Figure 3.2a). Like in CTRL, Txx rises less than mean temperature in northern latitudes. Oppositely, Txx increases more than mean temperature in Central Europe and in the core of the Amazon (Figure 3.3b).

Changes in PHYS are smaller than those in CTRL and ATMO but can be regionally higher than +2 K, thus reinforcing extremes in several regions. In other regions, the change in Txx compared to the mean due to PHYS can be negative thus mitigating the ATMO increase of Txx, such as in Louisiana (Figure 3.9c). Txx increases in PHYS compared to the mean temperature around the equator, in Central Europe, in South America, in the eastern part of Asia, in central Australia and northern North America. The increase is larger than the mean temperature increase in Central Europe, in Northern latitudes, in North-Eastern Asia, in Amazonia and in Australia. This means that physiological effects there tend to reinforce the

radiative effect of increasing Txx, while the reverse effect is relevant in Southern USA, Eastern Brazil, Africa, and South-Eastern Asia (Figure 3.6a), where physiological effects tend to dampen the ATMO effect of increasing Txx. Altogether, this result indicates that CTRL changes are dominated by the greenhouse gas, radiative, effect of climate change, but that the physiological effects on Txx can be regionally large and of varying sign and magnitude. We therefore decided to highlight specific regions displaying contrasting behaviors.

AMZ, CNA and CEU exhibit large Txx increases in CTRL (Figure 3.2), consistently with previous studies (Vogel et al. 2017). In those regions, physiological effects account for 5 (CNA) to 25% (CEU) of the effects in CTRL in the end of the simulation, in the same range of amplitude as soil moisture effects on Txx (Vogel et al. 2017). SAF and NAU show a more limited increase of Txx and little PHYS influence.

Txx increases in AMZ by about +8 K in 140 years in CTRL (Figure 3.2b) and is driven by a large sensible heat flux increase (Figure 3.6b), and a corresponding large EF decrease of -15%. The contribution of physiological effects to EF changes (Figure 3.3i) is of the same order of magnitude as the radiative effects. The corresponding increase in sensible heat flux warms up the atmosphere and then ultimately impacts Txx. LAI slightly decreases in CTRL (Figure 3.3j), as the LAI increase in PHYS (Figure 3.3l) due to the positive fertilization effect is compensated by an LAI decrease in ATMO (Figure 3.3k) due to the negative effect of the temperature increase. However, physiological feedbacks remain an important contributor (~13%) to the total CTRL Txx increase in the region. The physiological effect is reinforcing the large-scale radiative effect on Txx (Figure 3.2b), and follows the increase in local mean temperature (Figure 3.2c).

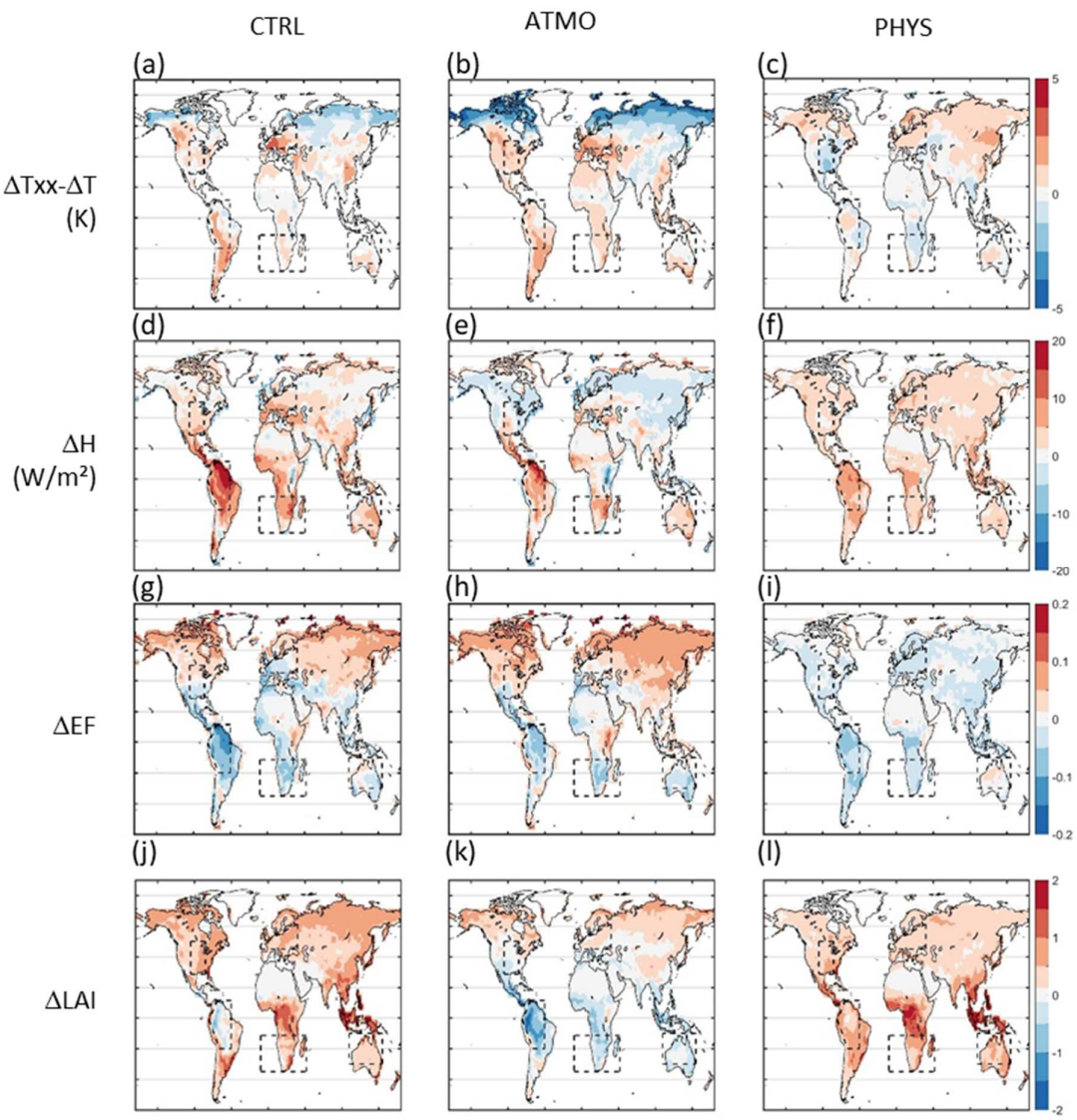

Figure 3.3 Drivers of the Txx change.
*Projected changes between Years 89-118 and 1-20 of Txx minus local mean temperature (K) (**a**, **b**, **c**), sensible heat flux (W/m²) (**d**, **e**, **f**), evaporative fraction (W/m² / W/m²) (**g**, **h**, **i**), and leaf area index (m^2/m^2) (**j**, **k**, **l**), for CTRL (left column), ATMO (middle column) and PHYS (right column). Each colorbar corresponds to the according row. Dashed areas correspond to Amazonia (AMZ), Central Europe (CEU), Central North America (CNA), Northern Australia (NAU), and Southern Africa (SAF). For Txx change (**a**, **b**, **c**), only pixels with more than 3 models in agreement on the sign change are shown.*

CEU also exhibits a large Txx increase of more than +8 K in 140 years in CTRL (Figure 3.2d). CEU has been documented as a region with a strong increase in extreme heat-wave episodes in recent decades (Schär et al. 2004), largely due to soil moisture feedbacks (Seneviratne et al. 2006). Here we show that physiological effects are also strong contributors to the Txx increase over CEU. EF decreases in CEU (Figure 3.3g), driven by the physiological effect (Figure 3.3i). The LAI increase (Figure 3.3j and Figure 3.3l), which tends to increase the latent heat flux, does not sufficiently compensate the stomatal closure and the corresponding increase in water use efficiency. The latent heat flux does not increase as much as sensible heat flux, thus driving down EF in the region. Long-term mean soil moisture does not increase nor decrease on average in this region centered on CEU (Figure 3.7) in the simulations analyzed here, emphasizing that radiative and physiological effects, even in the absence of soil moisture changes can strongly regulate Txx. Physiological effects and associated feedbacks account for about 25% of the radiative effects in CEU at the end of the simulation, comparable with previously assessed regional soil moisture feedbacks on Txx in CEU (Vogel et al. 2017). The Txx trend in PHYS over CEU is rather large (~0.2 K/decade), as well as the difference between the CTRL (0.6 K/decade) and ATMO (~0.4 K/decade) (Figure 3.2d). As a result of those physiological feedbacks, Txx in CTRL increases more than the mean temperature, while ATMO Txx follows the mean temperature trend tightly (Figure 3.2e).

In CNA, the large Txx increase (Figure 3.2f) is even larger than the regional mean temperature increase in CTRL (Figure 3.2g, Figure 3.3a). The increase in sensible heat flux due to the greenhouse gas effect is a driving factor of both the mean temperature and Txx increases. The increase in sensible heat flux is primarily due to ATMO (Figure 3.3e) but with a non-negligible impact of PHYS (Figure 3.3f) and therefore of reduced stomatal conductance. Txx in ATMO increases at a higher rate than the mean temperature (Figure 3.3b, Figure 3.2g), as soil is predicted to become drier in this region (Figure 3.7, Vogel et al. 2017). Txx increases

only moderately in PHYS (Figure 3.2f), compared to CTRL (~10% at the end of simulation of the CTRL changes). Whereas EF increases in ATMO (Figure 3.3h), EF decreases in PHYS (Figure 3.3i), so that EF remains mostly steady in CTRL (Figure 3.2f). The decrease in PHYS is due to the reduced stomatal conductance, which is not compensated by the increased LAI due to fertilization effects in PHYS (Figure 3.3l). CNA also shows a consistent decreasing trend of soil moisture in large parts of the region (Figure 3.7), and the soil moisture decrease feeds back onto the atmosphere and increases Txx (Vogel et al. 2017). However, the increased LAI (Figure 3.4l), largely mitigates the increase of Txx so that the increase in Txx in CTRL is comparable to ATMO (Figure 3.2g), i.e. physiological effects (stomatal regulation, fertilization and soil moisture feedback) compensate each other and are overall small over CNA.

The SAF increase of Txx is smaller in CTRL (+7 K in 140 years) than over the three previous regions (Figure 3.2h), and is comparable to the mean temperature increase (Figure 3.3b, Figure 3.2i). In agreement with those results, PHYS trends of Txx are close to 0 (Figure 3.2h). Since this semi-arid to arid area is seasonally very dry the impact of vegetation effects in PHYS are limited and the change in sensible and latent heat fluxes are small (Figure 3.3f). As a result, the ATMO and CTRL trends are similar (Figure 3.2f). The physiological effects on Txx changes are thus small in SAF (about 5% at most of CTRL), yet slightly negative (Figure 3.6a, Figure 3.2i).

Similarly, NAU shows a more moderate change in Txx (+6 K in 140 years) compared to AMZ, CEU and CNA (Figure 3.3a, Figure 3.10a). Only limited physiological effects are observed in this monsoonal regions (Figure 3.10a). NAU is indeed a region much less sensitive to land-atmosphere interactions than CEU, and where carbon uptake is dominated by interannual climate variability (Perkins et al. 2015; Poulter et al. 2014). The Txx increase in this region follows strikingly the mean temperature change (Figure 3.10b), indicating that PHYS effects are indeed very small. Soil moisture feedbacks on Txx have been shown to be

consistently small in this region (Vogel et al. 2017), as this monsoonal region is mostly impacted by oceanic influence.

We note that except for NAU, vegetation physiological effects on temperature extremes are particularly important in transitional dry-to-wet regions, like the Certão or the Sahel (Figure 3.6a), which are well known hotspots of biosphere-atmosphere interactions (Green et al. 2017; Koster et al. 2004). At Northern latitudes, in the models, the mean temperature increase trends are much larger than the Txx increasing trends (Figure 3.3a), which may be contradictory with recent evidence (Tingley & Huybers 2013). This departure from observations might be due to challenges in the model representation of cold processes such as the stable boundary layer and snow related processes. Interestingly though, the changes in Txx in this region is not only due to radiative effects but also to some physiological effects (Figure 3.6a). In fact, the PHYS impact on Txx is positive in the region (Figure 3.6a), while the effect of ATMO is negative (Figure 3.3b). The stomatal regulation increases sensible heat flux (Figure 3.3f) over this extended (and non-water limited region) region, thus increasing Txx.

Chapter 15: Discussion

The increasing trend of temperature extremes (Txx) is globally driven by radiative effects, but we demonstrated that physiological effects due to increased CO_2 at the leaf level, account for about 15% of the radiative greenhouse gas CO_2 effects, globally. However, global averages hide substantial variability across regions. In the Amazon and Central Europe, physiological effects strongly increase temperature extremes, while they tend to mitigate radiative greenhouse effects in Central North America because of the increase in leaf area index there. Vegetation indeed modulates the partitioning of energy fluxes. If stomatal regulation is the dominant surface CO_2 response mechanism then the evaporative fraction is reduced and sensible heat flux increases. If biomass increases (fertilization) then increased roughness and increased turbulent exchange tend to cool the surface and near-surface air. These two mechanisms, in turn, affect seasonal soil moisture depletion, especially during heat-waves or droughts (Lemordant et al. 2016). The degree of variation of those three mechanisms (direct physiological effects, biomass increase, soil moisture feedbacks), summarized in Figure 3.1, explains the wide variety of physiological responses observed across the globe.

We showed that physiological effects tend to play a negligible effect in regions dominated by ocean variability, such as Southern Africa and Northern Australia, consistent with the fact that land-atmosphere feedbacks are weak in those regions. These regions are sensitive to precipitation variability (Green et al. 2017; Poulter et al. 2014), which is expected to decline in the future (Scheff & Frierson 2015) under oceanic influence (Mason 2001; Poulter et al. 2014; Richard et al. 2001) so that droughts will increase in occurrence and length (Prudhomme et al. 2014). It is also an important factor in regions prone to a climate change towards a transitional regime, such as Central Europe. Central North America and Central Europe show larger influence of the physiological effects, consistently with the impact of soil

moisture on Txx (Vogel et al. 2017), which is large in those regions. These regions are indeed hotspots of biosphere-atmosphere interactions (Green et al. 2017).

CO_2 fertilization representation in models is still relatively uncertain. First, extreme weather conditions (Ciais et al. 2005; Obermeier et al. 2016; Reichstein et al. 2013) might limit on the long run the trend of CO_2 fertilization, a negative impact not correctly represented in current models. Secondly, biogeochemical processes and nutrient limitations (Reich et al. 2014) might also limit plant growth stimulation by CO_2, in comparison with model simulations. On top of these uncertainties, the representation of stomatal conductance in current models may lead to an under-estimation of the intensity of the future extreme temperatures (Kala et al. 2016). Given that we could only use four models for this study, there is an inherent noise in the results presented but we believe that the results still present a useful assessment of the impacts of surface CO_2, which likely will be better assessed in the CMIP6 and future Model Intercomparison Projects. Future simulations should try to disentangle the effects of stomatal CO_2 effects from the fertilization and soil moisture effects to correctly assess their relative contributions to temperature extremes.

Chapter 16: Supplementary Materials of Part III

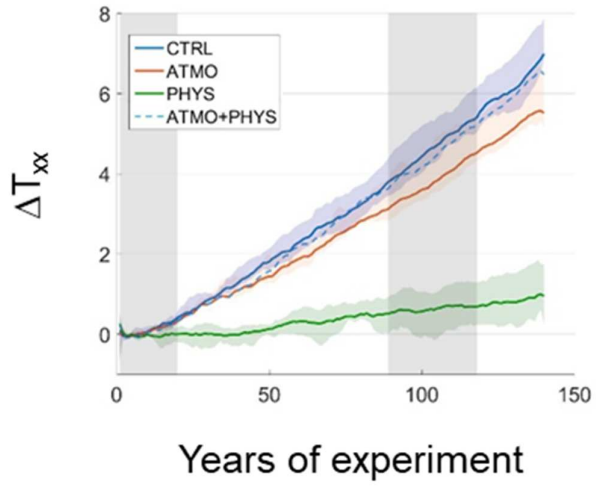

Figure 3.4 Global terrestrial Txx anomalies and quantification of the physiological effect. The global terrestrial Txx anomalies (K) are plotted against time in years for CTRL (blue), ATMO (red) and PHYS (green). The colored shaded areas present the minimum and maximum values of the individual models. Txx intermodel average is smoothed using a 10-years moving mean algorithm. Anomalies are calculated against the mean of years 1 to 10. Grey shaded area indicate the historical and future periods.

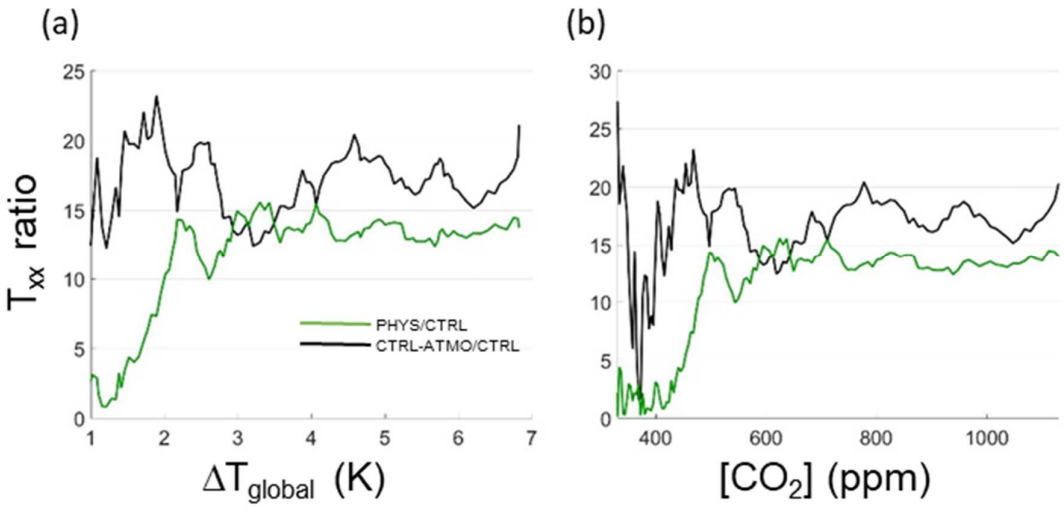

Figure 3.5 Comparison of the PHYS simulation with the hypothesized equivalent CTRL-ATMO.
*The Txx physiological effect in % is presented against global mean temperature anomalies (**a**) and against [CO2] in ppm (**b**). It is calculated as the ratio of the PHYS anomaly to the CTRL anomaly (green), and the ratio between the difference between the CTRL anomaly and the ATMO anomaly to the CTRL anomaly (black).*

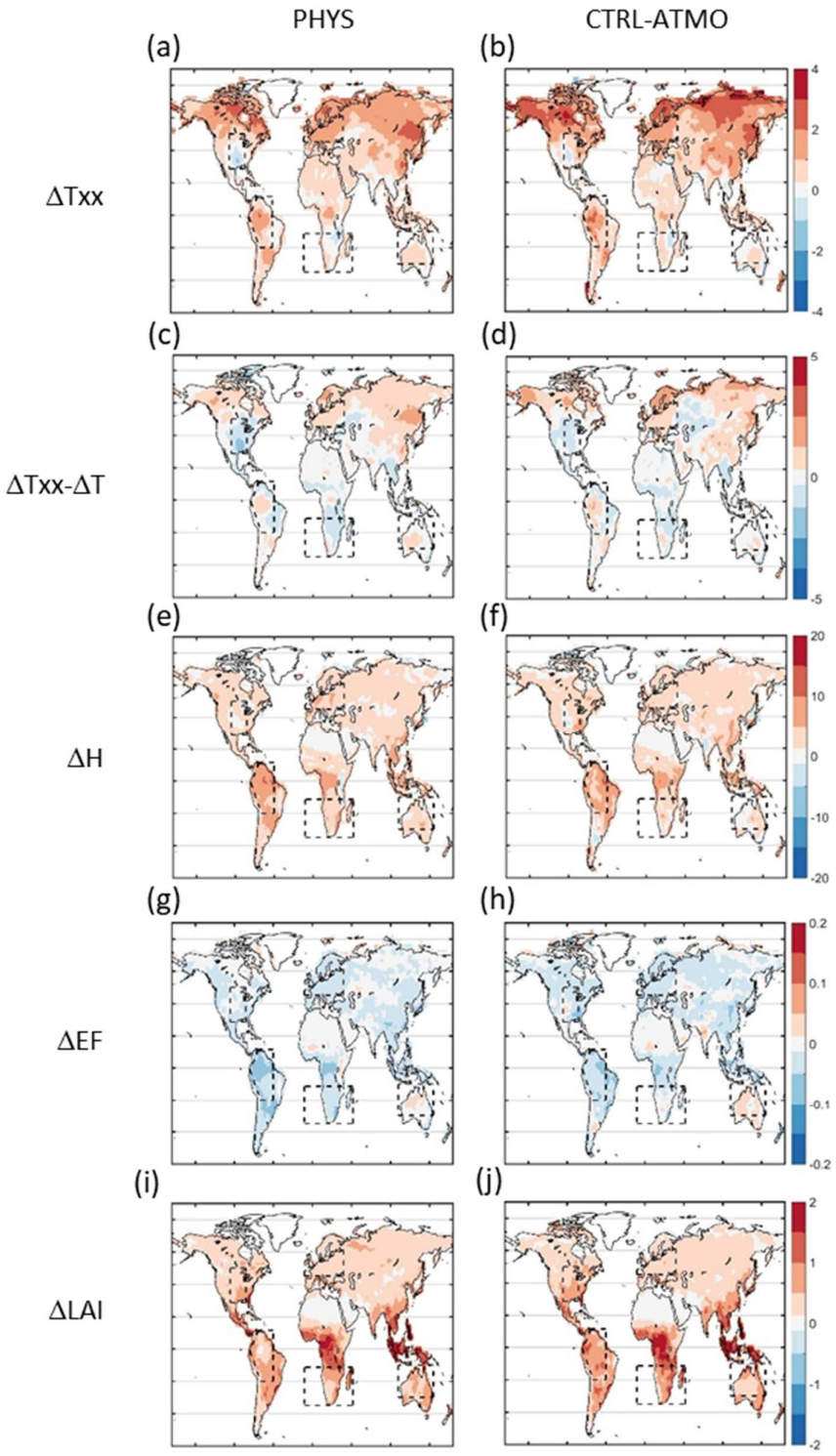

Figure 3.6 Projected changes of Txx.
*Change is calculated between Years 89-118 and 1-20 for the increase of Txx (**a**, **b**), Txx minus mean local temperature (**c**, **d**), sensible heat flux (**e**, **f**), evaporative fraction (**g**, **h**) and*

*leaf area index (**i**, **j**), for the runs PHYS (left column), and CTRL - ATMO (right column). Each colorbar corresponds to the according row.*

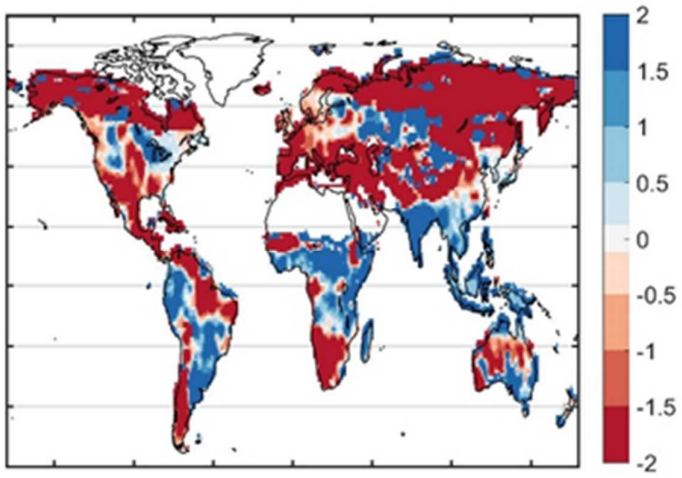

Figure 3.7 Standardized changes in CTRL of soil moisture at 2m.
Change is quantified by the difference of the years 89-118 of the simulation and the years 1-20, normalized by the standard deviation of CTRL over the years 1-20 (Methods).

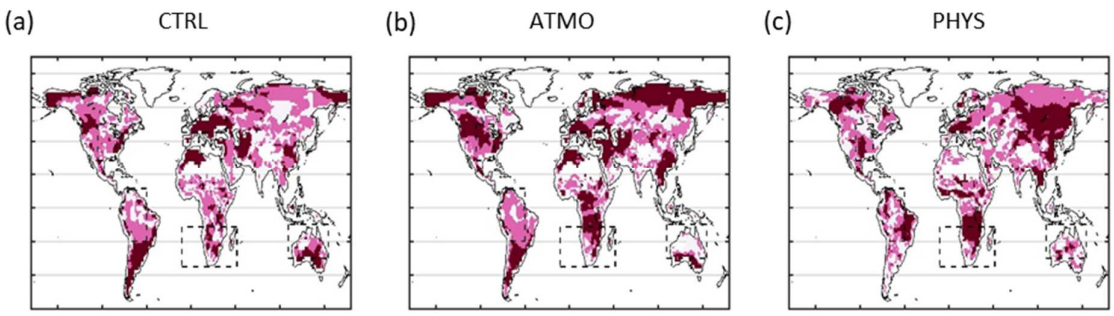

*Figure 3.8 Significance of Txx change for CTRL (**a**), ATMO (**b**), and PHYS (**c**). Light and dark pink indicates that 3 and 4 models respectively agree on the sign change of Txx between Years 89-118 and 1-20. White pixels indicate that only 2 models agree on the sign change.*

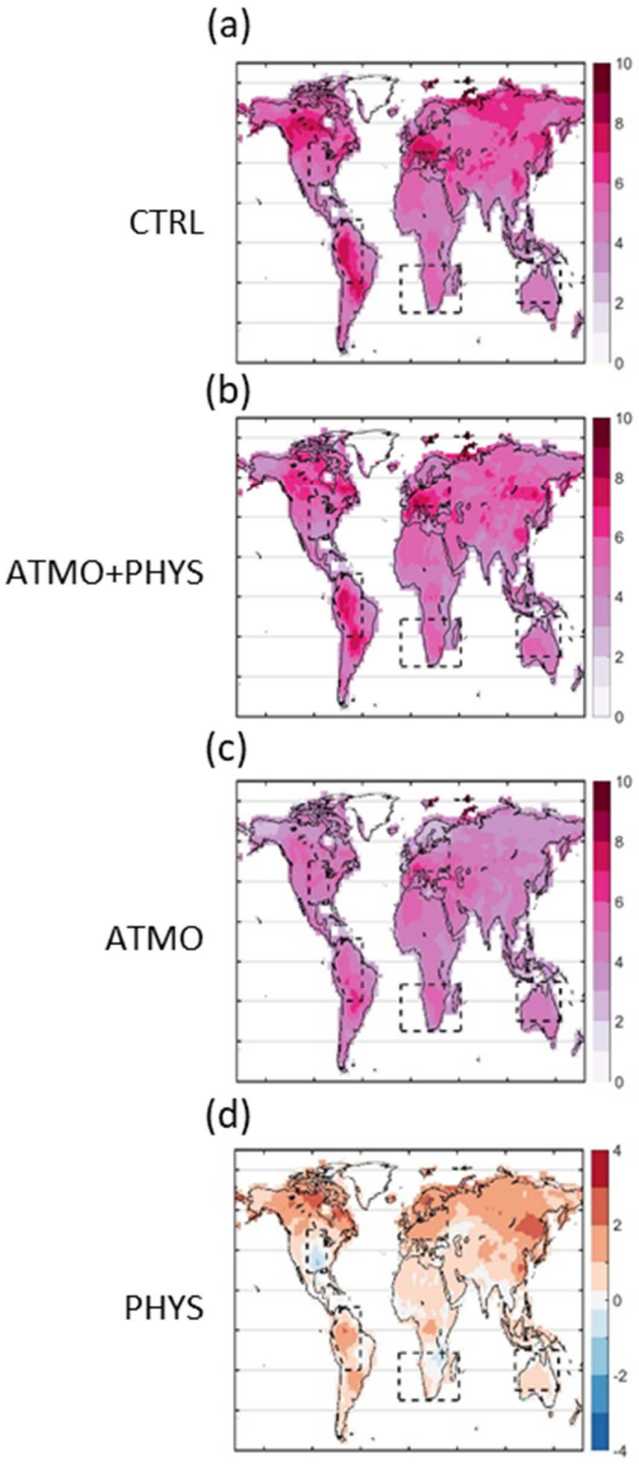

Figure 3.9 Coherence of projected changes of Txx.
*Change is calculated between Years 89-118 and 1-20 for the increase of Txx, additional to the local mean increase for the CTRL (**a**), ATMO+PHYS (**b**) ATMO (**c**) and PHYS (**d**).*

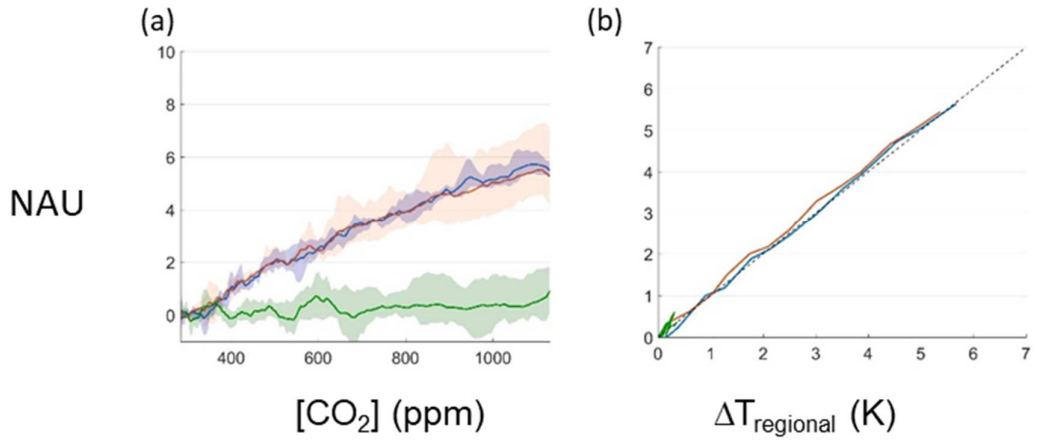

Figure 3.10 Terrestrial regional NAU Txx anomalies and quantification of the physiological effect.
*The regional NAU terrestrial Txx anomalies (K) are plotted against [CO2] in ppm for CTRL (blue), ATMO (red) and PHYS (green) (**a**). The colored shaded areas present the minimum and maximum values of the individual models.*
*Regional NAU Txx anomalies in K are presented against regional mean temperature anomalies in K for CTRL (blue), ATMO (red) and PHYS (green) (**b**). The Txx intermodel average is smoothed using a 10-years moving average. Anomalies are calculated against the years 1 to 10 average. Anomalies can be small, translating into shorter lines. Data of only 4 models was available, explaining some of the noise in the results.*

CONCLUSIONS AND PERSPECTIVES

This study explored the role and importance of the physiological processes in the changes of the hydrologic cycle in an atmosphere enriched in CO_2. Altogether, the three parts strongly highlight the key role of the vegetation will play in the future. In the first part, we showed that vegetation is not only responding to the hydrological cycle with rising [CO_2], but also that direct physiological effects and feedbacks are the main drivers of hydrological changes on land. For the first time, a model study quantifies the role of the vegetation in regulating the terrestrial water cycle and finds that it will be more important in that respect than either precipitation or radiation, contrary to current wisdom.

In part II and III, the focus has been put on extreme events, a crucial consequence of the water cycle changes. The extreme events are indeed of vital importance for both ecosystems and societies. We showed that for heat-waves and extreme temperatures are also influenced by physiological effects and feedbacks. The European case study of part II points out a seasonal feedback originated by the vegetation reaction to higher [CO_2] levels. As a consequence, the severity of the heat-wave is attenuated and the stress caused by heat-waves is partially diminished. In the Part III, we look more systematically and globally at the extreme temperatures. The maximum daily temperatures are shown to increase globally, in a trend that is larger or in the same ballpark than the mean temperature except in Northern latitudes. The physiological effects contribute globally to about 15% of the full trend, with large local variations. The physiological effect does indeed depend on regions, and is contradictory between Europe and North America. If in Europe, the extreme temperature increasing trend is expected to be reinforced by physiological direct and indirect feedbacks, in North America, the vegetation tend to dampen it.

The results presented above open a path for future work. First of all, these results highlight the fundamental role land processes will play in the future in regulating the climate and the hydrological cycle at the local, regional and global levels, as well as at various temporal

scales. It should incite the model community to systematically use coupled models, and spend resources to improve the land models. Vegetation and biogeochemical processes in models are sometimes represented too simplistically, are not even represented. There lies a way to improve significantly both the accuracy of climate model performance and prediction.

The number of models that have taken part to the CMIP5 experiments used in this dissertation is limited. The quantitative accuracy of the findings presented here are necessary limited by the number of realizations, and the variety of models used. However, this type of idealized experiments have proven to be very useful to disentangle the complexity of the interactions in the climate system. CMIP6 is in its launching phase. We hope that more model groups will participate to the idealized runs, and at least run the PHYS-like experiments.

Lastly, this study focused on some aspects only of the water cycle. Further work should investigate all other aspects. For example, minimum temperature, and especially minimum temperature during a heat-wave, should be affected dramatically by the physiological feedbacks. Nighttime temperature, though a very important parameters for ecosystem health, is relatively neglected in the literature. How the vegetation feedbacks on nighttime temperature could be of great importance.

BIBLIOGRAPHY

Ainsworth, E. a. & Long, S.P., 2005. What have we learned from 15 years of free-air CO2 enrichment (FACE)? A meta-analytic review of the responses of photosynthesis, canopy properties and plant production to rising CO2. *New Phytologist*, 165(2), pp.351–372.

Ainsworth, E.A. & Rogers, A., 2007. The response of photosynthesis and stomatal conductance to rising [CO2]: mechanisms and environmental interactions. *Plant, Cell & Environment*, 30(3), pp.258–270. Available at: http://doi.wiley.com/10.1111/j.1365-3040.2007.01641.x.

Alexander, L. V et al., 2006. Global observed changes in daily climate extremes of temperature and precipitation. *Journal Of Geophysical Research*, 111, pp.1–22.

Alkama, R. & Cescatti, A., 2016. Biophysical climate impacts of recent changes in global forest cover. *Science*, 351(6273), pp.600–604.

Anav, A. et al., 2010. A validation of heat and carbon fluxes from high-resolution land surface and regional models. *Journal of Geophysical Research: Biogeosciences*, 115(4), pp.1–20.

Arora, V.K. et al., 2011. Carbon emission limits required to satisfy future representative concentration pathways of greenhouse gases. *Geophysical Research Letters*, 38(5), pp.3–8.

Bader, M.K.F. et al., 2013. Central european hardwood trees in a high-CO2 future: Synthesis of an 8-year forest canopy CO2 enrichment project. *Journal of Ecology*, 101, pp.1509–1519.

Ball, J.T., Woodrow, I.E. & Berry, J.A., 1987. A Model Predicting Stomatal Conductance and Its Contribution to the Control of Photosynthesis Under Different Environmental Conditions. *Journal of Progress in Photosynthesis Research*, 4(5), pp.221–224. Available at: http://link.springer.com/10.1007/978-94-017-0519-6.

Bateni, S.M. & Entekhabi, D., 2012. Relative efficiency of land surface energy balance components. *Water Resources Research*, 48(4), pp.1–8.

Bentsen, M. et al., 2013. The Norwegian Earth System Model, NorESM1-M – Part 1: Description and basic evaluation of the physical climate. *Geoscientific Model Development*, 6(3), pp.687–720. Available at: https://www.geosci-model-dev.net/6/687/2013/.

Berg, A. et al., 2014. Impact of soil moisture-atmosphere interactions on surface temperature distribution. *Journal of Climate*, 27, pp.7976–7993.

Berg, A., Findell, K., et al., 2016. Land–atmosphere feedbacks amplify aridity increase over land under global warming. *Nature Climate Change*, (May), pp.1–7. Available at: http://www.nature.com/doifinder/10.1038/nclimate3029.

Berg, A., Sheffield, J. & Milly, P.C.D., 2016. Divergent surface and total soil moisture projections under global warming. *Geophysical Research Letters*, pp.2079–2087.

Betts, R.A. et al., 2007. Projected increase in continental runoff due to plant responses to increasing carbon dioxide. *Nature*, 448(August), pp.1037–1041.

de Boer, H.J. et al., 2011. Climate forcing due to optimization of maximal leaf conductance in subtropical vegetation under rising CO2. *Proceedings of the National Academy of Sciences*, 108(10), pp.4041–4046. Available at: http://www.pnas.org/cgi/doi/10.1073/pnas.1100555108.

Boisier, J.P. et al., 2015. Projected strengthening of Amazonian dry season by constrained climate model simulations. *Nature Climate Change*, 5(7), pp.656–660. Available at: http://www.scopus.com/inward/record.url?eid=2-s2.0-84932110744&partnerID=tZOtx3y1.

Byrne, M.P. & O'Gorman, P.A., 2013. Land–Ocean Warming Contrast over a Wide Range of Climates: Convective Quasi-Equilibrium Theory and Idealized Simulations. *Journal of Climate*, 26(12), pp.4000–4016. Available at: http://dx.doi.org/10.1175/JCLI-D-12-00262.1.

Byrne, M.P. & O'Gorman, P.A., 2015. The Response of Precipitation Minus Evapotranspiration to Climate Warming : Why the '" Wet-Get-Wetter , Dry-Get-Drier "' Scaling Does Not Hold over Land *. *Journal of Climate*, 28, pp.8078–8092.

Byrne, M.P. & O'Gorman, P.A., 2016. Understanding Decreases in Land Relative Humidity with Global Warming : Conceptual Model and GCM Simulations. *Journal of Climate*, 29, pp.9045–9061. Available at: http://journals.ametsoc.org.ezproxy.cul.columbia.edu/doi/pdf/10.1175/JCLI-D-16-0351.1.

Campbell, J.E. et al., 2017. Large historical growth in global terrestrial gross primary production. *Nature*, 544(7648), pp.1–16. Available at: http://dx.doi.org/10.1038/nature22030.

Canouï-Poitrine, F., Cadot, E. & Spira, A., 2006. Excess deaths during the August 2003 heat wave in Paris, France. *Revue d'Épidémiologie et de Santé Publique*, 54(2), pp.127–135.

Cheaib, A. et al., 2012. Climate change impacts on tree ranges: model intercomparison facilitates understanding and quantification of uncertainty. *Ecology Letters*, 15(6), pp.533–544. Available at: http://doi.wiley.com/10.1111/j.1461-0248.2012.01764.x.

Christian, J.R. et al., 2010. The global carbon cycle in the Canadian Earth system model (CanESM1): Preindustrial control simulation. *Journal of Geophysical Research: Biogeosciences*, 115(3), pp.1–20.

Ciais, P. et al., 2005. Europe-wide reduction in primary productivity caused by the heat and drought in 2003. *Nature*, 437(7058), pp.529–533.

Collatz, G.J. et al., 1991. Physiological and environmental regulation of stomatal conductance, photosynthesis and transpiration: a model that includes a laminar boundary layer. *Agricultural and Forest Meteorology*, 54(2–4), pp.107–136.

Collatz, G.J., Ribas-Carbo, M. & Berry, J. a., 1992. Coupled photosynthesis-stomatal conductance model for leaves of C4 plants. *Australian Journal of Plant Physiology*, 19(1139), pp.519–539. Available at: http://www.publish.csiro.au/?paper=PP9920519.

Coumou, D. & Rahmstorf, S., 2012. A decade of weather extremes. *Nature Climate Change*, 2(7), pp.1–6. Available at: http://dx.doi.org/10.1038/nclimate1452.

Cox, P.M., Huntingford, C. & Harding, R.J., 1998. A canopy conductance and photosynthesis model for use in a GCM land surface scheme. *Journal of Hydrology*, 212–213(1–4), pp.79–94.

D'Andrea, F. et al., 1998. Northern Hemisphere atmospheric blocking as simulated by 15 atmospheric general circulation models in the period 1979-1988. *Climate Dynamics*, 14(6), pp.385–407.

Dai, A.G., 2013. Increasing drought under global warming in observations and models. *Nature Climate Change*, 3(1), pp.52–58.

Dee, D.P. et al., 2011. The ERA-Interim reanalysis: Configuration and performance of the data assimilation system. *Quarterly Journal of the Royal Meteorological Society*, 137(656), pp.553–597.

Ding, T., Qian, W. & Yan, Z., 2010. Changes in hot days and heat waves in China during 1961 – 2007. *International Journal of Climatology*, 1462(August 2009), pp.1452–1462.

Donat, M.G. et al., 2016. Temperature and precipitation extremes in century-long gridded observations, reanalyses, and atmospheric model simulations. *Journal of Geophysical Research: Atmospheres*. Available at: http://doi.wiley.com/10.1002/2016JD025480.

Drobinski, P. et al., 2014. HyMeX: A 10-Year Multidisciplinary Program on the Mediterranean Water Cycle. *Bulletin of the American Meteorological Society*, 95(7), pp.1063–1082. Available at: http://journals.ametsoc.org/doi/abs/10.1175/BAMS-D-12-00242.1.

Drobinski, P. et al., 2012. Model of the Regional Coupled Earth system (MORCE): Application to process and climate studies in vulnerable regions. *Environmental Modelling and Software*, 35, pp.1–18.

Dunne, J.P. et al., 2013. GFDL's ESM2 global coupled climate-carbon earth system models. Part II: Carbon system formulation and baseline simulation characteristics. *Journal of Climate*, 26(7), pp.2247–2267.

Dunne, J.P. et al., 2012. GFDL's ESM2 global coupled climate-carbon earth system models.Part I: Physical Formulation and Baseline Simulation Characteristics. *Journal of Climate*, 25(19), pp.6646–6665.

Durack, P.J., Wijffels, S.E. & Matear, R.J., 2012. Ocean Salinities Reveal Strong Global Water Cycle Intensification During 1950 to 2000. *Science*, 336(April), pp.455–458.

Etheridge, D.M. et al., 1996. Natural and anthropogenic changes in atmospheric CO2 over the last 1000 years from air in Antarctic ice and firn. *Journal of Geophysical Research Atmospheres*, 101(95), pp.4115–4128.

Farquhar, G.D., Caemmerer, S. & Berry, J.A., 1980. A biochemical model of photosynthetic CO2 assimilation in leaves of C3 species. *Planta*, 149(1), pp.78–90. Available at: http://dx.doi.org/10.1007/BF00386231%5Cnhttp://www.springerlink.com/index/10.1007/BF00386231.

Fatichi, S., Pappas, C. & Ivanov, V.Y., 2015. Modeling plant-water interactions: an ecohydrological overview from the cell to the global scale. *Wiley Interdisciplinary Reviews: Water*, p.n/a-n/a. Available at: http://doi.wiley.com/10.1002/wat2.1125.

Fischer, E.M. et al., 2007. Contribution of land-atmosphere coupling to recent European summer heat waves. *Geophysical Research Letters*, 34(6), p.L06707. Available at: http://doi.wiley.com/10.1029/2006GL029068.

Fischer, E.M. & Schär, C., 2010. Consistent geographical patterns of changes in high-impact European heatwaves. *Nature Geoscience*, 3(6), pp.398–403. Available at: http://dx.doi.org/10.1038/ngeo866.

Frank, D.C. et al., 2015. Water-use efficiency and transpiration across European forests during the Anthropocene. *Nature Climate Change*, 5(6), pp.579–583. Available at:

http://www.nature.com/nclimate/journal/v5/n6/full/nclimate2614.html.

Gentine, P. et al., 2013. A Probabilistic Bulk Model of Coupled Mixed Layer and Convection. Part II: Shallow Convection Case. *Journal of the Atmospheric Sciences*, 70(6), pp.1557–1576. Available at: http://journals.ametsoc.org/doi/abs/10.1175/JAS-D-12-0146.1.

Gentine, P. et al., 2016. An allometry-based model of the survival strategies of hydraulic failure and carbon starvation. *Ecohydrology*, 9(3), pp.529–546. Available at: http://onlinelibrary.wiley.com/doi/10.1002/eco.1654/epdf.

Gentine, P. et al., 2007. Analysis of evaporative fraction diurnal behaviour. *Agricultural and Forest Meteorology*, 143(1–2), pp.13–29. Available at: http://linkinghub.elsevier.com/retrieve/pii/S016819230600339X.

Gentine, P., Entekhabi, D. & Polcher, J., 2011. The Diurnal Behavior of Evaporative Fraction in the Soil–Vegetation–Atmospheric Boundary Layer Continuum. *Journal of Hydrometeorology*, 12(6), pp.1530–1546. Available at: http://journals.ametsoc.org/doi/abs/10.1175/2011JHM1261.1.

Giorgi, F. & Lionello, P., 2008. Climate change projections for the Mediterranean region. *Global and Planetary Change*, 63(2–3), pp.90–104. Available at: http://ac.els-cdn.com/S0921818107001750/1-s2.0-S0921818107001750-main.pdf?_tid=9edab9a0-3ef1-11e6-a1b5-00000aacb35e&acdnat=1467311995_1502b3dc861140b7ccb75506fd8934be.

Good, S.P., Noone, D. & Bowen, G., 2015. Hydrologic connectivity constrains partitioning of global terrestrial water fluxes. *Science*, 349(6244), pp.175–177.

Granier, A. et al., 2007. Evidence for soil water control on carbon and water dynamics in European forests during the extremely dry year: 2003. *Agricultural and Forest Meteorology*, 143(1–2), pp.123–145. Available at: http://linkinghub.elsevier.com/retrieve/pii/S0168192306003911.

Gray, S.B. et al., 2016. Intensifying drought eliminates the expected benefits of elevated carbon dioxide for soybean. *Nature Plants*, 2(9), pp.1–8. Available at: http://dx.doi.org/10.1038/nplants.2016.132.

Green, J.K. et al., 2017. Regionally strong feedbacks between the atmosphere and terrestrial biosphere. *Nature Geoscience*, 10, pp.410–414. Available at: http://dx.doi.org/10.1038/ngeo2957%0Ahttp://10.0.4.14/ngeo2957%0Ahttp://www.nature.com/ngeo/journal/vaop/ncurrent/abs/ngeo2957.html#supplementary-information.

Greve, P. et al., 2014. Global assessment of trends in wetting and drying over land. *Nature Geoscience*, 7(10), pp.716–721. Available at: http://www.nature.com.are.uab.cat/ngeo/journal/v7/n10/full/ngeo2247.html.

Greve, P. & Seneviratne, S.I., 2015. Assessment of future changes in water availability and aridity. *Geophysical Research Letters*, 5, pp.1–7.

Hartmann, D.L., 2016. *Global physical climatology*, Available at: http://www.sciencedirect.com/science/book/9780123285317 [Accessed May 23, 2017].

Hauser, M., Orth, R. & Seneviratne, S.I., 2016. Role of Soil Moisture vs. Recent Climate Change for the 2010 Heat Wave in Western Russia. *Geophysical Research Letters*, p.n/a-n/a. Available at: http://doi.wiley.com/10.1002/2016GL068036.

He, J. & Soden, B.J., 2016. A re-examination of the projected subtropical precipitation decline. *Nature Climate Change*, 1(November), pp.1–6. Available at: http://www.nature.com/doifinder/10.1038/nclimate3157.

Held, I.M. & Soden, B.J., 2006. Robust responses of the hydrological cycle to global warming. *Journal of Climate*, 19(21), pp.5686–5699.

Hu, X.M., Nielsen-Gammon, J.W. & Zhang, F., 2010. Evaluation of three planetary boundary layer schemes in the WRF model. *Journal of Applied Meteorology and Climatology*, 49(9), pp.1831–1844. Available at: http://journals.ametsoc.org/doi/pdf/10.1175/2010JAMC2432.1.

Iversen, T. et al., 2013. The Norwegian Earth System Model, NorESM1-M – Part 2: Climate response and scenario projections. *Geoscientific Model Development*, 6(2), pp.389–415. Available at: https://www.geosci-model-dev.net/6/389/2013/.

Jasechko, S. et al., 2013. Terrestrial water fluxes dominated by transpiration. *Nature*, 496(7445), pp.347–350. Available at: http://www.ncbi.nlm.nih.gov/pubmed/23552893.

Ji, J., 1995. A Climate-Vegetation Interaction Model: Simulating Physical and Biological Processes at the Surface. *Journal of Biogeography*, 22(2/3), pp.445–451. Available at: http://www.jstor.org/stable/2845941?origin=crossref.

Jones, C.D. et al., 2011. The HadGEM2-ES implementation of CMIP5 centennial simulations. *Geoscientific Model Development*, 4(3), pp.543–570.

Kala, J. et al., 2016. Impact of the representation of stomatal conductance on model projections of heatwave intensity. *Scientific reports*, 6(January), p.23418. Available at: http://www.nature.com/srep/2016/160321/srep23418/full/srep23418.html.

Katul, G.G. et al., 2012. Evapotranspiration: A process driving mass transport and energy exchange in the soil-plant-atmosphere-climate system. *Reviews of Geophysics*, 50(3), p.RG3002.

De Kauwe, M.G. et al., 2013. Forest water use and water use efficiency at elevated CO_2: a model-data intercomparison at two contrasting temperate forest FACE sites. *Global Change Biology*, 19(6), pp.1759–1779. Available at: http://doi.wiley.com/10.1111/gcb.12164.

Keel, S.G. et al., 2007. Stomatal conductance in mature deciduous forest trees exposed to elevated CO2. *Trees*, 21(2), pp.151–159. Available at: http://link.springer.com/10.1007/s00468-006-0106-y.

Kimball, B.A. et al., 1993. Effects of increasing atmospheric CO2 on vegetation. In *Vegetatio*. Kluwer Academic Publishers, pp. 65–75.

Konings, A.G. & Gentine, P., 2016. Global Variations in Ecosystem-Scale Isohydricity. *Global Change Biology*, p.In press. Available at: http://onlinelibrary.wiley.com/doi/10.1111/gcb.13389/epdf.

Konings, A.G., Williams, A.P. & Gentine, P., 2017. Sensitivity of grassland productivity to aridity controlled by stomatal and xylem regulation. *Nature Geoscience*, 10(4), pp.284–288. Available at: http://www.nature.com/doifinder/10.1038/ngeo2903.

Koster, R.D. et al., 2004. Regions od Strong Coupling Between Soil Moisture and Precipitation. *Science*, 305(5687), pp.1138–1140. Available at:

http://www.jstor.org/stable/3837616.

Krasting, J.P. et al., 2013. Future Changes in Northern Hemisphere Snowfall. *Journal of Climate*, 26, pp.7813–7828.

Krinner, G. et al., 2005. A dynamic global vegetation model for studies of the coupled atmosphere-biosphere system. *Global Biogeochemical Cycles*, 19(1), p.GB1015. Available at: ftp://nacp.ornl.gov/synthesis/2008/firenze/continental/model_output/ORCHIDEE/references/krinner_etal_2005GBC.pdf%5Cnpapers3://publication/doi/10.1029/2003GB002199.

Kull, O. & Kruijt, B., 1998. Leaf photosynthetic light response: A mechanistic model for scaling photosynthesis to leaves and canopies. *Functional Ecology*, 12, pp.767–777.

Lafont, S. et al., 2012. Modelling LAI, surface water and carbon fluxes at high-resolution over France: comparison of ISBA-A-gs and ORCHIDEE. *Biogeosciences*, 9(1), pp.439–456. Available at: http://www.biogeosciences.net/9/439/2012/.

Lammertsma, E.I. et al., 2011. Global CO2 rise leads to reduced maximum stomatal conductance in Florida vegetation. *Proceedings of the National Academy of Sciences*, 108(10), pp.4035–4040. Available at: http://www.pnas.org/cgi/doi/10.1073/pnas.1100371108.

Lawrence, D.M. et al., 2011. Parameterization improvements and functional and structural advances in Version 4 of the Community Land Model. *Journal of Advances in Modeling Earth Systems*, 3(1). Available at: http://doi.wiley.com/10.1029/2011MS00045.

Lemordant, L. et al., 2018. Critical impact of vegetation physiology on the continental hydrologic cycle in response to increasing CO 2. *Proceedings of the National Academy of Sciences*. Available at: http://www.pnas.org/content/early/2018/03/29/1720712115.

Lemordant, L. et al., 2016. Modification of land-atmosphere interactions by CO2 effects: implications for summer dryness and heatwave amplitude. *Geophysical Research Letters*. Available at: http://doi.wiley.com/10.1002/2016GL069896.

Leuning, R., 1995. A critical appraisal of a combined stomatal - photosynthesis model for C3 plants. *Plant, Cell & Environment*, 18, pp.339–355. Available at: http://onlinelibrary.wiley.com/doi/10.1111/j.1365-3040.1995.tb00370.x/full.

Leuzinger, S. et al., 2015. The 'island effect' in terrestrial global change experiments: a problem with no solution? *AoB Plants*, 7, p.plv092. Available at: http://aobplants.oxfordjournals.org/lookup/doi/10.1093/aobpla/plv092.

Leuzinger, S. & Körner, C., 2007. Water savings in mature deciduous forest trees under elevated CO2. *Global Change Biology*, 13(12), pp.2498–2508.

Leuzinger, S., Zotz, G. & Asshoff, R., 2005. Responses of deciduous forest trees to severe drought in Central Europe. *Tree Physiology*, 25(6), pp.641–650. Available at: http://treephys.oxfordjournals.org/content/25/6/641.full.pdf+html?sid=ff667a93-b8a3-47ce-b2c7-a8de8319a32c.

Lindsay, K. et al., 2014. Preindustrial-control and twentieth-century carbon cycle experiments with the Earth system model CESM1(BGC). *Journal of Climate*, 27(24), pp.8981–9005.

Mason, S.J., 2001. El Niño, climate change, and Southern African climate El Nin.

Environmetrics, 12(July 1999), pp.327–345.

Mccarthy, H.R. et al., 2007. Temporal dynamics and spatial variability in the enhancement of canopy leaf area under elevated atmospheric CO2. *Global Change Biology*, 13(12), pp.2479–2497. Available at: http://onlinelibrary.wiley.com/doi/10.1111/j.1365-2486.2007.01455.x/epdf.

Mcdowell, N.G., 2011. Mechanisms Linking Drought , Hydraulics , Carbon Metabolism , and Vegetation Mortality. *Plant physiology*, 155(March), pp.1051–1059.

Meehl, G.A. & Tebaldi, C., 2004. More intense, more frequent, and longer lasting heat waves in the 21st century. *Science*, 305(5686), pp.994–997.

Milly, P.C.D. & Dunne, K.A., 2016. Potential evapotranspiration and continental drying. *Nature Climate Change*, (June).

Miralles, D.G. et al., 2014. Mega-heatwave temperatures due to combined soil desiccation and atmospheric heat accumulation. *Nature Geoscience*, 7(5), pp.345–349. Available at: http://www.nature.com/doifinder/10.1038/ngeo2141.

Morgan, J.A. et al., 2011. C4 grasses prosper as carbon dioxide eliminates desiccation in warmed semi-arid grassland. *Nature*, 476(7359), pp.202–205. Available at: http://www.nature.com/doifinder/10.1038/nature10274.

Morgan, J.A. et al., 2004. Water relations in grassland and desert ecosystems exposed to elevated atmospheric CO2. *Oecologia*, 140(1), pp.11–25.

Morison, J.I.L., 1985. Sensitivity of stomata and water use efficiency to high CO2. *Plant, Cell and Environment*, 8, pp.467–474. Available at: http://onlinelibrary.wiley.com.ezproxy.cul.columbia.edu/doi/10.1111/j.1365-3040.1985.tb01682.x/epdf.

Moss, R.H. et al., 2010. The next generation of scenarios for climate change research and assessment. *Nature*, 463(7282), pp.747–56. Available at: http://www.ncbi.nlm.nih.gov/pubmed/20148028.

Norby, R.J. & Zak, D.R., 2011. Ecological Lessons from Free-Air CO2 Enrichment (FACE) Experiments. *Annual Review of Ecology, Evolution, and Systematics*, 42(1), pp.181–203.

Obermeier, W.A. et al., 2016. Reduced CO2 fertilization effect in temperate C3 grasslands under more extreme weather conditions. *Nature Climate Change*, 1(December), pp.1–6. Available at: http://www.nature.com/doifinder/10.1038/nclimate3191.

Penman, H.L., 1948. Natural Evaporation from open water, bare soil and grass. *Proceedings of the Royal Society*, 193(1032). Available at: http://rspa.royalsocietypublishing.org.ezproxy.cul.columbia.edu/content/193/1032/120.

Peñuelas, J., Canadell, J.G. & Ogaya, R., 2011. Increased water-use efficiency during the 20th century did not translate into enhanced tree growth. *Global Ecology and Biogeography*, 20(4), pp.597–608.

Perkins-Kirkpatrick, S.E. & Gibson, P.B., 2017. Changes in regional heatwave characteristics as a function of increasing global temperature. *Scientific Reports*, 7, pp.1–12. Available at: http://dx.doi.org/10.1038/s41598-017-12520-2.

Perkins, S.E., Alexander, L. V & Nairn, J.R., 2012. Increasing frequency , intensity and

duration of observed global heatwaves and warm spells. *Geophysical Research Letters*, 39(October), pp.1–5.

Perkins, S.E., Argüeso, D. & White, C.J., 2015. Relationships between climate variability, soil moisture, and Australian heatwaves. *Journal of Geophysical Research: Atmospheres*, 120, pp.8144–8164.

Pieruschka, R., Huber, G. & Berry, J.A., 2010. Control of transpiration by radiation. *Proceedings of the National Academy of Sciences of the United States of America*, 107, pp.13372–13377.

Poulter, B. et al., 2014. Contribution of semi-arid ecosystems to interannual variability of the global carbon cycle. *Nature*, 509(7502), pp.600–603. Available at: http://www.nature.com/doifinder/10.1038/nature13376.

Prudhomme, C. et al., 2014. Hydrological droughts in the 21st century, hotspots and uncertainties from a global multimodel ensemble experiment. *Proceedings of the National Academy of Sciences of the United States of America*, 111(9), pp.3262–7. Available at: http://www.pubmedcentral.nih.gov/articlerender.fcgi?artid=3948235&tool=pmcentrez&rendertype=abstract.

Quesada, B. et al., 2012. Asymmetric European summer heat predictability from wet and dry southern winters and springs. *Nature Climate Change*, 2(10), pp.736–741. Available at: http://dx.doi.org/10.1038/nclimate1536.

Reich, P.B., Hobbie, S.E. & Lee, T.D., 2014. Plant growth enhancement by elevated CO2 eliminated by joint water and nitrogen limitation. *Nature Geoscience*, 7(12), pp.920–924. Available at: http://www.nature.com/doifinder/10.1038/ngeo2284.

Reichstein, M. et al., 2013. Climate extremes and the carbon cycle. *Nature*, 500(7462), pp.287–295. Available at: http://www.nature.com.are.uab.cat/nature/journal/v500/n7462/full/nature12350.html.

Richard, Y. et al., 2001. 20th Century Droughts in Southern Africa: Spatial and Temporal Variability, Teleconnactions with Oceanic and Atmospheric Conditions. *International Journal of Climatology*, 21, pp.873–885.

Sarah B. Kapnick & Delworth, T.L., 2013. Controls of Global Snow under a Changed Climate. *Journal of Climate*, 26, pp.5537–5562.

Saurer, M., Siegwolf, R.T.W. & Schweingruber, F.H., 2004. Carbon isotope discrimination indicates improving water-use efficiency of trees in northern Eurasia over the last 100 years. *Global Change Biology*, 10(12), pp.2109–2120.

Schär, C. et al., 2004. The role of increasing temperature variability in European summer heatwaves. *Nature*, 427(6972), pp.332–336.

Scheff, J. & Frierson, D.M.W., 2014. Scaling Potential Evapotranspiration with Greenhouse Warming. *Journal of Climate*, 27(4), pp.1539–1558. Available at: http://journals.ametsoc.org/doi/abs/10.1175/JCLI-D-13-00233.1.

Scheff, J. & Frierson, D.M.W., 2015. Terrestrial aridity and its response to greenhouse warming across CMIP5 climate models. *Journal of Climate*, 28(14), pp.5583–5600.

Schlesinger, W.H. & Jasechko, S., 2014. Transpiration in the global water cycle. *Agricultural and Forest Meteorology*, 189–190, pp.115–117. Available at:

http://dx.doi.org/10.1016/j.agrformet.2014.01.011.

Seager, R. et al., 2014. Causes of increasing aridification of the mediterranean region in response to rising greenhouse gases. *Journal of Climate*, 27(12), pp.4655–4676.

Sellers, P.J. et al., 1996. Comparison of Radiative and Physiological Effects of Doubled Atmospheric CO_2 on Climate. *Science*, 271(5), pp.1402–1406. Available at: http://adsabs.harvard.edu/cgi-bin/nph-data_query?bibcode=1996Sci...271.1402S&link_type=ABSTRACT%5Cnpapers2://publication/doi/10.1126/science.271.5254.1402.

Seneviratne, S.I. et al., 2016. Allowable CO2 emissions based on regional and impact-related climate targets. *Nature*, 1870(Gt C), pp.1–7. Available at: http://www.nature.com/doifinder/10.1038/nature16542.

Seneviratne, S.I. et al., 2012. *Changes in climate extremes and their impacts on the natural physical environment*, Cambridge Univ. Press, Cambridge, U. K., and New York. Available at: https://www.ipcc.ch/pdf/special-reports/srex/SREX-Chap3_FINAL.pdf.

Seneviratne, S.I. et al., 2010. Investigating soil moisture-climate interactions in a changing climate: A review. *Earth-Science Reviews*, 99(3–4), pp.125–161. Available at: http://dx.doi.org/10.1016/j.earscirev.2010.02.004.

Seneviratne, S.I. et al., 2006. Land-atmosphere coupling and climate change in Europe. *Nature*, 443(7108), pp.205–209.

Sherwood, S. & Fu, Q., 2014. A Drier Future? *Science*, 343(6172), pp.737–739. Available at: http://www.sciencemag.org/content/343/6172/737.short.

Sillmann, J. & Croci-Maspoli, M., 2009. Present and future atmospheric blocking and its impact on European mean and extreme climate. *Geophysical Research Letters*, 36(10), pp.1–6.

Skamarock, W.C. et al., 2008. A Description of the Advanced Research WRF Version 3. *Technical Report*, (June), p.113.

Stéfanon, M. et al., 2012. Effects of interactive vegetation phenology on the 2003 summer heat waves. *Journal of Geophysical Research: Atmospheres*, 117(24), pp.1–15.

Stocker, T.F. & Qin, D. eds., 2013. *IPCC Climate Change 2013: The Physical Science Basis*, Cambridge University Press.

Strain, B.R., 1987. Direct Effects of Increasing Atmospheric CO2 on Plants and Ecosystems. *Trends in ecology & evolution*, 2(I), pp.18–21.

Swann, A.L.S. et al., 2016. Plant responses to increasing CO2 reduce estimates of climate impacts on drought severity. *Proceedings of the National Academy of Sciences*, 113(36), pp.10019–10024. Available at: www.pnas.org/cgi/doi/10.1073/pnas.1604581113.

Taylor, K.E., Stouffer, R.J. & Meehl, G. a, 2011. A Summary of the CMIP5 Experiment Design. *World*, 4(January 2011), pp.1–33. Available at: http://cmip-pcmdi.llnl.gov/cmip5/docs/Taylor_CMIP5_design.pdf.

Taylor, K.E., Stouffer, R.J. & Meehl, G.A., 2012. An overview of CMIP5 and the experiment design. *Bulletin of the American Meteorological Society*, 93(4), pp.485–498.

Teuling, A.J. et al., 2010. Contrasting response of European forest and grassland energy

exchange to heatwaves. *Nature Geoscience*, 3(10), pp.722–727. Available at: http://dx.doi.org/10.1038/ngeo950.

Tingley, M.P. & Huybers, P., 2013. Recent temperature extremes at high northern latitudes unprecedented in the past 600 years. *Nature*, 496(7444), pp.201–205. Available at: http://dx.doi.org/10.1038/nature11969.

Tjiputra, J.F. et al., 2013. Evaluation of the carbon cycle components in the Norwegian Earth System Model (NorESM). *Geoscientific Model Development*, 6(2), pp.301–325.

Vogel, M.M. et al., 2017. Regional amplification of projected changes in extreme temperatures strongly controlled by soil moisture- temperature feedbacks. *Geophysical Research Letters*, 44(3), pp.1511–1519. Available at: http://onlinelibrary.wiley.com/doi/10.1002/2016GL071235/pdf.

Walker, a. P. et al., 2014. Comprehensive ecosystem model-data synthesis using multiple data sets at two temperate forest free-air CO2 enrichment experiments: Model performance at ambient CO2 concentration. *Journal of Geophysical Research: Biogeosciences*, 119, pp.937–964.

Warren, J.M. et al., 2011. Ecohydrologic impact of reduced stomatal conductance in forests exposed to elevated CO2. *Ecohydrology*, 4, pp.196–210.

Watts, N. et al., 2017. The Lancet Countdown on health and climate change : from 25 years of inaction to a global transformation for public health. *The Lancet*, 6736(17).

Wu, T. et al., 2013. Global carbon budgets simulated by the Beijing Climate Center Climate System Model for the last century. *Journal of Geophysical Research Atmospheres*, 118(10), pp.4326–4347.

Wullschleger, S., 2002. Sensitivity of stomatal and canopy conductance to elevated CO2 concentration – interacting variables and perspectives of scale. *New Phytologist*, 153, pp.485–496.

Wullschleger, S.D., Tschaplinski, T.J. & Norby, R.J., 2002. Plant water relations at elevated CO2 - implications for water-limited environments. *Plant Cell and Environment*, 25, pp.319–331.

Zaehle, S. et al., 2014. Evaluation of 11 terrestrial carbon-nitrogen cycle models against observations from two temperate Free-Air CO2 Enrichment studies. *New Phytologist*, 202(3), pp.803–822.

Zaehle, S. & Friend, A.D., 2010. Carbon and nitrogen cycle dynamics in the O-CN land surface model: 1. Model description, site-scale evaluation, and sensitivity to parameter estimates. *Global Biogeochemical Cycles*, 24(1), pp.1–13.

Zhang, X. et al., 2011. Indices for monitoring changes in extremes based on daily temperature and precipitation data. *Wiley Interdisciplinary Reviews: Climate Change*, 2(6), pp.851–870. Available at: http://onlinelibrary.wiley.com.ezproxy.cul.columbia.edu/doi/10.1002/wcc.147/pdf.

Zhu, Z. et al., 2016. Greening of the Earth and its drivers. *Nature Climate Change*, (April), pp.1–6.